CHALMERS
UNIVERSITY OF TECHNOLOGY

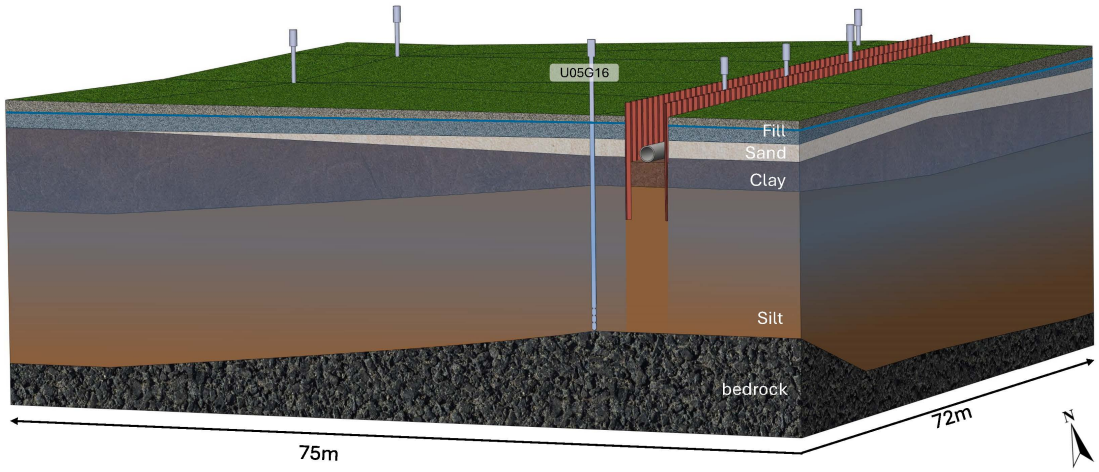

On the effects of unloading and reloading of excavations in clay and silt

A Case Study of the Varberg Tunnel Project

Master's thesis in Infrastructure and Environmental Engineering

ALICE HULTIN
AXEL RECKMAN

DEPARTMENT OF ARCHITECTURE AND CIVIL ENGINEERING
CHALMERS UNIVERSITY OF TECHNOLOGY
Gothenburg, Sweden 2024
www.chalmers.se

Master's thesis 2024

On the effects of unloading and reloading of excavations in clay and silt

A case study of the Varberg Tunnel Project

ALICE HULTIN
AXEL RECKMAN

CHALMERS
UNIVERSITY OF TECHNOLOGY

Department of Architecture and Civil Engineering
Division of Geology and Geotechnics
Geotechnics Research group
Chalmers University of Technology
Gothenburg, Sweden 2024

On the effects of unloading and reloading of excavations in clay and silt
A case study of the Varberg Tunnel project
ALICE HULTIN
AXEL RECKMAN

Supervisor: Mats Karlsson, Department of Architecture and Civil Engineering
Supervisor: Daniel Baltrock, Implenia Sverige AB
Examiner: Jelke Dijkstra, Department of Architecture and Civil Engineering

Master's Thesis 2024
Department of Architecture and Civil Engineering
Division of Geology and Geotechnics
Geotechnics Research group
Chalmers University of Technology
SE-412 96 Gothenburg
Telephone +46 31 772 1000

Cover: A visualization showing the ground profile and geotechnical structure on the site.

Typeset in LaTeX
Printed by Chalmers Reproservice
Gothenburg, Sweden 2024

On the effects of unloading and reloading of excavations in clay and silt
A Case Study from the Varberg Tunnel Project

ALICE HULTIN
AXEL RECKMAN
Department of Architecture and Civil Engineering
Chalmers University of Technology

Abstract

In connection with pipe laying in an excavated trench supported by steel sheet piles in clay with underlying layered silty soil, large settlements were measured on a newly laid pipe in a project in Varberg, Sweden. This work aims to investigate possible causes of the settlement by numerical modelling of the geotechnical design. The work also aims to draw conclusions that can help in future excavation work in similar soil profiles. The project initially identified relevant sounding points with in-situ geotechnical tests and laboratory tests. A soil profile was developed from the empirical interpretation of CPTu logs using soil behaviour type (SBT) classification systems. Soil parameters were determined from field and laboratory tests. A numerical modelling was performed of the unloading and reloading effects of a supported excavation. The numerical analysis shows that the excavation bottom heaves during unloading and mechanical swelling. During reloading and pipe laying, there is an immediate settlement and a consolidation settlement. The settlement of the excavation bottom (and the pipe) during reloading in the numerical model may be due to an elastic rebound effect of the bottom under the pre-consolidation pressure in the soil. A difference arises between the total heave and total settlement corresponding to the magnitude of the mechanical swelling. The work also identifies other potential causes of the actual settlement of the excavation bottom (and the pipe) but which were omitted in the numerical modelling. These factors are briefly addressed and include hydraulic uplift, water flows along the soil-sheet pile interface due to penetration of permeable water-bearing subsoil layers, installation and removal effects of sheet piles, and the influence on the strength properties of the soil from vibrations during sheet pile driving in layered silty soils and compaction works in the shafts.

Keywords: excavation, unloading effects, reloading effects, layered soil, vertical displacement, heave, mechanical swelling, settlement, embedded retaining structures, sheet piling.

Om effekterna av avlastning och återbelastning av schakter i lera och silt
En fallstudie från projekt Varbergstunneln
ALICE HULTIN
AXEL RECKMAN
Institutionen för arkitektur och samhällsbyggnadsteknik
Chalmers tekniska högskola

Sammanfattning

I samband med rörläggning i en schaktad ledningsgrav inom stålspont i lera med underliggande skiktad siltig jord uppmättes stora sättningar på en nylagd ledning i ett projekt i Varberg, Sverige. Detta arbetet syftar till utreda möjliga orsaker till sättningen genom numerisk modellering av den geotekniska konstruktionen. Arbetet strävar också efter att dra slutsatser som kan vara behjälpliga i framtida schaktarbeten i liknande jordprofiler. Projektet identifierade inledningsvis relevanta sonderingspunkter med utförda in-situ geotekniska tester samt laboratorietester. En markprofil utvecklades från empirisk tolkning av CPTu-loggar genom diagram för jordklassificering. Jordparmeterar bestämdes utifrån fält- och laboratorieförsök. En numeriska modellering utfördes av av- och återbelastningseffekter av en spontad schakt. Den numeriska analysen visar att schaktbotten häver sig vid avlastning samt på mekanisk svällning. Vid återbelastning och ledningsläggning sker en omedelbar sättning samt en konsolideringssättning. Sättningen av schaktbotten (och ledningen) vid återbelastning i den numeriska modellen kan bero på en elastisk återfjädring av botten under förkonsolideringstrycket i jorden. En differens uppstår mellan den totala hävningen och totala sättningen som motsvarar storleken på den mekaniska svällningen. I arbetet identifieras också andra potentiella orsaker till den verkliga sättningen av schaktbotten (och ledningen) men som utelämnades i den numeriska modelleringen. Dessa faktorer behandlas kortfattat och innefattar hydraulisk bottenupptryckning, vattenflöden längs kontaktytan mellan jord och spont på grund av penetration av permeabla vattenförande underliggande skikt, installations- och dragningseffekter av spontar och påverkan på jordens hållfasthetsegenskaper från vibrationer under spontdrivning i skiktad siltig jord samt packningsarbeten i schakten.

Nyckelord: schaktning, avlastningseffekter, återbelastningseffekter, skiktad jord, vertikala rörelser, hävning, mekanisk svällning, sättning, nedsänkt stödkonstruktion, spontning.

Acknowledgements

This master thesis was carried out during the spring of 2024 as part of the master's programme in Infrastructure and Environmental Engineering at Chalmers University of Technology, in collaboration with Implenia Sverige AB and the Varberg Tunnel project.

We would like to thank Daniel Baltrock at Implenia Sverige AB for proposing this thesis topic, providing supervision, and sharing valuable project insights. We also thank the project team for their assistance in gathering data.

At Chalmers University of Technology, we thank our supervisor, Mats Karlsson, for his excellent feedback and sharing of insights from engineering practice. We also thank Jelke Dijkstra for accepting the responsibility of being our examiner and for his valuable feedback.

We extend our heartfelt thanks to our families and friends for their support during the work.

Alice Hultin, Gothenburg, June 2024
Axel Reckman, Gothenburg, June 2024

List of Acronyms

Below is the list of acronyms that have been used throughout this thesis listed in alphabetical order:

B	Billion
CAL	Calibrated
CAUC	Consolidated Anisotropic Undrained Compression
CPT	Cone Penetration Test
CPTu	Cone Penetration Test with Piezocone
CRS	Constant Rate of Strain
DSS	Direct Simple Shear
ECI	Early Contractor Involvement
FCT	Fall Cone Test
FEM	Finite Element Method
FVT	Field Vane Test
IL	Incremental Loading
M	Million
MC	Mohr Coulomb
MUR	Soil Survey Report (Markteknisk undersökningsrapport)
NC	Normally Consolidated
OC	Over Consolidated
OCR	Over Consolidation Ratio
POP	Pre-overburden Pressure
PS	Parametric Study
SBT	Soil Behaviour Type
SGU	Geological Survey of Sweden (Sveriges geologiska undersökning)
SQD	Specimen Quality Designation
SS	Soft Soil
SSC	Soft Soil Creep

Nomenclature

Below is the nomenclature of indices, sets, parameters, and variables that have been used throughout this thesis.

Latin letters

A	Area
a_s	Swelling index
B_q	Normalized Pore Pressure Ratio
b	Load factor (swelling)
c'	Effective cohesion
c_u	Undrained shear strength
c_v	Consolidation coefficient (vertical)
$C_{\alpha e}$	Secondary consolidation index (void ratio)
e	Void ratio
f'_c	Yield surface
f_s	Sleeve resistance
F_r	Normalized Friction Ratio
g	Gravity
H	Height
i	Hydraulic gradient
I_r	Soil behavior type index
k_i	Permeability
K_0	Lateral earth pressure ratio at rest
K_0^{NC}	Lateral earth pressure at rest in the NC-region
M_0	Constant constrained modulus below the effective vertical preconsolidation pressure, Swedish method
M_c	Stress ratio at critical state in triaxial compression

M_e	Stress ratio at critical state in triaxial extension
M_L	Constant constrained modulus between the stresses σ'_c and σ_L, Swedish method
M_{ul}	Unloading modulus
M'	Modulus number
m_v	Volumetric compressibility
p'	Mean effective stress
p'_0	Magnitude of the yield surface
q	Deviatoric stress
q_c	Tip resistance
q_n	Net cone resistance
q_t	Corrected Cone Resistance
Q_t	Normalized Cone Resistance
S_t	Sensitivity
S_u	Undrained shear strength
t	Time
u	Pore water pressure
u_0	Equilibrium pore pressure based on water table depth
u_2	Measured pore pressure
v_{ur}	Poisson's ratio for unloading-reloading
w_L	Liquid limit
w_n	Natural water content

Greek letters

ϵ_1	Axial strain
σ'_c	Apparent preconsolidation pressure
γ	Unit weight
ρ	Density
σ_L	Stress limit
σ_{vo}	Total Overburden Stress
σ'_{vo}	Effective Overburden Stress
σ'_{cv}	Ratio between the preconsolidation stress and the vertical effective stress
σ_h	Horizontal effective stress

σ'_n	Normal effective stress
τ	Strength index
τ_f	Shear stress
μ	Correction factor
ϕ'	Friction angle
ϕ'_c	Critical state friction angle
κ^*	Modified swelling index
λ^*	Modified compression index
μ^*	Modified creep index

Contents

List of Figures

List of Tables

1

Introduction

The Swedish systems for stormwater, drinking water and wastewater management will need large investments following an increased urbanisation, a growing need for maintenance, and climate adaption for increased resilience against growing precipitation (Svenskt Vatten AB, 2023). The investments in new stormwater, drinking water and wastewater pipes in Sweden amounted in 2021 to SEK 8.363 billion (B) and in existing pipes to SEK 5.090 B. This corresponds to a total yearly expenditure of SEK 13.461 B in the pipe network and 60% of the total investment in the systems. Nevertheless, an additional SEK 10 B is needed to cope with the growing demand for maintenance works in the system that was mainly built in the 1950s-1970s. These drivers are together challenging the systems performance. Solutions that contribute to the development of the pipe systems are essential for people, the environment, and society. The construction industry could play a key role by conducting cost-effective projects for laying of new pipes and replacement of existing pipes approaching the end of their serviceable life.

The laying of pipes in soft clay is typically performed in excavated trenches supported by sheet pile walls in urban areas, where open-cut excavations are not suitable (Franzén et al., 2000). This approach often results in significant pipe settlements, impacting serviceability and leading to additional construction works and increased project costs. Moreover, construction of transportation infrastructure can sometimes require pipes to be relocated. Consequently, an improved understanding of the ground movements in trench excavations for pipes and more reliable predictions of settlements can increase the profitability in construction projects.

Currently, there is a lack of knowledge about the properties of silt and the mechanisms linked to settling problems. Therefore, SGI, together with the Swedish Traffic Agency and Chalmers, has chosen to delve more deeply into the behavior and properties of silt, according to (Löfroth et al., 2024). The report concludes that hydrogeological and topographic conditions create high pore water pressure in the most permeable areas of layered soils with varying hydraulic conductivity (Löfroth et al., 2024). This leads into this master's thesis, which will also explore the problem of silt related to settlement, situating this report within the existing body of knowledge on silt behavior.

The Swedish Transport Administration (Trafikverket) invests SEK 7.9 B in the development of Sweden's main west coast railway line through the the Varberg tunnel project (Swedish Transport Administration, 2022). The railway route is important for passenger and freight traffic in Western Sweden. The project will add double-tracks to the link and thus improved railway capacity and increase the robustness of the system. The execution undertaken by Implenia Construction GmbH and Implenia Sweden AB, under an Early Contractor Involvement (ECI) contract with Trafikverket, comprises 9 km of double-tracks, a 2.8 km drill & blast tunnel, a 300 m cut & cover concrete tunnel, a 900 m concrete trough, and associated civil engineering works (Implenia AG, n.d.).

The city of Varberg manages a wastewater treatment plant located in the north of Varberg. In the planning stage of the new tunnel project, the railway track area adjacent to the treatment plant was projected to expand, reducing the accessibility to existing pipes. Consequently, the pipes were relocated to a free corridor to ensure accessibility for future maintenance and renovations.

1.1 Problem statement

The contractor laid pipes in excavated trenches supported by sheet pile walls and bracing. The walls were driven to the prescribed level. The trench was excavated to the final excavation level. Pipes and vertical displacement gauges monitoring the position were installed according to the instructions. During backfilling large pipe settlements arose and soon stabilised. The pipe settled more than the tolerances allowed and the construction approach was revised.

1.2 Aim

The aim of this thesis is to investigate the mechanisms controlling the unloading and reloading effects in both the short and long term for excavations (3.2 m wide and 4-5 m deep). Additionally, it seeks to explain the pipe settlements and the mechanisms contributing to the observed behaviour in the considered case study.

1.3 Objectives

The research questions for this project are as follows:

- What are the mechanisms influencing the ground movements typically associated with excavations with a depth of 4-5 meters?
- What influences the unloading and reloading response of a deep excavation?
- What geotechnical project risks exist given the site investigation?

- How can the pipe settlements from the site be explained?
- How do alternative approaches for trenched excavations compare against each other?

1.4 Limitations

The numerical modelling will only capture the unloading and reloading response of the excavation and the subsequent pipe settlements. The soil geometry employed will be based on the developed ground profile. The ground movements and soil disturbance arising from wall installation, wall removal, and workmanship will not be modelled, as the exact mechanisms and modelling procedures are not clear. Additionally, the swelling behaviour of expansive soils will not be included in the analysis.

1.5 Project outline

The project will encompass a literature review of embedded wall design and associated ground movements, ground profiles typically associated with geotechnical risks, and numerical modelling of excavations. The site investigation will start with a desk study. Soundings will be selected and assessed, yielding a 3D ground profile for the site. Soil behaviour will be assessed, and soil properties evaluated from in-situ and laboratory tests. The next step is to identify the key factors in the ground profile and at the site that are believed to be important for recreating the pipe settlement in the numerical model. This will lead to the development of soil geometry for the numerical modelling, which will be performed using the geotechnical finite element software PLAXIS 2D. The evaluated properties will be validated by simulating stress paths in the SOIL TEST module in the software. A sensitivity analysis will identify the principal parameters controlling the behaviour in the model. Ultimately, a parametric study will seek the ultimate soil properties that yield the pipe settlements observed at the site.

2

Site description

This chapter provides background information of the site, the excavation, and describes the local soil conditions. Additionally, it presents the construction methods used for the new pipe, the geotechnical structure, and the existing structures.

2.1 History of the area

The West Coast Railway between Malmö and Gothenburg was inaugurated in 1886 and has since been used to transport people and goods(Varberg Kommun, 2021). The railway station and the station house were built on what was then filled seabed. A goods depot, with railway tracks right outside, was built in 1900 north of the station house on land that resembled a swamp but was filled in. The West Coast Railway became very popular, and in 1920, the track was relaid, and the station area expanded. With an increasing population and trade, the traffic authority decided in 2019 to expand to a double track and a train tunnel through Varberg. The area by the old warehouse, where a former railroad track lay, will now have a wastewater pipeline built on the land previously characterised by filled marshland.

To understand the local conditions of the site, it is important to assess the existing constructions in the area and their foundations. The foundations of the structures and facilities adjacent to the new wastewater line, marked in red, are illustrated in Figure (*Figure 2.1*) below. The existing Getterö Bridge and the new Getterö Road, marked in grey, are foundation-reinforced with piles. The building to the east of the line, where the old warehouse once stood, is now replaced by a new construction with a foundation reinforced with a slab on land, marked in yellow. The buildings west of the line are foundation-reinforced with piles marked in blue. The red area in Figure (*Figure 2.1*) indicates where the new wastewater line will be built. This area previously had a railroad track, which has been removed and replaced by a low noise barrier. The embankment was removed in connection with the construction of the new wastewater line. Additionally, there is a temporary road where the new line will be built, allowing all construction traffic to pass through.

Figure 2.1: Overview of building foundations in the surrounding area (Golder Associates AB, 2020)

2.2 Geology and hydrogeology overview

The geological historical site of Varberg creates complex conditions as the ground consists of many different deposits, both post-glacial and glacial (Påsse, 1990). The location under investigation is located right along the coastline, providing unique geotechnical conditions. The rock formation under the Varberg tunnel is presumed to mainly be banded gneiss with smaller part of mafic rocks. This rock formation was formed approximately 1420 million years ago and consists of alternating layers of quartz-feldspar and garnet. Most of the soil types and layers have been formed from this bedrock. Other soil types present are embedded within the others, such as flint, which formed in Skåne and was transported here by sea ice. The material above the bedrock is assumed to be moraine/till, which is also classified as a firm material. The soil layer overlying the bedrock is characterised by glacial clay or post-glacial clay. Both glacial clay and post-glacial clay can occur as both homogeneous and laminated layers. In the laminated clay, layers of sand, gravel, shell layer may occur. Above the clay, there are a few meters of wave-washed gravel and postglacial sand mixed with or overlain by fill material. The different soil types are presented in the soil map from SGU in the figure (*Figure 2.2*) below.

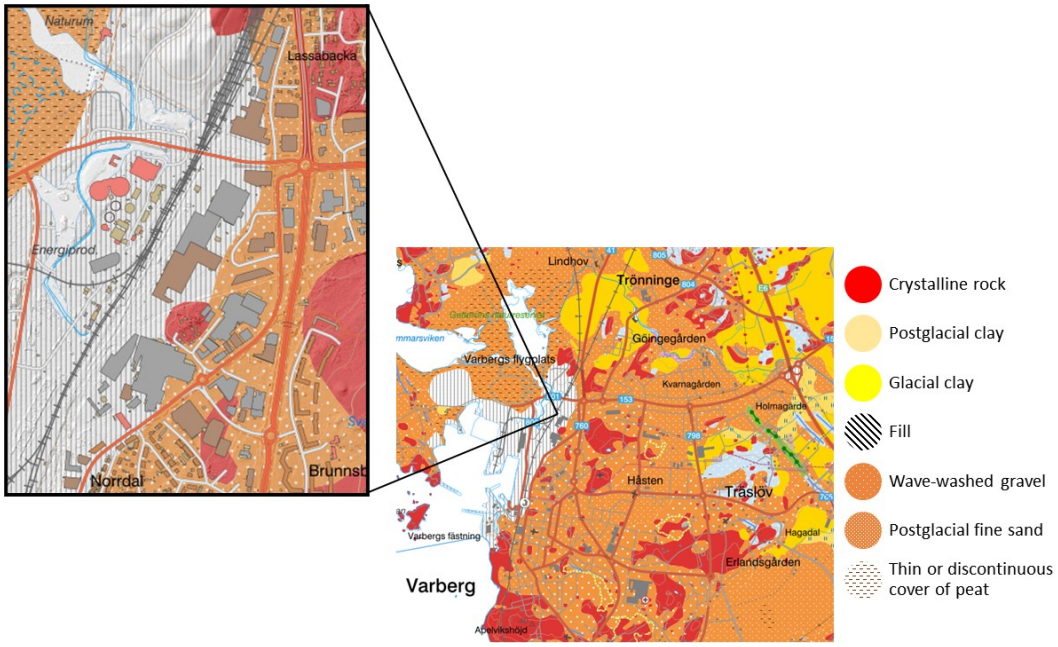

Figure 2.2: Soil map (Geological Survey of Sweden, 2023)

A general cross-section of the soil layer sequence developed by Implenia from surveys and material from the Soil Survey Report (MUR) is presented at the beginning of the process. The soil profile was taken from material from the soil type map from SGU, CPT surveys, interpretation of CPT using the computer program CONRAD and piston sampling. This survey indicates that the ground level is located at a depth of +2m to +3m above sea level and that groundwater levels are located at 1-2 meters below ground level. The top layer was fill with elements of sand, gravel and brick and had a varying thickness from 0m to -1m up to ground level. Under the fill, an area of sand/fine sand with a maximum thickness of 1.8m occurs in some parts, mainly in the south. The sand and fill layers are underlain by a clay layer that varies between 0m and -8m. The clay layer above goes to a silty clay/clayey silt layer down to a depth of 18m. The next layer is a solid layer consisting of moraine that overlays the rock surface, where the rock surface starts at a depth of approximately 16-20 meters.

This geological locale and the produced cross-section described above types on a system with two aquifers, partly an unconfined aquifer in the sand layer/fill layer and partly a confined aquifer in the silty clay/clay silt. The clay layer in between will act as a confining bed. The first cross-section from Implenia is reported in (*Figure 2.6*) below under the conceptual site model chapter.

2.3 Construction works

The City of Varberg manages a wastewater treatment plant located to the north of Varberg. In the planning stage of the tunnel, the railway track area adjacent to

the treatment plant was projected to expand, reducing accessibility to the existing underground utility lines connecting to the plant. Consequently, to enhance accessibility to perform future maintenance and renovation works, the pipe was realigned to an open corridor along the east side of the railway tracks.

The new wastewater pipe was planned with a length of 580m using precast concrete pipe segments of diameter 1200mm, 1000mm and 800mm installed in an excavated trench. The pipe that starts in the south uses 1000 mm concrete segments with an excavation bottom situated between -1.6 m and -0.2 m. In the middle, a 1200 mm pipe was installed at the bottom of the excavation, between -1.9 m and -2.1 m. At the northern end, an 800 mm pipe was installed with an excavation bottom at a level between -1.4 m and -1.9 m. The ground surface level is at approximately +2 m.

The construction approach involved laying the pipe in a braced excavation using 10 m long sheet pile walls. The wall type was VL603 with steel quality S355GP. The bracing was HEB300 with steel quality S355N/M/J. The walls was installed by means of vibration using a side grip vibratory-type sheet pile driver until the top of the walls was at +2,5m. The material properties of the wall and the bracing is presented in *Table 4.1* and *Table 4.2*. The excavation proceeded to the final excavation level was at -1,9m. The backfilling began with constructing a reinforced pipe bed of 0,5m thickness. A vibratory plate compactor was used inside. Subsequently, the pipe was installed and settlement gauges connected (*Figure 2.4*). Lastly, the walls were removed. The gauges recorded significant pipe settlements during the backfilling of the excavation (*Figure 2.5*).

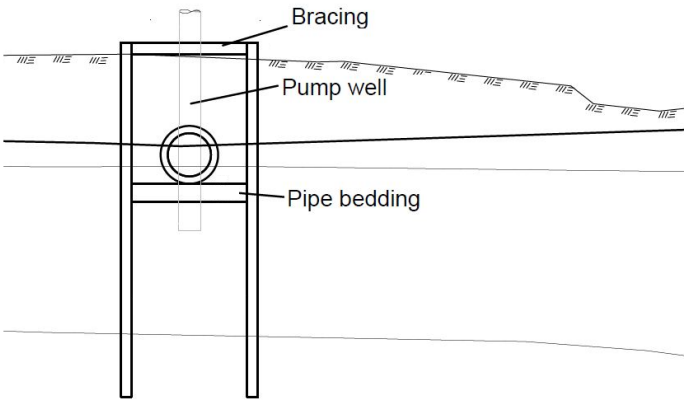

Figure 2.3: Geotechnical structure for the new pipeline with sheet pile walls and bracing

Figure 2.4: Plan over the settlements gauges that was used during the pipe construction.

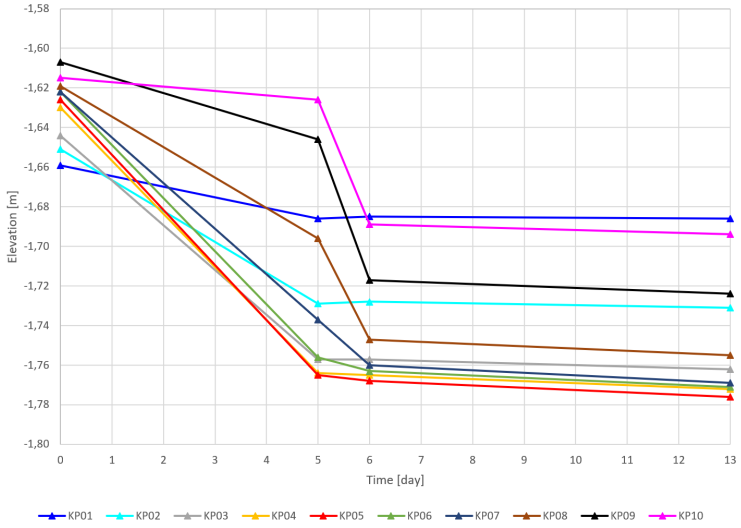

Figure 2.5: Monitoring of pipe settlement through displacement gauges.

2.4 Conceptual site model

The first step in developing a numerical model that illustrates important aspects of the real world is to create a conceptual site model. This model is a simplification of reality used to understand the problem. The conceptual model developed for the pipeline project in Varberg is presented in (*Figure 2.6*). This model shows adjacent structures, rail ways and roads. The conceptual site model highlights the adjacent structures, infrastructures, and that soil tests are only available on the west side of the projected pipeline.

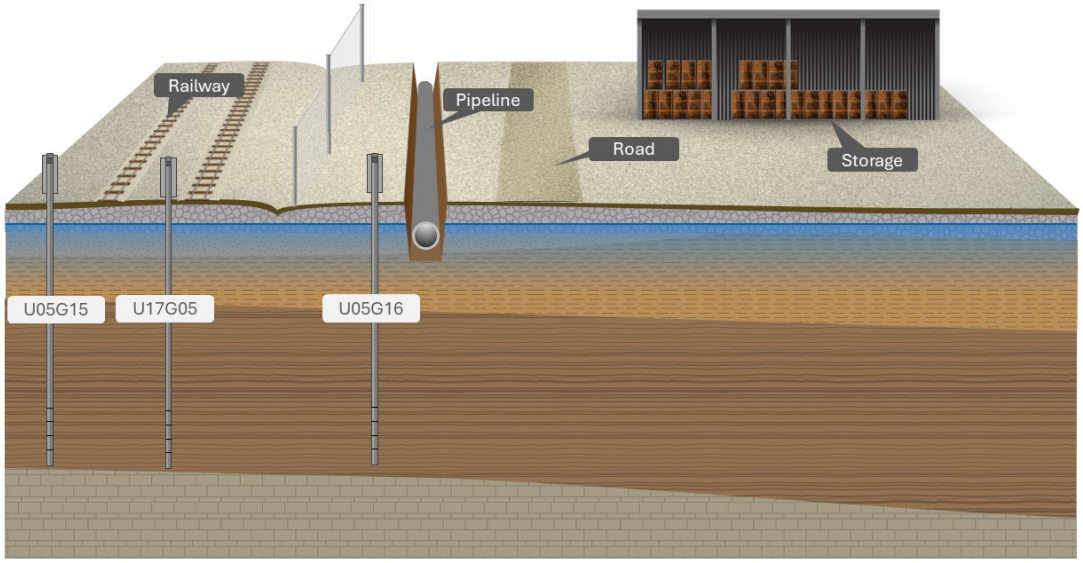

Figure 2.6: Conceptual Site Model

3

Theory

The chapter presents key concepts relevant to the considered case and summaries the main findings of the literature review.

3.1 Groundwater flow in soils

The groundwater flow through soil can be estimated using Darcy's Law, as shown in *Equation 3.1.* The flow depends on the cross-sectional area (A), the permeability of the soil (k), and the hydraulic gradient (i), which can be derived from *Equation 3.2* (Brown et al., 2023a).

$$q = Aki \tag{3.1}$$

$$i = \frac{dh}{dx} \tag{3.2}$$

Natural soils formed under varying depositional environments can exhibit anisotropic features in the macro-structure(Brown et al., 2023a). Distinct alternations in particle sizes, as in partings, laminations, and layering influences the soil permeability and ground water flow conditions. Layering on a macroscopic level can result in the horizontal permeability being 100 to 1000 times larger than the vertical. In engineering practice, a reliable estimate of a soil's permeability is derived from in-situ measurements. Laboratory tests use a limited number of samples, and sampling can result in disturbed specimens, affecting the specimen's permeability.

3.2 Unloading/reloading response

The unloading response of soils depends on the unloading stiffness (Persson, 2004). The unloading modulus is thus relevant for estimating heave in excavations. The stress dependency of the unloading modulus was analysed for a soft clay deposit in the Gothenburg region. The study encompassed field monitoring in a deep excavation and laboratory testing, including triaxial, IL oedometer, and Bender element tests of specimens. As the overburden pressure was reduced, the unloading modulus decreased. Moreover, the initial large unloading modulus can be explained by the fact that secondary consolidation is acting in the opposite direction of the swelling

(Persson, 2004). The swelling rate must thus be larger than the secondary consolidation rate for heave to develop. A relationship for the unloading modulus in soft clay is presented in *Equation 3.3* (Persson, 2007). The showed unloading modulus is a refined numerical fitting of the relationships recognised earlier by Persson (2004). The equation depends on the pre-consolidation pressure (σ'_c) and the over-consolidation ratio (OCR), being $OCR = \sigma'_c/\sigma'_v$. S is the total swelling.

$$M_{ul} = 35\sigma'_c \cdot e^{\frac{3.5}{OCR}} \tag{3.3}$$

The unloading behaviour in silt is characterised by swelling, and the unloading modulus can be calculated from *Equation 3.4*, using empirical values of the swelling index (α_s) ranging from 0.2 to 0.6 % (R. Larsson, 1995).

$$M_{ul} = \frac{\sigma' v}{a_s} \tag{3.4}$$

The reloading behaviour and modulus of soft soils are influenced by previous swelling as seen in *Equation 3.5* (R. Larsson, 1986). The load factor (b) corresponds to the stress state at which swelling develops in the soil. The reloading modulus in a stress range $\sigma'_v < b \cdot \sigma'_c$ can be calculated with *Equation 3.5* and will be near constant. For $\sigma'_v > b \cdot \sigma'_c$, *Equation 3.6*.

$$M_{rl} = \frac{b \cdot \sigma'_c - \sigma'_v}{a_s \cdot ln\left(\frac{b \cdot \sigma'_c}{\sigma'_v}\right)} = \frac{b \cdot \sigma'_c - \sigma'_v}{S} \tag{3.5}$$

$$M_{rl} \simeq \frac{\sigma'_v}{a_s} \tag{3.6}$$

3.3 Settlements

Loading saturated soil with low permeability results in undrained (ρ_u), primary consolidation (ρ_c) and sometimes secondary/creep settlements (ρ_s) (Brown et al., 2023a). *Equation 3.7* shows the total settlement (ρ_t).

$$\rho_t = \rho_u + \rho_c + \rho_s \tag{3.7}$$

Primary consolidation settlements (ρ_c) in soils with a low permeability arise from the loading response and the subsequent consolidation process (Knappett & Craig, 2019). Loading increases the overburden pressure. The soil particles want to rearrange to take up less space, but such a movement is counteracted by the incompressible nature of water. The water flow rate through the boundaries of the soil is lower than the loading rate, resulting in an increased excess pore water pressure (u_e) and an undrained condition. A seepage gradient develops, draining the soil

and reducing the pore water pressure. The consolidation rate is governed by the soil's permeability (k). The consolidation continues until $u_e = 0$, and the pore water pressure equals the static pore water pressure. At this stage, the consolidation is completed and the soil is drained. The resulting vertical displacement is the primary consolidation settlement.

At the same time as the primary consolidation occurs, the soil can exhibit secondary consolidation/creep settlements that depends on the soil viscosity (Knappett & Craig, 2019). The secondary consolidation index is calculated using *Equation 3.8* (Olsson, 2010). The secondary consolidation is dependent on the degree of consolidation.

$$C_{\alpha e} = \frac{\Delta e}{\Delta log(t)} \tag{3.8}$$

3.4 Excavations with embedded retaining walls

Earth retaining structures provide lateral support to the ground (Gaba et al., 2017). Various types exist, encompassing gravity retaining walls, hybrid designs, and embedded retaining walls. For an embedded wall, lateral support for the retained ground is achieved by driving the wall below the excavation base. Various types of embedded retaining walls exist, including sheet pile walls, king post walls, contiguous bored pile walls, secant bored pile walls, and diaphragm walls. Deep and narrow excavations often use sheet pile walls, with additional support provided by bracing or props installed as the excavation progresses (Knappett & Craig, 2019).

3.4.1 Basal heave failure

The earth pressure outside excavation is exerted by the soil weight and a potential surface load. When the overburden pressure above the excavation level is equal to or exceeds the shear strength of the soil, basal heave failure can occur (Knappett & Craig, 2019). Failure occurs along a circular shearing plane below the excavation. Braced excavations in use one or more levels of props to maintain stability as they progress, resulting in larger stress reductions during excavation and, eventually, larger risk for bottom heave.

3.4.2 Hydraulic uplift

In dry excavations in fine-grained soil layers that overly coarser soil with higher permeability, high water pressures in the underlying formation can lead to instability and hydraulic uplift (Fredriksson et al., 2018). The stability of the excavation base against hydraulic uplift can be assessed using *Equation 3.9*, using the unit weight of water ρ_w, gravity g, height between ground water table and permeable stratum H, saturated soil density ρ_m, and the distance between excavation level and permeable stratum d. The partial factor γ_d depends on the safety class for the geotechnical

structure and is 0.83 for safety class (SF) 1, 0.91 for SF 2, and 1.00 for SF 3. Consequently, the overburden pressure of soil in the excavation has to be greater or equal to the water pressure in the more permeable coarse soil layer beneath to ensure stability.

$$\rho_w \cdot g \cdot H \leq \frac{0.9\rho_m \cdot g \cdot d}{\gamma_d \cdot 1.1} \tag{3.9}$$

The high water pressures beneath the excavation can be reduced by installing wells and thus reduce the risk for hydraulic uplift to develop in the excavation (Brown et al., 2023b). The excavation can be cut off from the water-bearing stratum by taking the embedded retaining walls into an underlying soil formation with lower permeability or by grouting and sealing the zone below the wall. A passive relief system for the water pressure can be installed in the excavation.

3.4.3 Ground movements

Excavations in front of embedded retaining structures result in ground movements, which depend on various factors and their complex interactions in three dimensions (Gaba et al., 2017). Factors contributing to ground movements within and around a deep excavation encompass wall installation, the excavation effect (changes in the stress state in the soil during unloading, excavation geometry, ground stiffness and strength, the type and stiffness of the wall and support system, changes in the groundwater regime and pore pressures, the construction procedure, and the quality of workmanship), groundwater flows, and project-specific procedures (e.g. sheet pile removal). This section covers soil movements from installing embedded retaining structures, excavation work before the wall, and elastic and time-dependent heave.

Wall installation

Sheet piles are installed through driving, hydraulic jacking or pressing depending on the ground conditions (Gaba et al., 2017). Smaller ground movements can arise during the installation procedure. Sheet pile driving also generates ground vibrations, resulting in compaction of loose coarse-grained soils.

Excavation works

Excavation between the retaining walls reduces lateral passive earth pressures. Mobilising shear stresses to the yield limit of the soil in excavation results in shear deformations and local plastic ground movements (Gaba et al., 2017).

Elastic and time-dependent heave

The overburden pressure exerted on the underlying soil is reduced as the excavation progresses (Gaba et al., 2017). This leads to an elastic displacements upwards of the excavation bottom in the short term. The soil stiffness determines the immediate heave for excavations in clay. The unloading effect on an excavation bottom in saturated clay also results in time-dependent swelling, which adds to the total

excavation heave in the long term (Knappett & Craig, 2019). The reduced overburden pressure increases soil volume and void space, resulting in decreased pore pressures and negative excess pore pressures. Swelling arises as the seepage restores the pore pressure within the soil to the long-term equilibrium, steady-state seepage and drained conditions. The soil permeability governs the swelling rate.

3.5 Reference projects on anisotropic permeability

The conceptual design of underground construction projects needs to account for the macro-structure of the soil, which is influenced by the depositional environment (Brown et al., 2023a). The characteristic features can also vary within a soil layer, e.g. coarse partings, layering, and lamination, resulting in anisotropic permeability.

The conceptual design of the New Palace Yard underground car park adjacent to Westminster Palace in London showed the importance of thorough ground investigations of the soil macro-structure and its implications on the construction procedure (Brown et al., 2023a). The setting with surrounding historical buildings meant small tolerances for ground movements, thus presenting a geotechnical engineering challenge for the project. The underground project involved an 18.5 m deep excavation supported by reinforced concrete diaphragm walls and struts. Geotechnical site investigations revealed 10mm thick fine sand and silt partings with a 50 mm spacing within the London clay between 19 and 30m depth, with a decreasing frequency with depth. A more homogeneous clay was estimated to extend from a depth of 30m. The presence of permeable partings in the clay meant that the horizontal permeability could be high. Assessments of the groundwater conditions on the site indicated hydrostatic water pressures. Consequently, the soil underlying the excavation could exhibit high pressures and present a geotechnical hazard, encompassing an increased risk for hydraulic uplift and base failure. Various mitigation measures were assessed. A relief system was inappropriate due to concerns about its effectiveness over time. Additionally, it was challenging to perform a representative seepage analysis for the design, as the flow properties can vary greatly in fine-grained soil with coarse partings. Ultimately, the approach employed 30m diaphragm walls extending into the underlying homogeneous clay, there by reducing the risk of hydraulic uplift and base failure.

A construction project for a sewer in a deep excavation in Southampton encountered difficulties due to a water-bearing stratum underlying the excavation level (Ward, 1957). The contractor used sheet piles to support the trench excavation, carried out in a stiff sandy clay overlaying a laminated soil layer between fine sand and silty. The sewer was constructed on a concrete slab on the excavation bottom. During excavation, hydraulic uplift arose from the high water pressures in the underlying formation and the subsequently constructed precast concrete sewer pipes settled and cracked after backfilling. The solution became a relief system for the water pressure in the underlying formation. A post-hole auger was driven into the excavation bot-

tom, filling the hole with gravel. Excess water was pumped during the construction. A permeable layer was constructed on the bottom, followed by the concrete slab and the sewer. This approach led to the successful completion of the project.

Hydraulic uplift was identified as a significant risk in a 10m deep excavation project in sensitive clay in central Ottawa (McRostie et al., 1996). The excavation would later accommodate the new Police headquarters complex. In 1981, it was the deepest open dry excavation in the city. A geotechnical site characterisation identified the subsurface as silty clay until 13 meters depth, clayey silt until 18 meters, a stratum of sandy silt, and glacial till at 21 meters. High water pressures in the more permeable stratum below the excavation level were recognised as a potential geotechnical hazard that could lead to hydraulic uplift. The risk was mitigated in the planning phase of the contract by developing a control system for the water pressures of wells and electro-osmosis. The contractor awarded the contract was concerned about the overall cost efficiency and the influence that it might have on the workmanship within the excavation and thus employed the observational approach. The unloading effect would result in negative pore pressures, and a groundwater gradient would develop to seek equilibrium. Nevertheless, a slow seepage gradient due to estimated low horizontal permeability would allow the excavation to be completed without additional measures. The excavation started with a test and then progressed in stages. Extensive monitoring of both heave and pore pressures was performed. In case of an uncontrolled rise in water pressure or heave, the contractor would install wick drains. When the bottom was reached, a raft foundation was installed. The contractor successfully employed the observational method and completed the excavation with minimal heave.

3.6 Reference projects on excavation heave

Full-scale field studies on bottom heave and deformation in trench excavations supported by sheet piles in Swedish soft clay have been performed by Magnusson (1975) and Franzén et al. (2000).

Magnusson (1975) analysed the heave behaviour in deep excavations and whether the unloading response was elastic and plastic. A proposed approach to predict the former was to use a bottom heave safety factor N. A value for N smaller than 4 signifies elastic heave and a greater plastic. Reloading of the excavation base by backfilling results in settlements, and the magnitude depends on the deformation behaviour of the base heave. In clay, the subsequent settlement, developing during the construction time, is equal to the elastic heave if the soil structure remains unchanged, and the reloading restores the stress state to the initial condition. Reloading to a restored stress state and with an unchanged clay structure on a base heave composed of both elastic and plastic deformations results in an additional settlement, apart from the elastic rebound, developing during 3 to 6 months. The additional settlement is sometimes associated with the retaining wall extraction and the following remaining cavity.

Franzén et al. (2000) performed full-scale field trials of pipe laying in trench excavation between temporary sheet pile walls in soft clay in the Gothenburg region. Bottom displacements were monitored and analysed during and after construction. Various approaches to minimise the total settlements were analysed. In all attempts, the initial bottom heave was followed by an even greater settlement of the pipe.

The study found that longer sheet piles reduced the mobilised shear stresses and the bottom heave, leading to smaller subsequent pipe settlements during backfilling. Longer sheet piles also created a larger cavity in the soil below the trench base, resulting in larger vertical settlements during wall extraction(Franzén et al., 2000). The removed walls contained 0-15 mm of soil, further increasing the cavity in the ground (Franzén & Spetz, 1998). Cutting the walls at the excavation level did not reduce bottom settlements (Franzén et al., 2000). Moreover, walking on the excavation bottom disturbed the clay, leading to larger pipe displacement. Ultimately, the study recognised that the total bottom displacement arose form was complex and arose from various sources.

3.7 Soil classification

A prevalent approach for soil classification is based on physical soil characteristics (e.g. grading) (Robertson, 2016). Soil classification in geotechnical projects could benefit from combining physical and behavioural characteristics, as it better represents the in situ condition of the soils. The in situ soil behaviour can be measured through a cone penetration test, and various approaches for subsequent data analysis and soil classification exist (e.g. Robertson (1990), Robertson (2009), Schneider et al. (2008) and Robertson (2016)).

Cone penetration testing at a constant rate in situ provides continuous logging of test properties in the ground (Brown et al., 2023a). Subsequent data analysis can accurately identify soil stratification, classification and various properties. The electric static cone penetrometer (CPT) continuously logs the tip resistance (q_c) and the sleeve resistance (f_s) on the sleeve above the cone. The piezoncone penetrometer (CPTU) also measures the pore water pressure during penetration. While this method can yield precise geotechnical property values for sand, additional in situ methods are necessary to complement it for clay and silt (Swedish Institute for Standards, 2023). Piston sampling and subsequent testing can better estimate density, water content, and liquidity index (Knappett & Craig, 2019).

Robertson (1990) presented a soil behaviour type classification (SBT) system from CPTU logs (*Figure 3.1* that classifies soils according to *Table 3.1*). Normalised parameters are obtained from the CPTU data with *Equation 3.10, 3.11 and 3.12* (Robertson, 2016). The SBT system presented by Robertson (1990) is a refinement of a previous method and considers an increase in effective overburden stress with depth in both penetration and sleeve resistances (Robertson, 2009). The semilog $Q_t - F_r$ space has limited accuracy for classifying softer, fine-grained soils, particularly within the lower Q_t range (< 10 kPa). In such cases, an alternative approach is to plot the CPTU parameters in the semilog $Q_t - B_q$ space, as the classification is linked to the penetration pore pressure.

$$Q_t = \frac{q_t - \sigma_{vo}}{\sigma'_{vo}} \tag{3.10}$$

$$F_r = \left[\frac{f_s}{q_t - \sigma_{vo}}\right] \cdot 100\% \tag{3.11}$$

$$B_q = \frac{u_2 - u_0}{q_t - \sigma_{vo}} = \frac{\Delta u}{q_t - \sigma_{vo}} \tag{3.12}$$

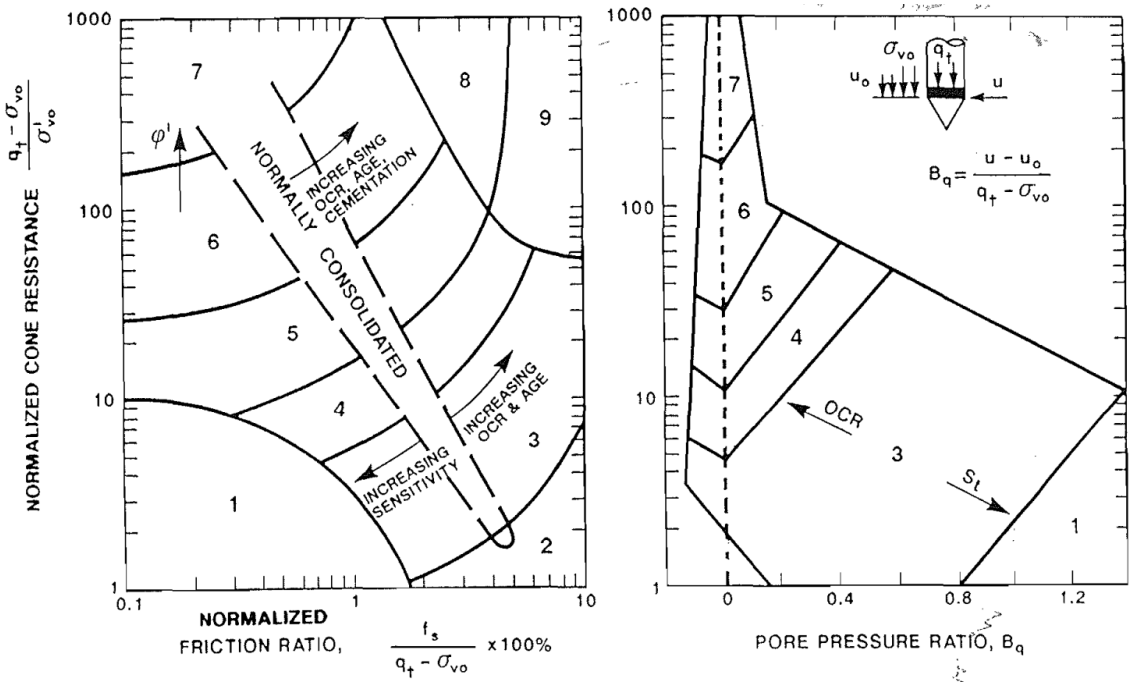

Figure 3.1: The soil behaviour type classification charts represented in the semilog $Q_t - F_r$ space and the semilog $Q_t - B_q$ space (Robertson, 1990).

Table 3.1: The soil behaviour type classes presented by Robertson (1990).

Zone	Soil Type
1	Sensitive fine-grained
2	Organic
3	Clay
4	Silt-mixtures
5	Sand-mixtures
6	Sand
7	Gravelly sand to sand
8	Very stiff sand to clayey sand
9	Very stiff fine-grained

Soil structure at the micro and macro scales contributes to the different behaviours observed in situ compared to ideal soils (Robertson, 2016). As a result, a refinement of the classification approach for soils with pronounced micro structure was developed. It is also recognised that the model presented by Robertson (1990) is reliable in ideal soils with a homogeneous macrostructure. The model presented by Schneider et al. (2008) is better suited for soils with pronounced macrostructure, as

the model has adjusted boundaries, especially in areas with higher F_r values. This adjustment creates clearer distinctions between silt, clay, and sand.

The approach for soil classification with SBTn charts presented by Robertson (1990) from CPTU logs is less reliable in soils with a considerable macrostructure, such as layering (Robertson, 2016). The prevalent SBTn charts are also less accurate in transitional soils (Schneider et al., 2008). Consequently, new charts were proposed based on the general tip resistance and the pore pressure, encompassing the following spaces: log-log $Q - \Delta u_2/\sigma'_{vo}$ (*Figure 3.2*), semilog $Q - \Delta u_2/\sigma'_{vo}$ and semilog $Q - B_q$, which uses B_q as the model by Robertson (1990) and new boundaries (Schneider et al., 2008). The soil behaviour in mixtures of clay, silt, and sand with $u_m = 0$ during testing is best represented in the log-log $Q - \Delta u_2/\sigma'_{vo}$ space as it emphasises the key features of these soils. However, all spaces will yield the same soil classification. The approach characterises the soils according to *Table 3.2*.

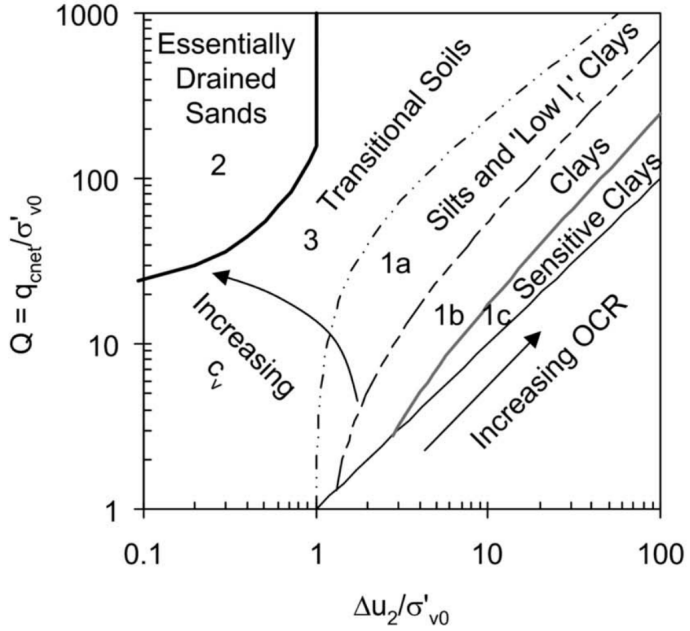

Figure 3.2: log-log $Q - \Delta u_2/\sigma'_{vo}$ SBTn chart as proposed by Schneider et al. (2008).

Table 3.2: The soil behaviour type classes according to Schneider et al. (2008).

Zone	Soil Type
1a	Silts and "Low I_r" clays
1b	Clays
1c	Sensitive clays
2	Essentially drained sands
3	Transitional soils

3.8 Evaluation of soil properties

Obtaining an established soil profile allows for the investigation of soil properties using Triaxial shear tests, Consolidation tests with a constant rate of strain (CRS), Direct simple shear tests (DSS), and sampling with piston samplers.

3.8.1 Piston sampler sampling

The initial parameters analysed included density ρ, water content w_n, liquidity index w_L, sensitivities and preconsolidation pressure (σ'_c) obtained from sampling with a piston sampler. Although triaxial shear tests, CRS, and DSS tests provided values for density and water content, samples from the piston sampler were considered more comprehensive and consequently prioritised highest in collecting these parameters. All values for density, moisture content, liquidity index, and sensitivity were compiled and plotted against depth, with trend lines drawn for each layer to determine the final value for the layer. Effective stress can be calculated using the soil layer's densities and known water level. The fill, sand and rock densities were evaluated according to TK GEO 13 and (R. Larsson, 1995).

From piston sampler sampling, fall cone tests and field vane (FVT) tests were also conducted in situ to determine the value of the strength index, τ. This value of the strength index was then used to calculate the undrained shear strength c_u by computing a correction factor μ according to Equations 3.13 to adjust the strength index, τ, to the undrained shear strength c_u according to Equations 3.14. The correction factor incorporates the soil's liquidity index to better account for soil behaviour and thus provide a more accurate value for the undrained shear strength. Finally, the preconsolidation pressure (σ'_c) was evaluated using Hansbo's empirical method for both fall cone tests and field vane (FVT) tests, as described in Equation and the undrained shear strength (uncorrected) was used Equations 3.15, (R. Larsson et al., 2007) and (Swedish Institute for Standards, 2007).

$$\mu = \left(\frac{0.43}{w_L}\right)^{0.45} \tag{3.13}$$

$$c_u = \tau * \mu \tag{3.14}$$

$$\tau = \sigma'_c * 0.45 * w_L \tag{3.15}$$

3.8.2 Triaxial shear test

Triaxial compression test is a prevalent testing approach for shearing of soils (Knappett & Craig, 2019). The shear strength of clay depends on the history of applied

stresses and thus the state of consolidation (Azizi, 1999). With increasing consolidation degree, the linear relationship between shear strength and applied normal effective stresses becomes non-linear. Hence, the relationship between the shear stress at failure for a heavily overconsolidated clay and the applied normal effective stresses follows *Equation 3.16*, and depends on the peak frictional angle (ϕ_p) and the apparent cohesion (c'). The parameter c' is the shear strength exhibited by the clay at zero normal effective stresses. The additional strength and stability within the clay result from increasing effective stresses from negative pore pressure, leading to suction. In practice, c' is challenging to measure accurately and can thus be set to zero as a conservative approach.

$$\tau_f = c' + \sigma'_n \tan \phi'_p \tag{3.16}$$

Normally consolidated clay and granular soils do not exhibit any apparent cohesion, and the relationship linking the shear strength to the effective normal stresses follows *Equation 3.17*, where ϕ_c is the critical frictional angle.

$$\tau_f = \sigma'_n \tan \phi'_c \tag{3.17}$$

3.8.3 Direct simple shear test (DSS)

The values from DSS tests were utilized to correct the shear strength obtained from fall cone and wing probing tests, complementing the results from Triaxial shear tests. According to Swedish Institute for Standards (1991b), DSS is employed to assess the controlling shear strength as a function of the normal stress acting on the shear plane. Both undrained shear strength and effective strength parameters are determined for DSS. Parameters obtained from the Direct Simple Shear (DSS) test included density (ρ), water content (w_n), undrained shear strength (c_u), and preconsolidation pressure (σ'_c).

Direct shear tests are conducted on undisturbed samples, primarily layered soil with alternating silt and clay TK GEO 13. The shear strength during direct shearing on a horizontal sliding surface is determined through direct shear tests. These tests are also particularly suitable for layered and varved soils, where the shearing is directed towards any potentially weaker layers in the soil (R. Larsson et al., 2007).

This indicates that compared to the corrected strength determined by field vane (FVT) and fall cone tests, active triaxial tests typically yield higher undrained shear strengths, while passive triaxial tests yield lower undrained shear strengths. The average undrained shear strength from active and passive triaxial tests and direct shear tests is slightly higher than the corrected strength from field vane (FVT) and fall cone tests, especially in low-plasticity clays (R. Larsson et al., 2007).

3.8.4 The constant rate of strain (CRS) consolidation test

From CRS, the calculations of the parameters density (ρ), preconsolidation pressure (σ'_c), limit stress (σ'_L), permeability (k), and oedometer modulus (M_0, M_L, M') were

performed.

An important parameter for obtaining information about the strength and deformation properties of the soil was the apparent pre-consolidation pressure (σ'_c). This parameter indicated the degree of soil consolidation and the maximum pressure to which the soil had previously been subjected, including creep deformation (Sällfors, 1975). Given the extensive past construction in the area, this parameter played an important role in understanding the loading history and predicting the soil's behaviour under the new loading. Consolidation was caused by two main mechanisms: vertical load exceeding the previous load and creep deformation resulting from particle movement, especially in clay particles that reorganised under constant effective stress (Bjerrum & Aitchison, 1973). To calculate the apparent preconsolidation pressure from CRS, Sällfors (1975) method was used in combination with Swedish Institute for Standards (1991a) to analyse CRS. M_0 Constant modulus at stresses below the apparent pre-consolidation pressure, M_L Constant modulus for stresses between the apparent preconsolidation pressure and the limit stress σ_L, and modulus number M' were also evaluated according to Swedish Institute for Standards (1991a) and Sällfors (1975). The parameters were evaluated according to *Figure 3.3*. The parameters for the compression modulus are assessed based on the plotted modulus-stress curve, which typically yields an M_0 value that tends to be lower than the actual field conditions, as per past experiences. As a common practice, the evaluated M_0 from a CRS test is often multiplied by a factor of 3-5 to approximate the field conditions better (Olsson, 2010)

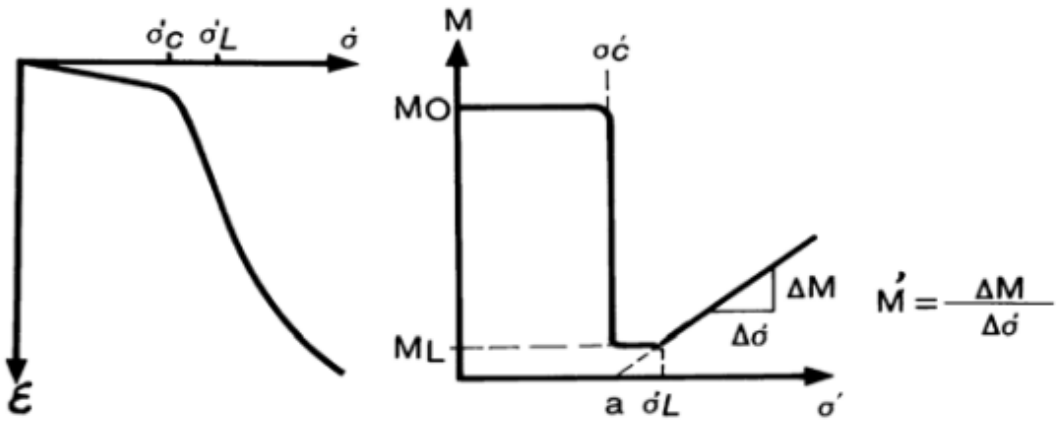

Figure 3.3: Evaluation of compressibility parameters from the CRS-test (Sällfors, 1975)

According to Karstunen and Amavasi (2017), the apparent preconsolidation pressure is an important parameter for the Soft Soil models in PLAXIS, as the pre-overburden pressure (POP) and the Overconsolidation Ratio (OCR) used in the material models depend on this parameter. POP was of significant importance for the model's response and its sensitivity. The apparent pre-consolidation pressure can be evaluated from Triaxial tests, DSS tests, fall cone tests (FC) and field vane test (FVT).

To calculate the Oedometer module from CRS tests, the definition provided by R. Larsson, 2008 is employed, utilizing the relationship between the vertical effective stress σ_v and strain ϵ_1 according to *Equation 3.18*. The oedometer module serves to assess the material's load-bearing capacity, particularly in settlement calculations. This module assumes that horizontal deformation is restrained and that the vertical effective stress increases continuously (R. Larsson, 1995).

$$M = \frac{\Delta\sigma'_v}{\Delta\epsilon_v} \tag{3.18}$$

3.8.5 Sample quality

To ensure a correct and accurate analysis, it is important that the samples are of high quality. Quality assessment is used to investigate possible sample disturbances by classifying whether and how disturbed the samples are. Several methods exist to determine the degree of disturbance in a sample. The methods used in this report are based on the theories of (Terzaghi et al., 1996) (which is based on (Andresen & Kolstad, 1979)), (Karlsrud & Hernandez-Martinez, 2013) and (R. Larsson et al., 2007).

The first two theories can be applied to both laboratory tests: the Oedometer (CRS) and triaxial tests. They are based on evaluating the volumetric strain ϵ_{v0} at the preconsolidation pressure σ'_p for the CRS samples and at the horizontal effective pressure σ'_{h0} for triaxial tests (Andresen & Kolstad, 1979; Terzaghi et al., 1996). The samples are then classified according to the Specimen Quality Designation (SQD) system, which ranting the disturbance level of the samples from A to E (Terzaghi et al., 1996). The range of the classes and their meanings are specified in *Table 3.3*.

Table 3.3: Sample quality estimation according to (Amundsen et al., 2015) compilation of different calculation methods for the CRS (oedometer) and triaxial test methods

Specimen Quality Designation (SQD) (Terzaghi et al. 1996)		M_0/M_L Karlsrud and Hernandez-Martinez (2013)	
Volumetric strain ϵ_{v0} (%)	SQD	Ratio M_0/M_L	Sample quality
<1	A	>2	Very good to excellent
1-2	B	1.5-2	Good to fair
2-4	C	1.5-2	Poor
4-8	D	1-1.5	Very poor
>8	E	<1	

The second method is used only for CRS samples and use the oedometer modules to determine a stiffness ratio, called the oedometer stiffness ratio. This relationship is defined between M_0 The initial consolidation modulus, which indicates the stiffness of the soil at the start of loading and M_L The consolidation modulus at a later stage of loading, which indicates the stiffness of the soil after some consolidation (Karlsrud & Hernandez-Martinez, 2013).

These values, M_0 and M_L, are determined according to the procedure shown in *Figure 3.4*. The classes and their meanings, which categorise the sample quality based on the oedometer stiffness ratio, are given in *Table 3.3* . This classification is important for assessing the degree of disturbance in the samples and is essential for the correct interpretation of the results of the CRS tests (Amundsen et al., 2015).

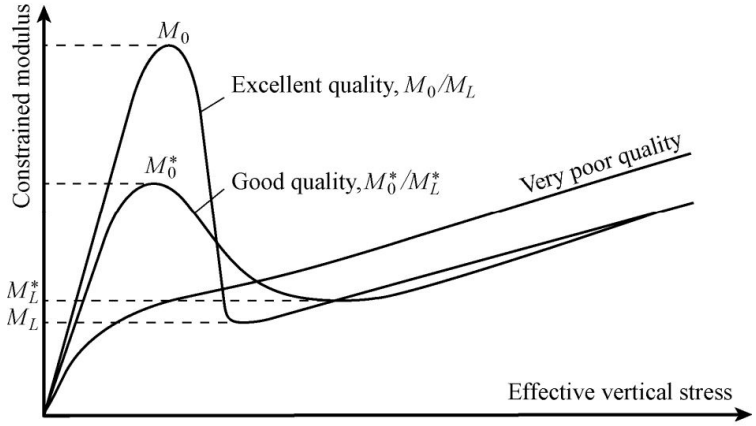

Figure 3.4: The reality and definition for the relationship between the modules for oedometer tests (Amundsen et al., 2015)

The last theory to evaluate the quality introduced by R. Larsson et al., 2007 is useful for both the Oedometer (CRS) and triaxial tests. R. Larsson et al., 2007 method is a further development of Lunne et al., 1997. The method uses the value for the volumetric strain, ϵ_{v0}, but instead of the preconsolidation pressure, σ'_p, the natural water content w_N is applied. The classes and their meanings, which categorize the sample quality based on the volumetric strain, are given in *Figure 3.5*.

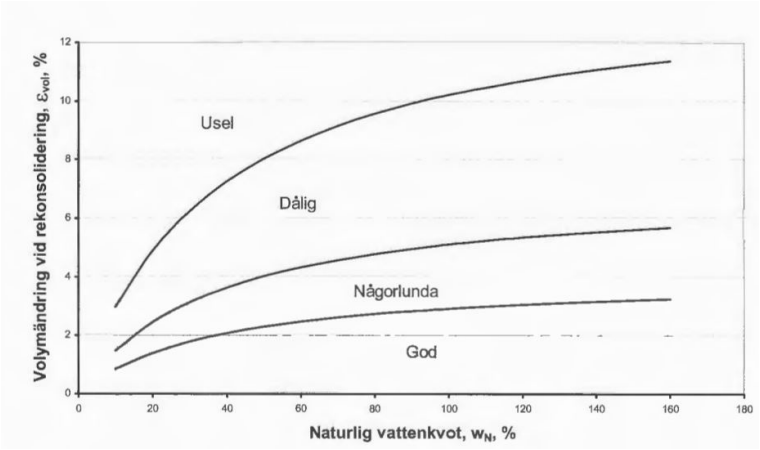

Figure 3.5: The definition for the relationship between the natural water content w_N and volumetric strain ϵ_{v0} for triaxial and oedometer tests (R. Larsson et al., 2007)

3.9 Numerical modelling

Elasto-plastic hardening models are suitable for numerical modelling of lightly over-consolidated soft soils (Karstunen & Amavasi, 2017). These constitutive models incorporate elastic properties, a yield function, a plastic potential, and a hardening rule. The associated hardening rule links plastic deformation to the progression of the yield surface. The internal hardening parameter allows the model to recognise distinct features of soft soils, such as the stiffness dependency on recent stresses and the strength increase along the normal compression line. Two elasto-plastic hardening models are the Soft Soil (SS) model and the Soft Soil Creep (SSC) model. The SS model uses a failure criterion defined by the Mohr-Coulomb model. The SSC model incorporates rate-dependency to recognise secondary consolidation/creep in the analysis.

The yield function of the SS model is influenced by the critical state (Karstunen & Amavasi, 2017). The critical state concept in geomechanics is an ultimate state condition, reached when continuous constant shearing results in no more changes in mean effective stress (p'), deviatoric stress (q), or void space (v) of a soil specimen (*Equation 3.19*) (Wood, 1991).

$$\frac{\partial p'}{\partial \epsilon_q} = \frac{\partial q}{\partial \epsilon_q} = \frac{\partial v}{\partial \epsilon_q} = 0 \tag{3.19}$$

At this state, the critical state stress ratio (η) evaluated as the ratio between the deviatoric stress (q_c) and the vertical effective stress (σ'_c) is equal to the critical state line (M) (*Equation 3.20*) (Wood, 1991).

$$\frac{q_c}{p'_c} = \eta = M \tag{3.20}$$

The frictional angle at critical state (ϕ'_c) can estimated from the critical state ratio in triaxial compression (M_c), typically given by a triaxial compression test (CAUC) (*Equation 3.21*) (Karstunen & Amavasi, 2017). Ultimately, the SS yield surface is defined.

$$\sin \phi'_c = \frac{3M_c}{6 + M_c} \tag{3.21}$$

The critical state ratio in extension (M_e) can be estimated from the ϕ_c using *Equation 3.22* (Karstunen & Amavasi, 2017). This value is typically given by a triaxal tests in extension (CAUE).

$$\sin \phi'_e = \frac{3M_e}{6 - M_e} \tag{3.22}$$

Moreover, the model parameters for the soft soil (SS) creep (SSC) model encompasses the modified swelling index (κ^*), the modified compression index (λ^*), and

Poisson's ratio at unloading/reloading (ν_{ur}), being different from the initial Poisson's ratio (ν) (Karstunen & Amavasi, 2017). Olsson (2010) has compiled empirical approaches for evaluating parameters for the SS/SSC model. κ^* can be derived through *Equation 3.23* and λ^* can be evaluated by using *Equation 3.24*. σ'_{vc} represents the vertical preconsolidation stress. The oedometer modulus (M) is stress dependent and is $M = M_0$ in the range $0 < \sigma'_v < \sigma'_c$ and $M = M_L$ in $\sigma'_c < \sigma'_v < \sigma'_L$ (R. Larsson, 2008).

$$\kappa^* \simeq \frac{2 * \sigma'_v}{M} \tag{3.23}$$

$$\lambda^* \simeq \frac{1.1 * \sigma'_{vc}}{M_L} \tag{3.24}$$

The slopes corresponding to stiffness parameters κ^* and λ^* are shown in the semilog $\epsilon_p - p'$ space from an oedometer test (*Figure 3.6*) (Karstunen & Amavasi, 2017). $\kappa*$ equals to the unloading (swelling) slope in the oedometer space. An alternative approach for evaluating κ^* is to use the initial loading slope with caution.

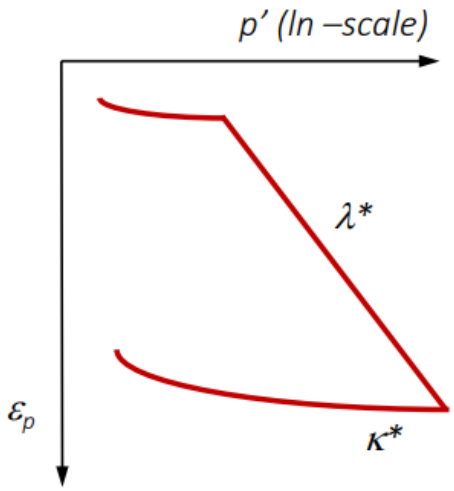

Figure 3.6: The modified stiffness parameters that are used in the SS/SSC model represented in the oedometer space (Karstunen & Amavasi, 2017).

A relationship exists between the modified soft soil strength parameters and the oedometer modulus, as shown in *Figure 3.7* (Olsson, 2010).

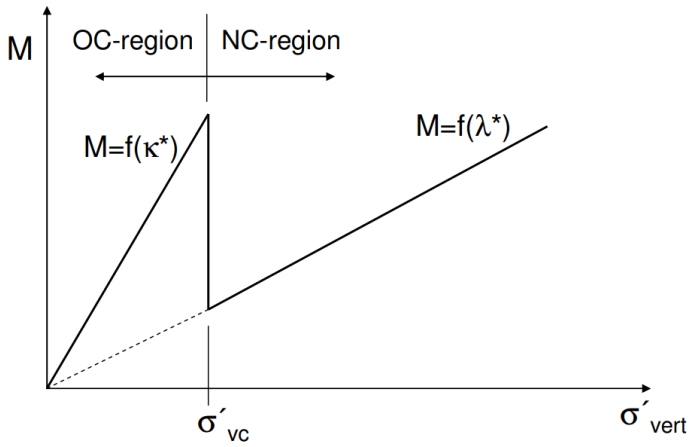

Figure 3.7: The relationship between κ^*, λ^*, and M in the overconsolidated (OC) region and the normal consolidated (NC) region (Olsson, 2010).

The creep parameter μ^* is typically evaluated from IL oedometer tests. Nevertheless, in engineering practice in Sweden, these test are rare due to their high cost (Olsson, 2010). An alternative approach to evaluate μ^* is first find the creep index r_1 from *Equation 3.25*, where W_N is the water content (Christensen, 1995). μ^* can be calculated from *Equation 3.26* (Olsson, 2010).

$$r_1 = \left(\frac{75}{w_N^{1.5}} \right) \tag{3.25}$$

$$\mu^* = \frac{1}{r_1} \tag{3.26}$$

An second alternative approach is to evaluate the coefficient of secondary compression at the apparent preconsolidation pressure ($\alpha_{s(max)}$) using the water content, as illustrated in *Figure 3.8* (P.-E. Larsson et al., 1997).

Clay and slightly organic clay			Organic clay, gyttja, sulphide clay, calcareous clay		
w_N %	$\alpha_{s\,max}$	β_{as}	w_N %	$\alpha_{s\,max}$	β_{as}
25	0.000	0.000	25	0.000	0.000
30	0.002	0.027	50	0.007	0.030
40	0.006	0.031	75	0.016	0.033
50	0.010	0.035	100	0.021	0.035
60	0.014	0.039	125	0.026	0.038
70	0.018	0.043	150	0.030	0.040
80	0.021	0.046	200	0.036	0.046
90	0.025	0.049	250	0.040	0.051
100	0.029	0.053	300	0.044	0.055
110	0.033	0.057	350	0.047	0.058
120	0.037	0.061	400	0.050	0.061

For peat, $\alpha_{s\,max}$ = 0.025 and $\beta_{\alpha\_}$ = 0.000 are normally used.

Figure 3.8: Coefficient of secondary compression $\alpha_{s(max)}$ at the apparent preconsolidation pressure for different water content (P.-E. Larsson et al., 1997)

$\alpha_{s(max)}$ is used to calculate μ^* according to *Equation 3.27*, as proposed by (Olsson, 2010).

$$\mu^* = \frac{\alpha_s}{ln10} \tag{3.27}$$

A third alternative approach is based on a constant representing the secondary compression behaviour of soil, denoted as the ratio C_α/C_c (Mesri & Castro, 1987). Essentially, the method follows the same principle as the relationship proposed by (Christensen, 1995), where μ^* is evaluated based on an r_1. Nevertheless, the third method incorporates the ratio between the preconsolidation stress σ'_c and the vertical effective stress σ'_v, along with the oedometer modulus M. This approach aligns more closely with the method used to evaluate the other parameters, κ^* and λ^*. *Equation 3.28* below illustrates this, as adapted by (Olsson, 2010) to match the Swedish parameters.

$$r_1 = \frac{M_L}{(0.04 \pm 0.01) * \sigma'_{vc}} \tag{3.28}$$

The calculation of soil parameters for the soft soil model in PLAXIS involves determining key factors such as the overconsolidation ratio (OCR), pre-overburden pressure (POP), and coefficients related to lateral earth pressure. From the apparent pre-consolidation pressure (σ'_c) and the vertical effective stress (σ'_c), the overconsolidation ratio (OCR) and the pre-overburden pressure (POP) could be evaluated according to *Equation 3.29 and 3.30* (Parry & Wroth, 1981).

$$OCR = \left(\frac{\sigma'_v}{\sigma'_c}\right) \tag{3.29}$$

$$POP = \sigma'_v - \sigma'_c \tag{3.30}$$

The soft soil models parameters OCR and POP can be assessed by plotting the in-situ effective vertical stress and the final evaluated trendline for (σ'_c) against depth in the same plot (*Equation 3.9*) (Karstunen & Amavasi, 2017).

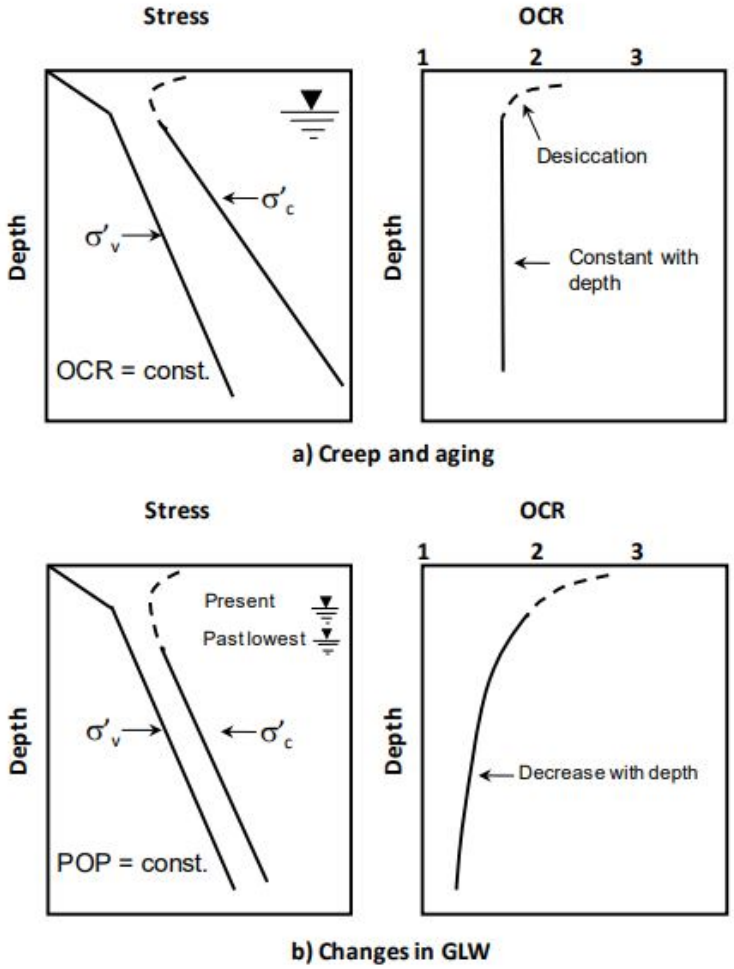

Figure 3.9: Effect from delayed consolidation and groundwater movements of geological history on the pre-consolidation pressure (Parry & Wroth, 1981)

The coefficient of lateral earth pressure at rest in the normally consolidated (NC) region, (K_0^{nc}), is calculated using Jaky's formula (*Equation 3.31*), as reported by Karstunen and Amavasi (2017). The coefficient of lateral earth pressure at rest for the overconsolidated (OC) state, (K_0), is determined using *Equation 3.32* (Swedish Institute for Standards, 2007).

$$K_0^{nc} = 1 - sin\Phi_c' \tag{3.31}$$

$$K_0 = (1 - sin\Phi_c')\sqrt{OCR} \tag{3.32}$$

R. Larsson et al. (2007) proposed another approach for calculating K_0 that is more appropriate for uniform clays and accounts for the water content.

4

Methods

This chapter presents the approach employed for developing a ground model for the construction site, evaluating soil properties for the numerical model, and validating the numerical model.

The soil profile and its input properties constitute the foundation of the modelling process and are essential for obtaining reliable results. Consequently, significant time and multiple steps are required to establish a detailed, accurate ground profile with reliable characteristics. The methodology employed to achieve maximum precision and reliability is described in the *Figure 4.1*. The investigation methods utilised in the various stages of the methodology and the derivation of soil properties are outlined in the *Figure 4.1*.

Many investigation methods produced similar parameters but with variations in the results. To ensure the highest possible accuracy, the tests were prioritised according to regulations from The challenge at the site was that only a limited number of borehole investigations and tests had been conducted. 32 boreholes were selected to create a representative 3D soil profile with as accurate soil properties as possible.

In order to obtain an accurate analysis with high quality, the samples were evaluated based on three different methods (Terzaghi et al., 1996), (Karlsrud & Hernandez-Martinez, 2013), and (R. Larsson et al., 2007). Sample quality assessment evaluates how disturbed the triaxial and oedometer tests were. This evaluation was conducted to determine which samples should be prioritized and which are of poor quality. The quality of the samples was assessed using ϵ_{v0}, σ'_p, σ'_{h0}, and w_N.

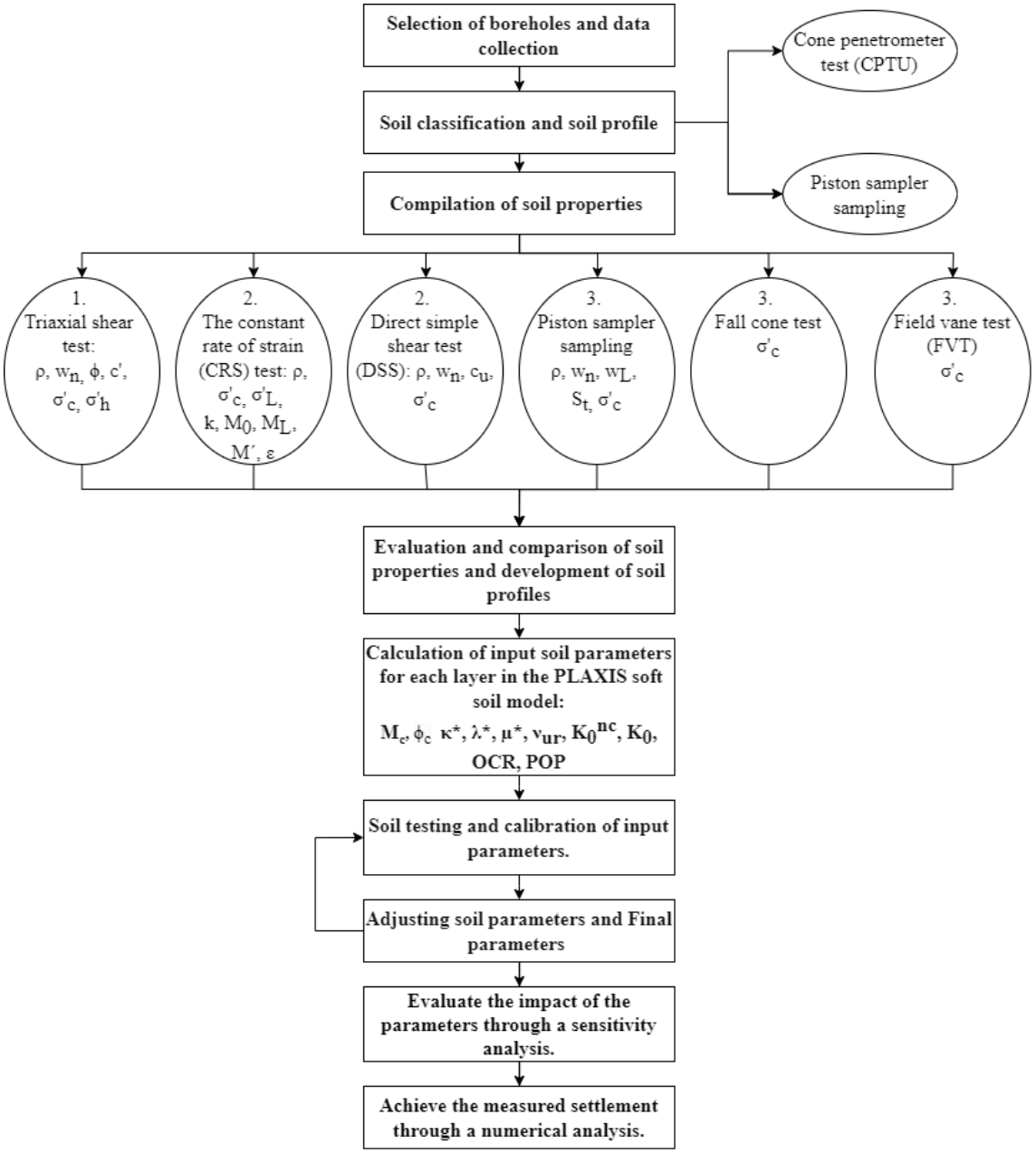

Figure 4.1: The Methodology employed for soil profile and soil properties.

4.1 Development of a soil profile

The development of a three-dimensional ground profile started with assessing the relevance of available field measurements on the site. A limited number of field tests conducted near the planned pipe were chosen and incorporated into the assessment.

In the approach, all Cone Penetration Testing with pore pressure measurements (CPTU) and piston sampling across the entire study area were selected to provide an overall understanding of the ground profile and the soil behaviour. During this phase, the homogeneity of soil behaviour across the area was evaluated, and any variations were examined.

The soil classification from CPTU was performed in line with the approaches involving normalized soil behaviour type (SBTn) charts proposed by Robertson (1990), Robertson (2016), and Schneider et al. (2008). The initial assessment was performed by assessing SBTn charts and comparing density, water content, and liquidity index from piston sampler sampling. CPTU test indicated various sudden significant increases in q_t and f_s, as well as decreases in u. The approach recognized the layering of silt in the clay. As a result, a second approach from (Schneider et al., 2008) was employed, where a more detailed profile was developed for the area where settlement issues were observed. This decision was based on the characterisation of this area as having larger volumes of silt than the rest, resulting in differences in density and water content compared to the overall area. The outcome was a general 3D soil profile across the entire area and a more specific 2D profile for the area experiencing settlement issues. The data from boreholes closer to the excavation were weighted higher.

4.2 Evaluation of soil properties

Piston sampling provided soil properties encompassing density (ρ), water content (w_n), liquid limit (w_L), sensitivities, and the preconsolidation pressure (σ'_c), which was calculated using Hansbo's empirical method for both fall cone tests and field vane (FVT) tests according to Equations 3.15.

The CRS tests provided the stiffness properties of the formations in the ground. The tests were evaluated according to Swedish Institute for Standards (1991a) and thereby provided the following properties: ρ, σ'_c, limit stress σ'_L, permeability k, and oedometer modulus (M_0, M_L, M'). The pre-consolidation pressure (σ'_c) and compression modulus were important for further analysis and development of input parameters in the subsequent numerical analysis.

Permeability k was assessed according to Swedish Institute for Standards (1991a) for the clay, where a trend-line that remained constant with depth was derived from the values obtained from CRS. A trend line was also drawn from the CRS values for the silt, but these values correspond more closely to those of the clay than those of the

silt. Therefore, that value was considered to represent the clay between the layers of silt and a new empirical value for the silt was derived from (R. Larsson, 1995). The permeability of the silt was then calculated by determining the percentage of silt compared to clay from the three closest boreholes and based on soil classification according to (Schneider et al., 2008). Finally, a weighted value for the silt was determined, taking into account the behaviour of the sieved silt. Permeability for the fill, sand, and rock was evaluated based on TK GEO 13 and (R. Larsson, 1995).

The parameters evaluated from the Triaxial shear test included ρ, w_n, ϕ', c_u, c', σ'_c, and σ'_h. The main parameters for further analysis and those whose final results were prioritised were ϕ', σ'_c, and c'. Parameters calculated from the Direct Simple Shear (DSS) test included ρ, w_n, c_u, and σ'_c.

The next step involved calculating the input parameters OCR, POP, M_c, κ^*, λ^*, μ, ν_{ur}, K_0^{nc}, and K_0 for Plaxis. To determine which POP and OCR to utilise, our values were evaluated and compared with our results, as shown in *Figure 3.9*. It suggests a constant POP and a decreasing OCR with depth due to changes in groundwater movements. Furthermore, only POP will be utilized in the PLAXIS analysis as its behaviour best corresponds to the soft clay in our area. Values for OCR and POP were determined for the silt and clay layers at the mid-depth of each layer, along with their corresponding σ'_c and σ'_c.

K_0 was calculated according to *Equation 3.32* from (Swedish Institute for Standards, 2007). Further methods were considered, but they did not meet the site-specific requirements demanded by the soil properties. The value for the friction angle was evaluated using the critical state line (M_c). The critical state line was used to achieve the best-fitted model.

Finally, the model-specific parameters for the soft soil model, κ^*, λ^*, μ, ν_{ur}, were evaluated. An important consideration when evaluating κ^* is that when assessing CRS oedometer tests within the overconsolidated zone, this often yields a value for κ^* that is too low compared to field conditions (Sällfors, 1975). It's crucial to consider that κ^*, λ^*, and $\mu*$ are based on mean values derived from σ'_v and σ'_c, rendering these parameters highly sensitive and reliant on accurate estimation of the mean value (Olsson, 2010). To mitigate this sensitivity, values are checked in soil tests and through sensitivity analysis.

The parameter κ^* is typically evaluated from the unloading/reloading path in a CRS test (Olsson, 2010). Nevertheless, no such test data were available for the construction site. This could result in an excessively large κ^*.

4.3 Calibration of soil parameters

The material properties in the numerical model were validated to verify the correspondence between the tests and the numerical interpretation by PLAXIS. The validation procedure involved using the soil test module in PLAXIS for the critical

layers, encompassing the clay and the silt layers. The numerical representation of the strength of the stiffness properties for a stratum was verified against one triaxial (CAUC) and one CRS test.

The strength parameters (ϕ' and c'_{ref}) were calibrated against a triaxial test assumed taken on a specimen from the clay formation on the site. The calibration was performed in the $p' - q$ plane to match the M_c line of the modelled soil layer with the peak of the stress path from the triaxial test. An acceptable match was achieved by increasing ϕ and the σ'_3 of the cell.

The κ^* was calibrated against the initial loading in the $\epsilon_1 - q$ plane of the triaxial test. Typically, the parameter is evaluated from the unloading/reloading path in a CRS test (Olsson, 2010). Nevertheless, no such tests were available for the construction site. As a result, this could potentially result in an excessively large κ^* in the model.

The λ in the model was calibrated against the M_L from CRS tests taken in the formation. The fit was made using a higher λ^* and shifting the curve to the right by slightly increasing the initial stress.

The μ^* in the representation of clay formation was verified against inSAR measurement from the site. The yearly creep rate is $0.49 mm/year$ and are presented in *Figure 4.2*.

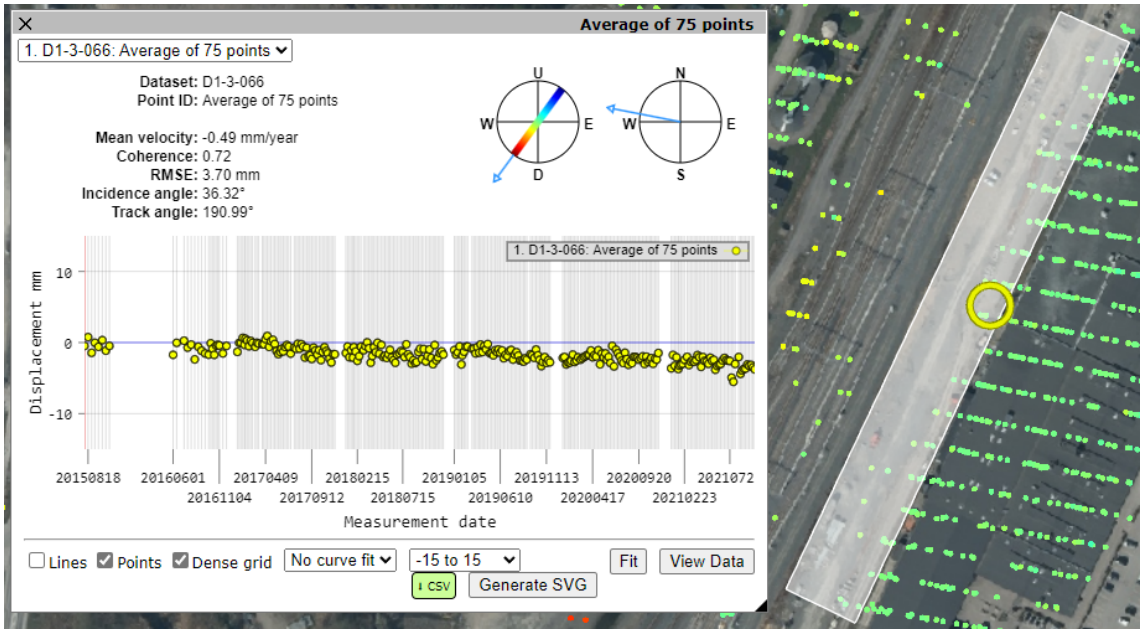

Figure 4.2: The inSAR measurement of the vertical displacement of the site for the excavation.

4.3.1 Numerical modelling of structural elements

The geotechnical structure encompass the sheet pile walls and the bracing. The walls was modelled as plate elements and material properties from *Table 4.1*. The bracing uses node-to-node anchors and properties from *Table 4.2*.

Table 4.1: Material properties used for numerical modelling of the embedded walls.

Parameters	Unit	Steal sheet pile wall, VL603, S355GP
Material type	-	Elastic
EA	(kN/m)	$2,43E6$
EI	(kNm^2/m)	31.20E3
d	(m)	0.3924
w	$(kN/m/m)$	1
v(nu)	-	0.3

Table 4.2: Bracing

Parameters	Unit	Bracing, HEB300, S355N/M/J2
Material type	-	Elastic
EA	(kN/m)	3,13E6
$L_{spacing}$	(kNm^2/m)	1

4.4 Method for assessing economic and environmental impacts

The economic and environmental impacts were evaluated for four different solutions: Sheet pile wall, trench box (kojapo), Slope, and Steered JT drilling. The method used to calculate the economic effects of the four different solutions was based on Implenia's own calculations for production costs. These calculations included all costs associated with each solution, such as the purchase of materials, machine costs, transport, and labor costs for the works.

The method used to evaluate the environmental impact was based on the standard SS-EN 15978:2011 (Swedish Institute for Standards, 2011). The environmental impact of the construction was assessed for the product stage and construction process

stage (A1-A5) as shown in *Figure 4.3*. The environmental impact was evaluated for three different solutions: Sheet pile wall, trench box (kojapo), and Slope.

For the sheet pile wall, raw material supply by a manufacturer in Holland included the transport within the production and manufacture of the sheet pile according to the manufacturer's own EPD. In the construction process stage (A4-A5) for the sheet pile, the transport from Holland to the project in Varberg was included, along with transport using excavators and trucks during the execution of the shaft and the backfilling, use of pumping, and finally the manufacture of the rock crusher used in the backfilling. This stage (A4-A5) was calculated according to two different cases defined by the Swedish Transport Administration: one for Earth excavation, case B road, and another for Earth excavation, case A road.

In Case B, soil masses are considered contaminated and must be transported to special facilities, with a transport distance of 83 km to a facility in Gothenburg. In Case A, soil masses are classified as clean but cannot be used for any other purpose in the project, resulting in transportation of the masses to a disposal site 3 km away. The installation impact from the driving of the sheet pile is not included due to missing information. The material used in the backfill was evaluated as crushed rock sourced from this project in Varberg. When calculating this, the emissions for all values, except those in parentheses, are based on the Swedish Transport Administration's climate calculation, which has been developed and adapted for Implenia's project using their own reference values.

For the trench box, two different cases were calculated. The first case used the same evaluated value as for the sheet piling in the product stage (A1-A3), and the second case excluded the influence from the product stage (A1-A3) to resemble a scenario where the trench box is rented out and therefore reused. In the construction process stage (A4-A5) for the trench box, transport from the company that rented out the trench box in Gothenburg to Varberg was calculated. In addition, the emissions for the trench box were included and calculated in the same way as for the sheet pile.

For slopes, no product stage (A1-A3) was included because the rock crusher material used is included in the construction process stage (A4-A5). The difference evaluated for the slope is a gradient of 1:1, which is considered slightly too low. The slope results in twice the volume of the shaft and the backfill. The impact in the construction process stage (A4-A5) was calculated in the same way but with the new larger volume.

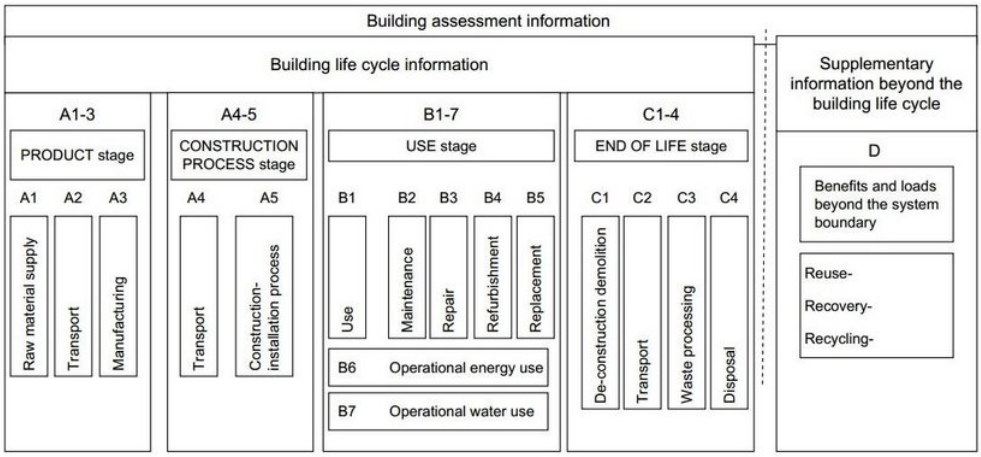

Figure 4.3: Buildings LCA stages according to EN 15978

5

Results form geotechnical site characterisation

5.1 The geotechnical site investigation

The geotechnical site investigation involved selecting high-quality soundings taken from the construction site and in an area extending 200 meters to develop a 3D ground profile. To obtain an accurate analysis, the quality of the samples was extensively evaluated using three different methods to ensure that our main probes were of high enough quality to give an accurate result. CPTU-tests were principally used to assess the stratification and pressure soundings to assess the level of firm ground/bedrock. The soil characterisation of the CPTU logs where performed according to Robertson (1990) and Schneider et al. (2008). For the three most relevant soundings (U05G16, U34G06 and U17G05) the results are presented in *Figure 5.1*. The CPTU logs losses of pore pressure on various occasions, which indicates a change in the soil macrostructure towards a more permeable deposit. This aligns with the results presented. Given the spread of soil types and the varying soil macrostructure, the approach proposed by Schneider et al. (2008) was implemented for soil characterisation. The result is presented in *Figure 5.2*.

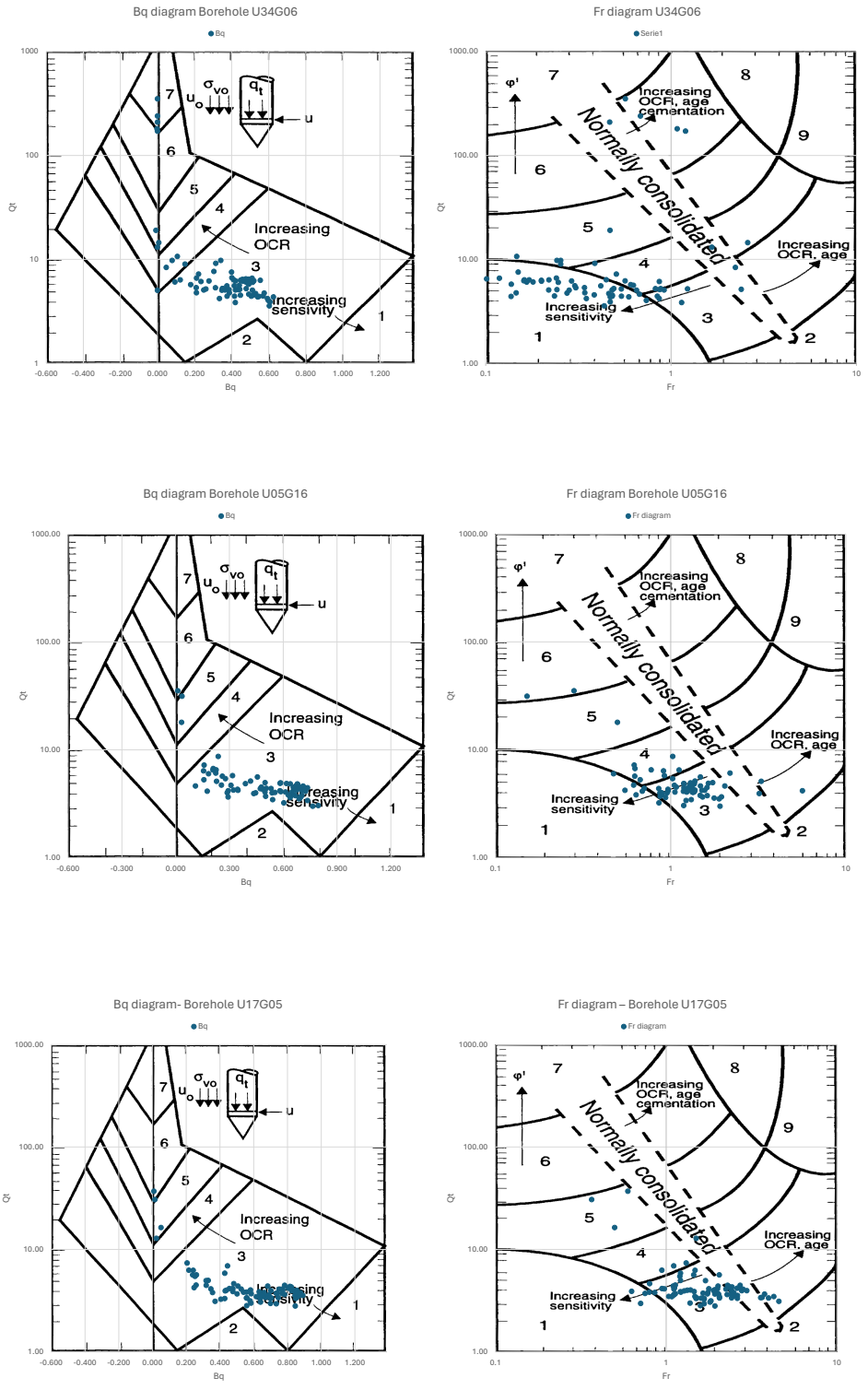

Figure 5.1: Results for borehole U34G06, U05G16 and U17G05 according to the (SBT_n) classification diagram based on Robertson's (1990) normalized parameters

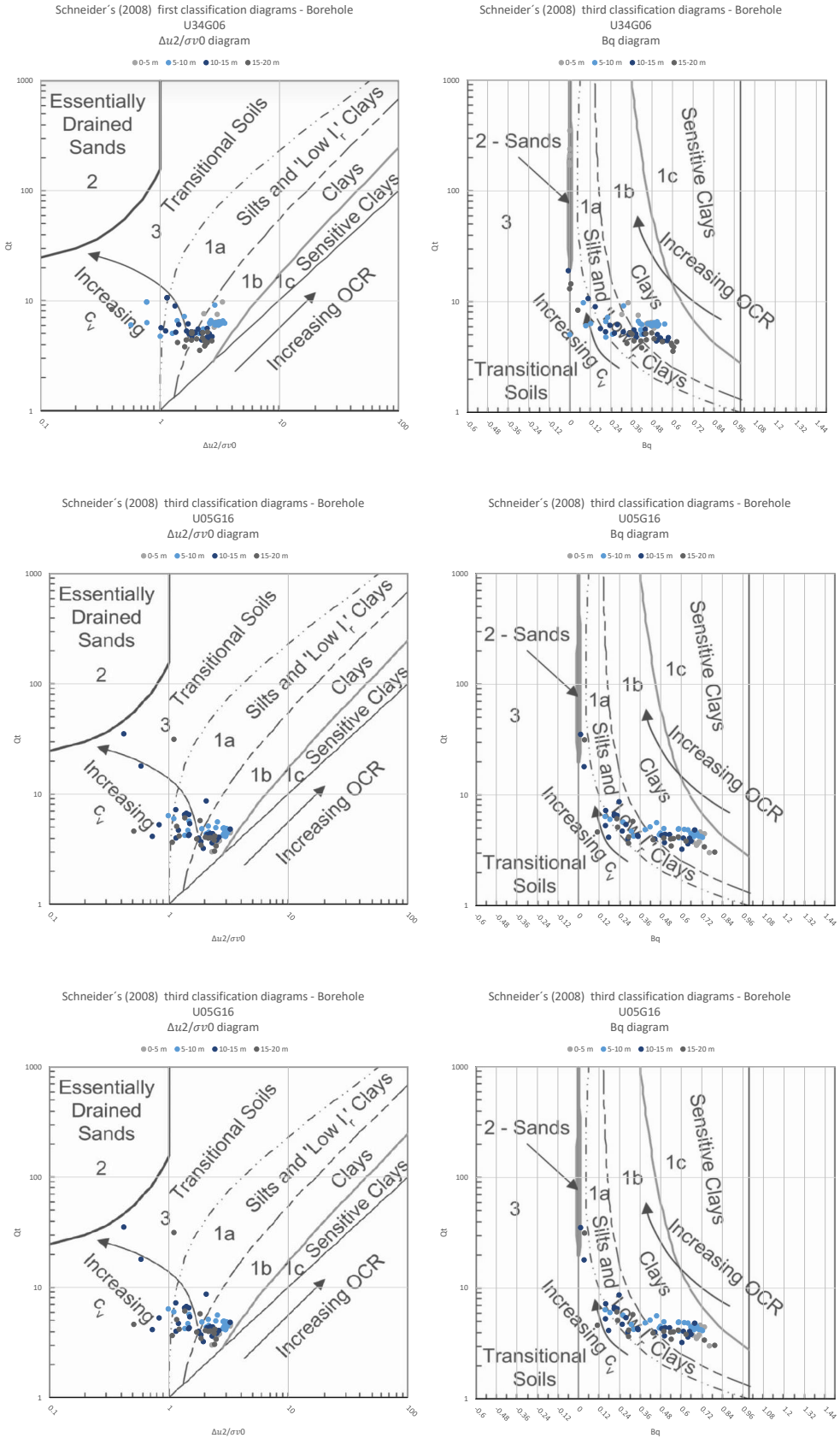

Figure 5.2: results of Soil classification diagrams in two different plotting formats from(Schneider et al., 2008)

5.2 Sample quality

After the soil profile had been determined, characteristic values for the soil layers were evaluated. To determine characteristic values for soil properties with high accuracy, the quality of the samples was examined using three different methods. The results for the quality of the samples are reported in *Figure 5.3* and *Table 5.1*. The results showed that the triaxial samples were of very high quality and will therefore have high importance in further analysis. However, these samples were unfortunately located far from the pipe. According to the SQD, none of the CRS samples were of good quality, in contrast to the methods by (Karlsrud & Hernandez-Martinez, 2013) and (R. Larsson et al., 2007), which indicated samples of higher quality. Based on the results of the quality assessment and the samples' locations, it was determined that samples U05G16, U34G06, and U17G05 were the most relevant and will be prioritized in further analysis.

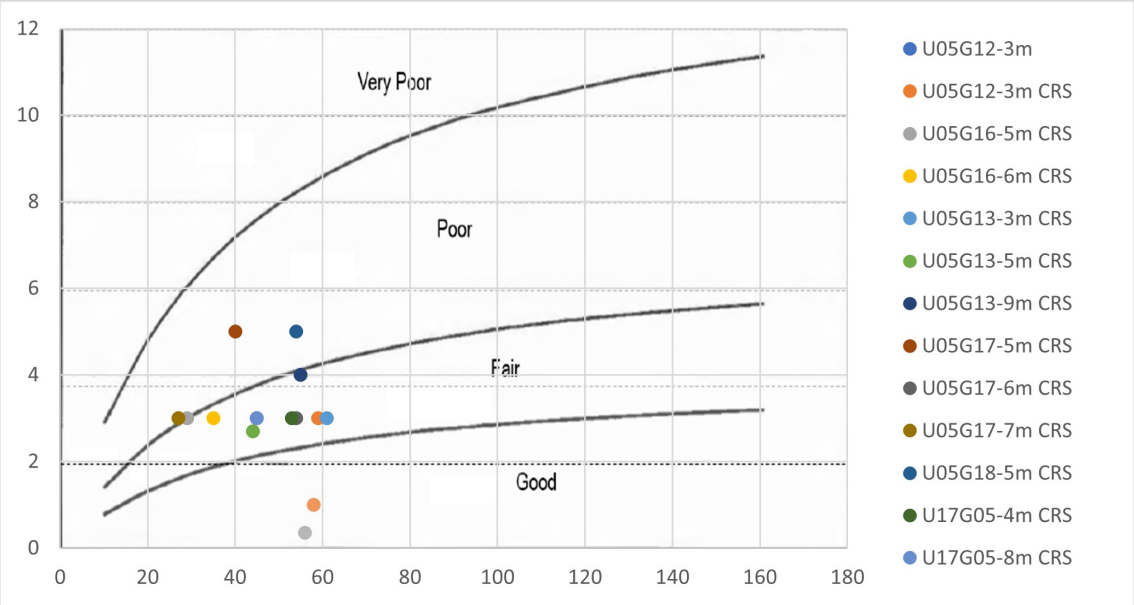

Figure 5.3: Result for sample quality with R. Larsson et al., 2007 method

Table 5.1: Sample quality

Sample	Type	ϵ_{v0} (%)	SQD	Sample quality	Ratio M_0/M_L	Sample quality
U05G12-3m	CRS	3	C	Poor	1.3	Poor
U05G12-4m	CRS	3	C	Poor	2.9	Very good
U05G16-5m	CRS	3	C	Poor	1.6	Good to fair
U05G16-6m	CRS	3	C	Poor	2.4	Very good
U05G13-3m	CRS	3	C	Poor	3.1	Very good
U05G13-5m	CRS	2.7	C	Poor	2.3	Very good
U05G13-9m	CRS	4	D	Very poor	2.1	Very good
U05G17-5m	CRS	5	D	Very poor	1.6	Good to fair
U05G17-6m	CRS	3	C	Poor	2.8	Very good
U05G17-7m	CRS	3	C	Poor	2.0	Good to fair
U05G18-5m	CRS	5	D	Very poor	1.4	Poor
U17G05-4m	CRS	3	C	Poor	1.2	Poor
U17G05-8m	CRS	3	C	Poor	2.3	Very good
U05G13-5m	Triaxial	1	B	Good to fair	-	-
U05G17-5m	Triaxial	0.35	A	Very good	-	-

5.3 Soil profile

The developed ground profile is principally based on the soil characterisation of U34G06 and is presented in *Figure 5.4*. The soil layer denoted "Silt" is in fact a stratum containing a significant amount of pronounced variations in the macrostructure. The global ground conditions of the site indicates that these variations are connected layers or larger lenses of coarser deposits in a finer-grained soil as the appear in multiple soundings logs. These layers have a thickness ranging from 0.2 m to several meters of soil type 1a, 2 and 3 according to Schneider et al. (2008). To capture the key feature being the higher permeability of this layer, it is modelled as a continuous silt layer. The layer denoted as "Friction material" has been indicated to be firm ground in pressure soundings and is thus thought of as a boundary condition with fixed deformation in the subsequent numerical analysis. The result for the produced 3D model with the final soil layer based on interpretations of all CPT according to the Schneider et al. (2008) method. The global ground profile was developed from the soundings compiled in *Table A.1* in *Appendix A*. The evaluated soil samples are shown in *Figure B.1*, *Figure B.2*, *Figure B.3*, *Figure B.4*, *Figure B.5*, *Figure B.6*, *Figure B.7*, *Figure B.8*, *Figure B.9*, *Figure B.10*, and *Figure B.11* in *Appendix B*.

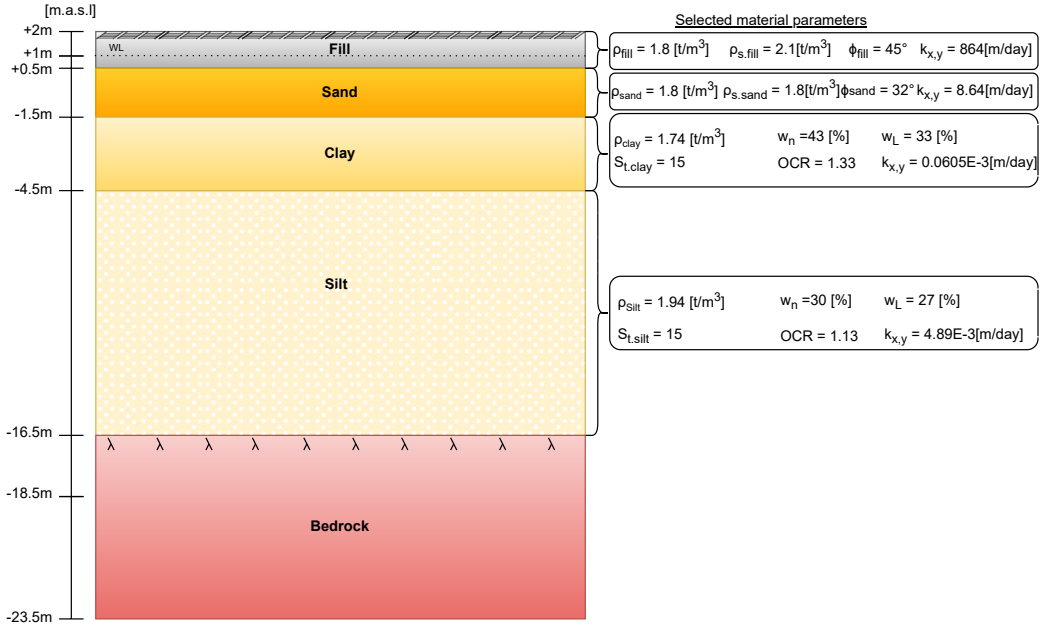

Figure 5.4: The picture shows the developed soil profile based on the method proposed by Schneider et al. (2008) and the evaluated soil properties is shown.

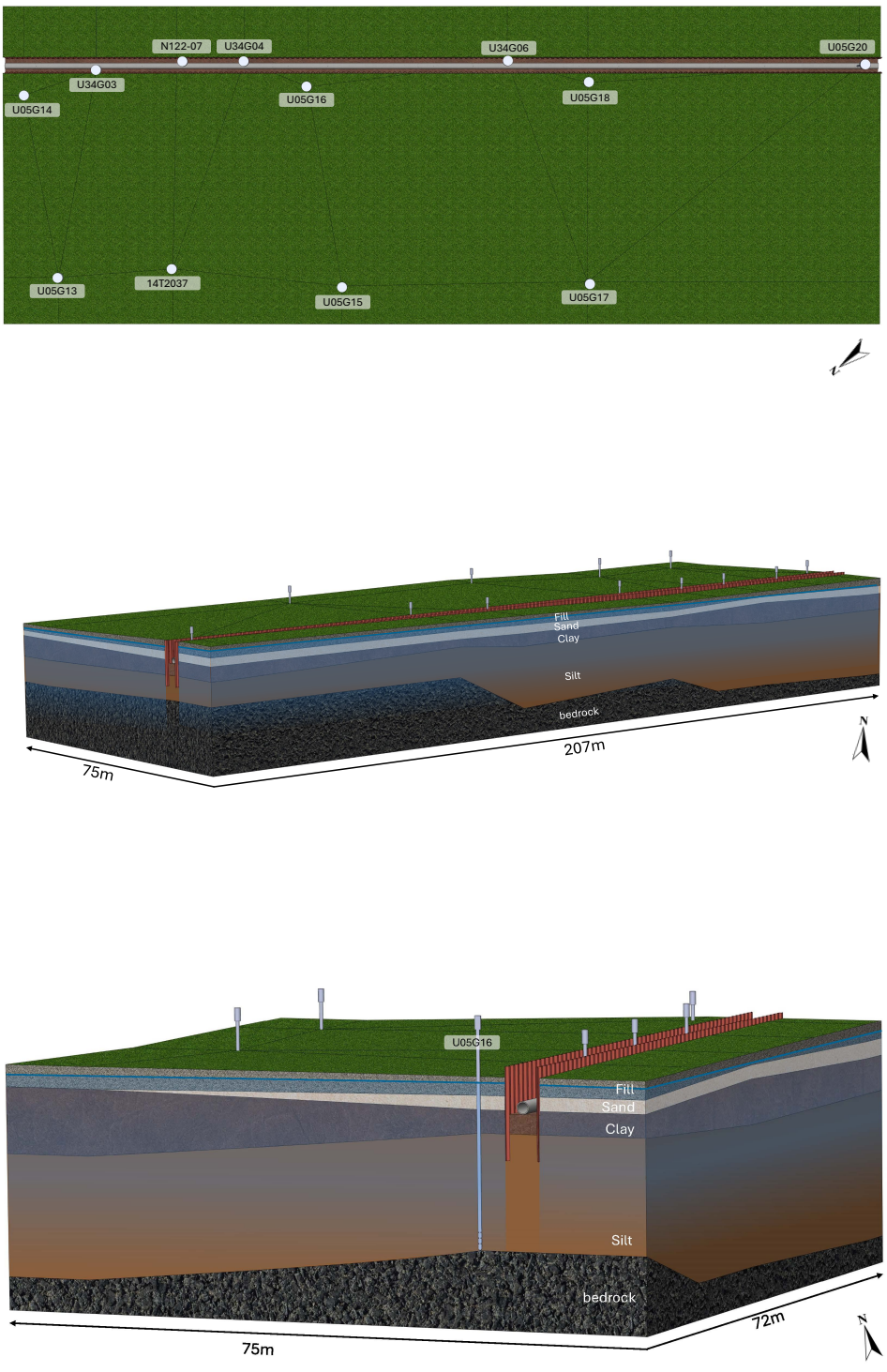

Figure 5.5: The illustrations show the developed soil profile in 3D from CPTu soundings, interpreted by empirical relations according to Schneider et al. (2008), and the geotechnical structure.

6

Results from the numerical analysis

A numerical model was developed to analyse the unloading and reloading effects at the excavation bottom. The aim of the numerical analysis was to compare the numerical output with the monitored pipe settlements to further understand the mechanisms acting on the site. This chapter presents the results of the numerical modelling and includes a compilation of evaluated and validated soil properties, sensitivity analysis, and a parametric study. Hereafter, the general movement of the excavation bottom is termed vertical displacement; the upward displacement is referred to as heave, and the downward movement as settlement.

The excavation was numerically modelled in PLAXIS 2D, version "22.02.00.452", using 15 noded elements. The soil geometry is presented in *Figure 6.1*. The mechanical boundary conditions used in the model are as follows: boundary XMin and XMax are normally fixed, YMin is fully fixed, and YMax is free. Groundwater flow was allowed in all directions except through boundary YMin.

The soil properties were evaluated using laboratory tests (CAUC and CRS) and field tests, empirical relations, and reference literature. The evaluated properties entered into the program's material models are compiled in *Table 6.1*.

The calculation steps for the staged construction in the numerical model was developed from the contractor's documentation and experiences. The adopted construction procedure is presented in *Table 6.2* and illustrated in *Figure 6.4*. The excavation was kept dry via a connected sump. This was modelled by adopting a custom hydraulic head inside the excavation. The ground water level inside the excavation was set to 0.2 m below the excavation level and the ground water level outside was governed by the static water level.

The evaluated properties in *Table 6.1* were validated by simulating stress paths (see Appendix C and Appendix D). This validation was done to ensure that the numerical interpretation of the entered material parameters corresponded to the stress paths recognised in CRS and CAUC tests of specimens taken from the site. Minor adjustments were made to achieve a better match and validate the evaluated

parameters.The validated soil properties are presented in *Table 6.3*. The deformed mesh from the numerical modelling with validated parameters are shown after the unloading in *Figure E.3* in *Appendix E* and after reloading and consolidation in *Figure E.4* in *Appendix E*.

A sensitivity analysis was performed to first assess the mesh quality and secondly to identify the material parameters controlling the unloading and reloading behaviour. The assessment of the mesh is shown in *Figure 6.2*. The influence on the vertical displacement is practically the same for the two finest mesh (fine and very fine) option with a coarseness factor of 0.5. The soil parameters were adjusted to values that are reasonable for the soil types and location. The analyses was benchmarked against the maximum settlements. The results from the sensitivity analysis of the soil model parameters are presented in *Figure 6.3*.

The parametric study was benchmarked against the monitored pipe settlements. The sensitivity analysis identified the key material parameters stearing the models response and these were adjusted to achieve the best match. The final parameters that resulted from the parametric study are shown in *Table 6.4*.

The unloading and reloading of the excavation resulted in significant vertical displacement of the excavation bottom during the construction time (*Figure 6.5*). A complete version of the graph showing the full consolidation time is available in *Figure E.1* in *Appendix E*. The vertical displacements are coupled with developments in the excess pore pressure beneath the excavation base as shown in *Figure 6.6* for the construction time. The excess pore pressure evolution for the hole consolidation time is shown in *Figure E.2* in *Appendix E*.

The monitored settlements of the pipe (*Figure 2.5*) are compared with the total settlements of the excavation bottom (and the pipe) from the numerical model in *Figure 6.7*. A similar settlement behaviour is observed in the monitored data and the numerical model.

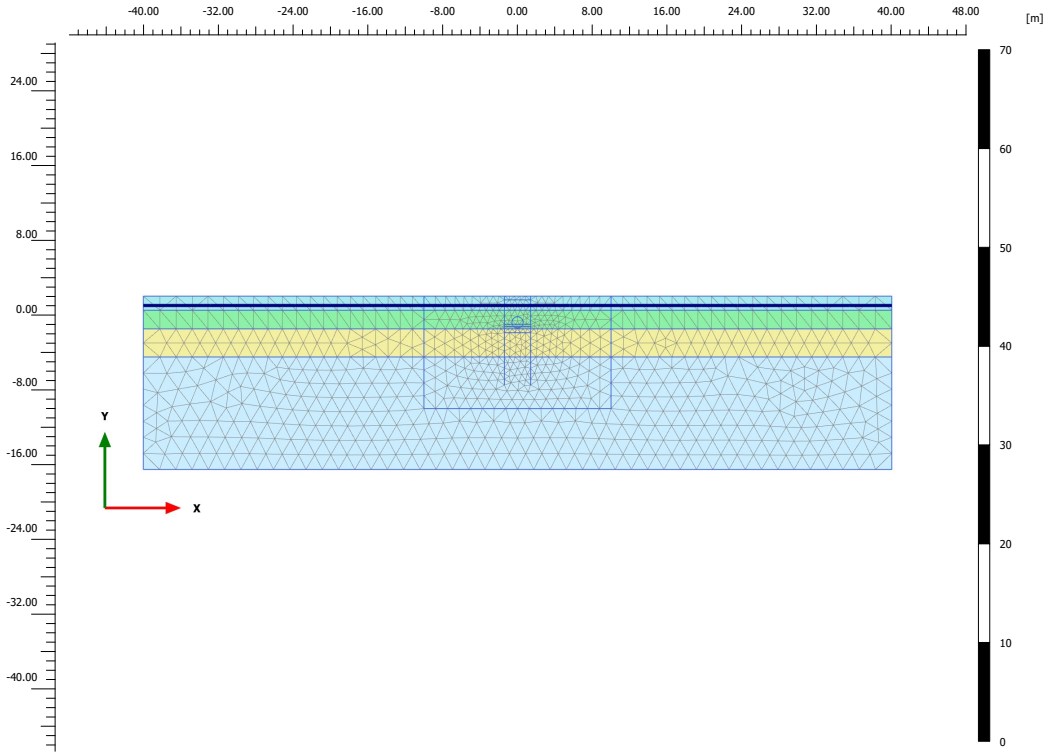

Figure 6.1: The soil geometry that was used in the numerical analysis.

Table 6.1: Input soil properties for validation with SOIL TEST in PLAXIS

	Fill	Sand	Clay	Silt	Backfill
depth (m)	0-1.5	1.5-3.5	3.5-6.5	6.5-18.5	-
γ_{unsat} (kN/m^3)	18	18	17.4	19.4	18
γ_{sat} (kN/m^3)	21	18	17.4	19.4	20
Model	MC	MC	SSC	SS	MC
Drainage type	Drained	Drained	Undrained (A)	Undrained (A)	Drained
E (kN/m^2)	20000	20000	-	-	50000
λ^*	-	-	0.1295	0.1394	-
κ^*	-	-	0.0168	0.0191	-
μ^*	-	-	0.0019	-	-
ν'	0.15	0.30	0.20	0.30	0.15
M_{c}	-	-	1.6	1.2	-
M_{e}	-	-	1[1]	0.9[1]	-
ϕ_{c} (°)	45	32	39[1]	30[1]	45
c'_{ref} (kN/m^2)	2	0	0	0	18
ψ	0	0	0	0	0
Soil class	Coarse	Coarse	Very fine	Fine	Coarse
k_{x} (m/day)	864	8.64	0.0605E-3	4.89E-3	864
k_{y} (m/day)	864	8.64	0.0605E-3	4.89E-3	864
K_0^{nc}	-	-	0.3684	0.5	-
$K_{0,\text{x}}$	0.2929	0.4701	0.4246	0.5317	0.2929
$K_{0,\text{z}}$	0.2929	0.4701	0.4246	0.5317	0.2929
OCR	-	-	1	1	-
POP	-	-	16	15	-
R_{inter}	0.67	0.67	0.5	0.67	0.67

[1] *The values for ϕ_c and M_e are derived from M_c, taken from CAUC tests.*

Table 6.2: Construction procedure of the excavation

Stage	Calculation type	Pore pressure calculation	Time (*days*)
Initial phase	K0 procedure	Phreatic	-
SPW installation (right)	Plastic	Phreatic	1
SPW installation (left)	Plastic	Phreatic	1
1st Excavation to +1.6m	Plastic	Phreatic	1
Bracing installation	Plastic	Phreatic	1
2nd Excavation to +0.5m	Plastic	Phreatic	1
3rd Excavation to -1m	Plastic	Phreatic	1
4th Excavation to -1.9m	Plastic	Phreatic	1
Consolidation	Consolidation	Phreatic	14
1st Refill to -1.5m	Plastic	Phreatic	1
Pipe installation and refill to -1.25m	Plastic	Phreatic	1
2nd Refill to -1.0m	Plastic	Phreatic	1
3rd Refill to +0.5m	Plastic	Phreatic	1
4th Refill to +1.6m	Plastic	Phreatic	1
Bracing Removal	Plastic	Phreatic	1
5th Refill to +1.6m	Plastic	Phreatic	1
SPW removal (left)	Plastic	Phreatic	1
SPW removal (right)	Plastic	Phreatic	1
Consolidation 2w	Consolidation	Phreatic	14
Consolidation 4w	Consolidation	Phreatic	28
Consolidation 3m	Consolidation	Phreatic	91

Table 6.3: Validated soil properties in the numerical model.

	Fill	Sand	Clay	Silt	Backfill
depth (m)	0-1.5	1.5-3.5	3.5-6.5	6.5-18.5	-
γ_{unsat} (kN/m^3)	18	18	17.4	19.4	18
γ_{sat} (kN/m^3)	21	18	17.4	19.4	20
Model	MC	MC	SSC	SS	MC
Drainage type	Drained	Drained	Undrained (A)	Undrained (A)	Drained
E (kN/m^2)	20000	20000	-	-	50000
λ^*	-	-	0.1100	0.1240	-
κ^*	-	-	0.02900	0.022	-
μ^*	-	-	0.00178	-	-
ν'	0.15	0.30	0.20	0.30	0.15
M_{c}	-	-	1.5[1]	1.2[1]	-
M_{e}	-	-	1[1]	0.9[1]	-
ϕ_{c} (°)	45	32	37.2	30	45
c'_{ref} (kN/m^2)	2[2]	0	0	0	18[2]
ψ	0	0	0	0	0
Soil class	Coarse	Coarse	Very fine	Fine	Coarse
k_{x} (m/day)	864	8.64	0.0605E-3	4.89E-3	864
k_{y} (m/day)	864	8.64	0.0605E-3	4.89E-3	864
K_0^{nc}	-	-	0.3954	0.5000	-
$K_{0,\text{x}}$	0.2929	0.4701	0.4557	0.5317	0.2929
$K_{0,\text{z}}$	0.2929	0.4701	0.4557	0.5317	0.2929
OCR	-	-	1	1	-
POP	-	-	16	15	-
R_{inter}	0.67	0.67	0.5	0.67	0.67

[1] *The values for M_c and M_e are calculated from ϕ_c.*
[2] *The value for c'_{ref} was applied along with an allowed tension. This was performed to prevent the model from collapsing due to the development of tensile stresses near the surface of heaving soils.*

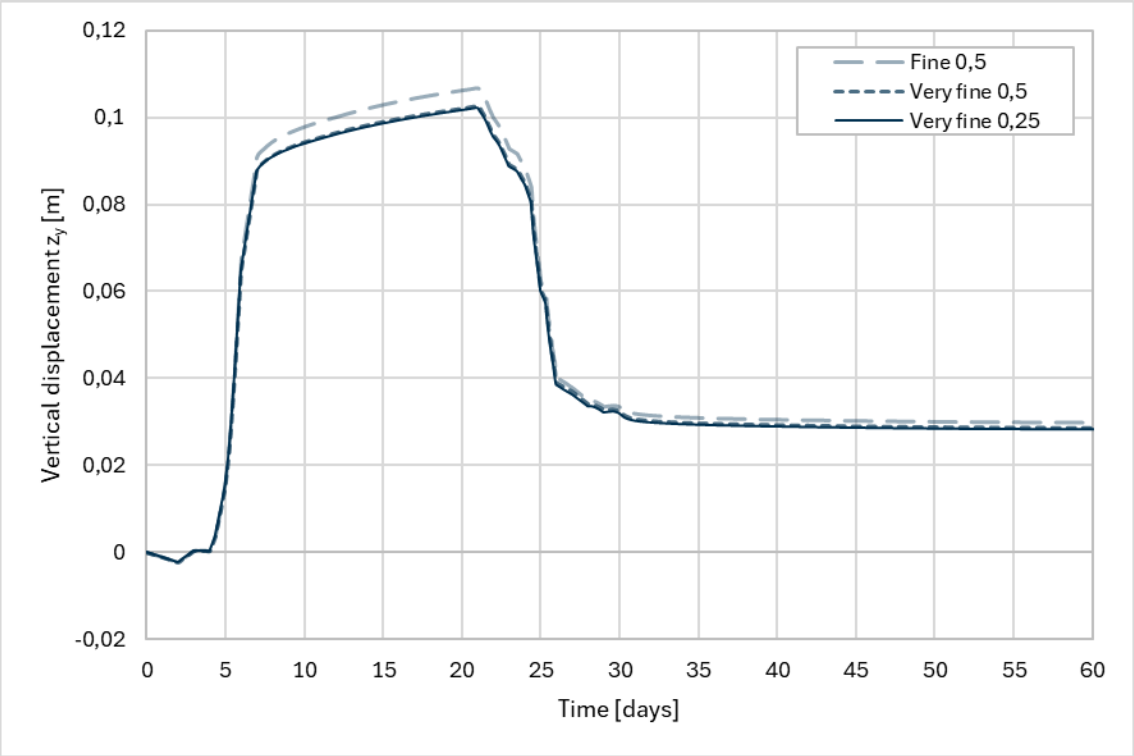

Figure 6.2: The figure shows the influence of the mesh quality on the vertical displacement in of the excavation bed. The factor written together with the name represents the coarseness factor for the respective element distribution.

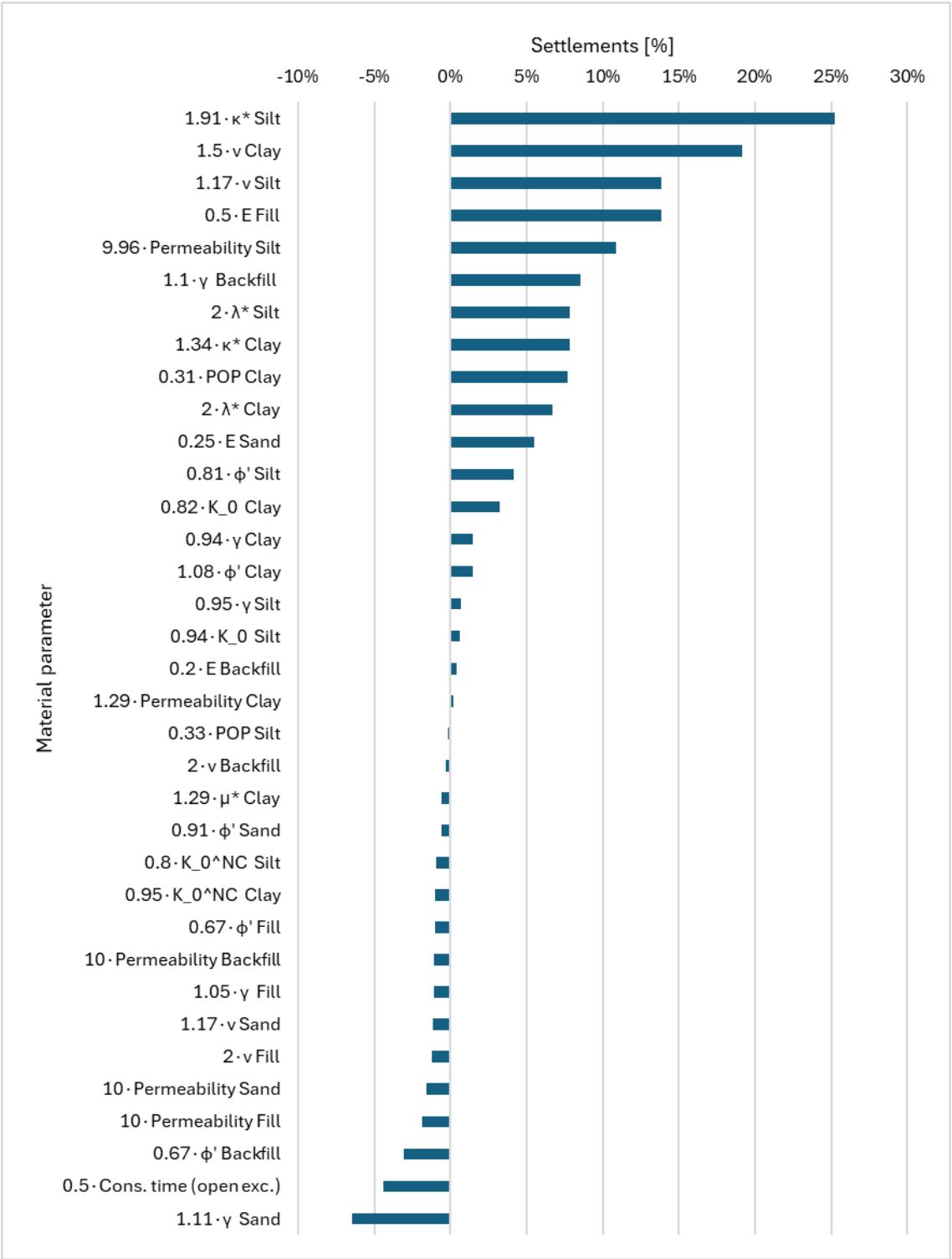

Figure 6.3: The results from the sensitivity analysis of the main material parameters are compiled in the figure. The material parameters were varied by the factors indicated. The settlement values represent the settlement occurring from the onset of reloading until the end of consolidation.

Table 6.4: The adopted soil properties from the parametric study.

	Fill	Sand	Clay	Silt	Backfill
depth (m)	0-1.5	1.5-3.5	3.5-6.5	6.5-18.5	-
γ_{unsat} (kN/m^3)	18	17.5	16.4	18.4	18
γ_{sat} (kN/m^3)	20	17.5	16.4	18.4	21
Model	MC	MC	SS	SSC	MC
Drainage type	Drained	Drained	Undrained (A)	Undrained (A)	Drained
E (kN/m^2)	10000	10000	-	-	5000
λ^*	-	-	0.1500	0.1640	-
κ^*	-	-	0.03500	0.028	-
μ^*	-	-	0.00178	-	-
ν'	0.15	0.20	0.20	0.30	0.15
M_{c}	-	-	1.5	1.3	-
M_{e}	-	-	1	0.9	-
ϕ_{c} (°)	45	32	40	37	45
c'_{ref} (kN/m^2)	2	0	0	0	18
ψ	0	0	0	0	0
Soil class	Coarse	Coarse	Very fine	Fine	Coarse
k_{x} (m/day)	864	8.64	0.0778E-3	0.0487	864
k_{y} (m/day)	864	8.64	0.0778E-3	0.0487	864
K_0^{nc}	-	-	0.3572	0.3982	-
$K_{0,\text{x}}$	0.2929	0.4701	0.3751	0.4235	0.2929
$K_{0,\text{z}}$	0.2929	0.4701	0.3751	0.4235	0.2929
OCR	-	-	1	1	-
POP	-	-	5	15	-
R_{inter}	0.67	0.67	0.5	0.67	0.67

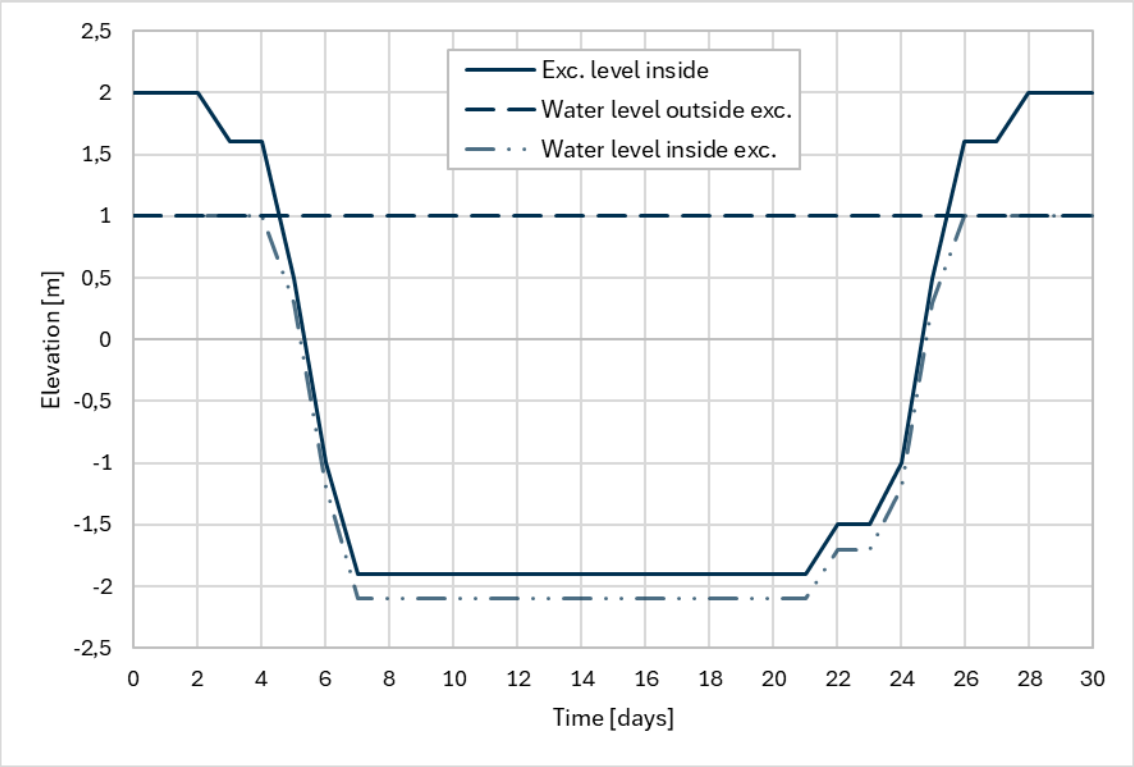

Figure 6.4: Presentation of the staged construction steps along with the prevalent water levels throughout the analysis. The water level outside the excavation is kept constant while the level inside is lowered 0.2 m below the excavation level.

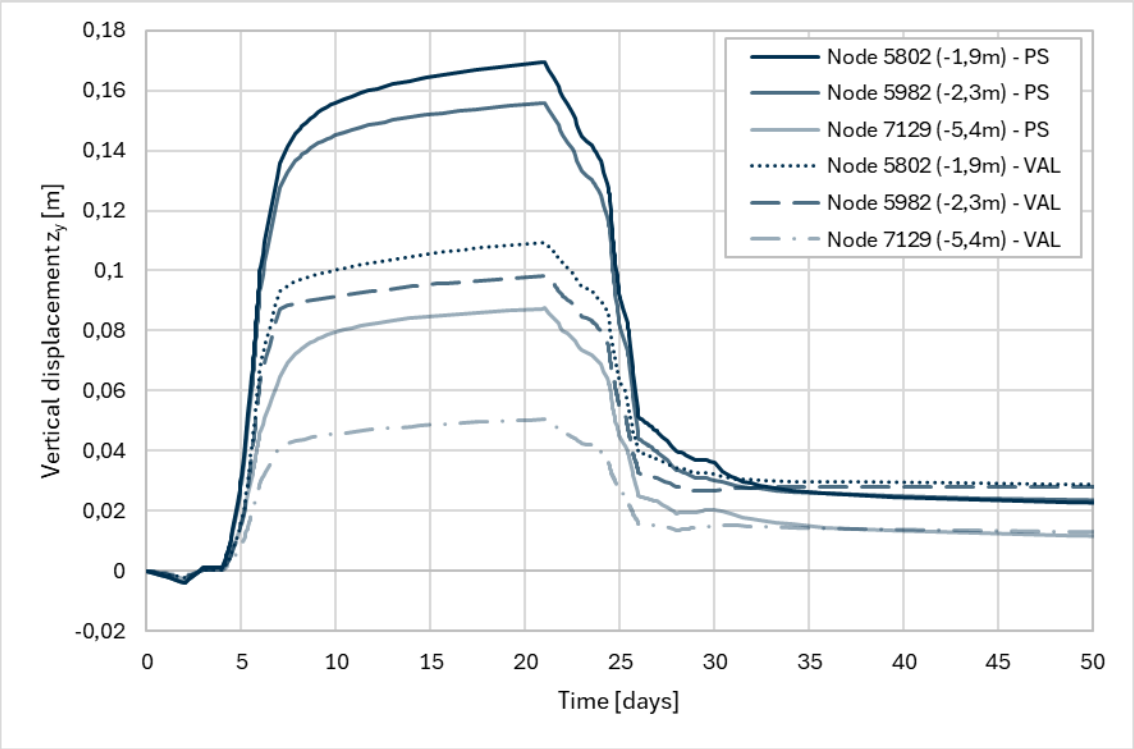

Figure 6.5: The vertical displacements that occurred during the construction works are presented here for the validated (VAL) model and the calibrated (CAL) model from the parametric study. The displacement measured from a node at -1.9 meters is used as the benchmark for comparison against pipe settlements.

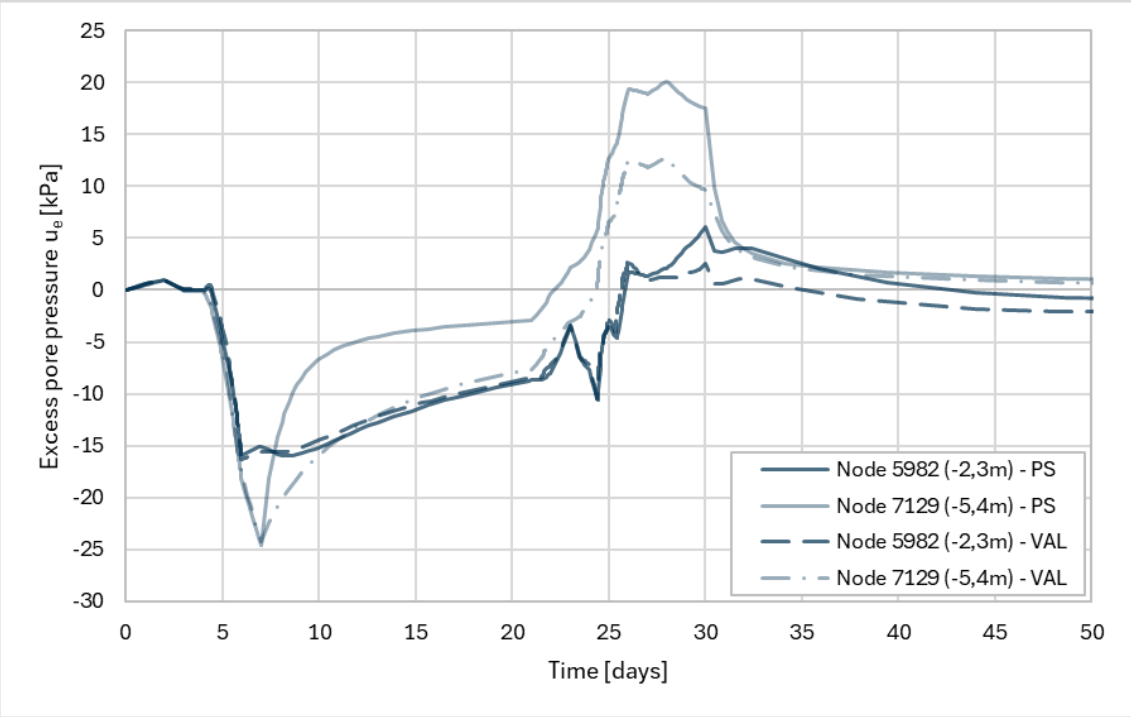

Figure 6.6: The excess pore pressure development that arose during the staged construction are shown at multiple depth (nodes).

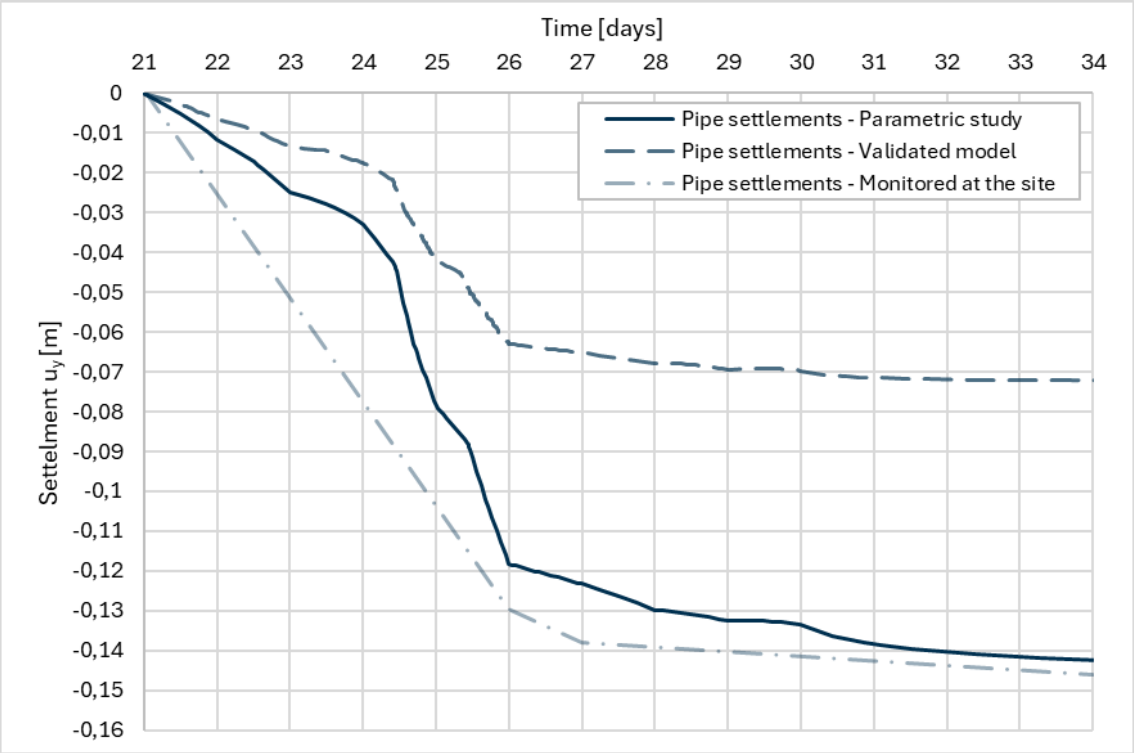

Figure 6.7: The pipe settlements in the case study are compared with the excavation bottom (and pipe) settlement measured from node 5802 at -1.9 m in the numerical model. Settlements are recorded from the onset of reloading and end on day 34, when site monitoring stops.

7

Results for economical and environmental impact

Below, the calculated carbon dioxide equivalents for various excavation construction methods are presented in *Table 7.1*, including Sheet pile wall, trench box (kojapo), Slope, and Steered JT drilling. Each result includes emissions from Excavator, truck, pumping, manufacturing, transport, and rock crusher. The emissions for all values, except those in parentheses, are calculated based on the Swedish Transport Administration climate calculation, which has been developed and adapted for Implenia's project using correct values. The values in parentheses for trench box (kojapo) represent calculations from kojapo's own sheet pile calculator, supplemented by the Swedish Transport Administration climate calculation. Manufacturing emissions are excluded for the kojapo solution, as it is rented out and not consumed in the same manner as a sheet pile.

The results are presented in two parts according to the Swedish Transport Administration: one for Earth excavation, case B road, and another for Earth excavation, case A road. In Case B, soil masses are considered contaminated and must be transported to special facilities, with a transport distance of 83 km to a facility in Gothenburg. In Case A, soil masses are classified as clean but cannot be used for any other purpose in the project, resulting in transportation of the masses to a disposal site 3 km away.

These results are based on theoretical values and should be viewed as a guide for comparing different solutions. The findings in *Table 7.1* indicate that the slope method has the lowest carbon dioxide emissions, with transportation representing a significant portion of the overall cost. Additionally, Case A, with less transport, yielded better results. The result with high emissions was sheet pile wall.

Finally, theoretical production costs are also presented in *Table 7.2* as part of the economic impact assessment. The results are derived from the same cases as before (case B and case A) and for the same methods. These values are based on production costs according to Implenia's tender calculation, providing theoretical costs to facilitate comparison of different solutions. It's important to note that these values do not reflect the actual costs incurred in reality, and thus, the calculations and

input parameters will not be detailed in the report.

According to the results in *Table 7.2*, case A was the most cost-effective for all methods, with the slope method being the least expensive option. However, due to limited space and the depth of the shaft, the slope method may not be feasible. The trench box (kojapo) also showed significantly lower costs compared to other proposals. Conversely, the sheet pile wall was the most expensive proposal.

Table 7.1: Results for environmental impact presented in tonnes of carbon dioxide equivalent (ton CO_2eq)

Type	Sheet pile wall (ton CO_2eq)	Trench box (Kojapo type) (ton CO_2eq)	Slope (ton CO_2eq)	Steered JT drilling (ton CO_2eq)
Earth excavation, case B road [1]	595	540 (172)	342	
Earth excavation, case A[1]	487	432 (64)	128	

[1] According to the Swedish Transport Administration

Table 7.2: Results for economical impact presented in million

Type	Sheet pile wall (million)	trench box (Kojapo type) (million)	Slope (million)	Steered JT drilling (million)
Earth excavation, case B road [1]	65	20	30	52
Earth excavation, case A[1]	58	15	10	49

[1] According to the Swedish Transport Administration

8

Discussion

8.1 Ground profile

An accurate soil profile was one of the most important aspects of producing a proper numerical model that simulates the measured settlement on the site. Soil classification is a central part of the Site Investigation in geotechnical projects and can involve the determination of physical properties and behavioural characteristics (Robertson, 2016). By combining physical and behavioural characteristics, a more comprehensive picture of the site conditions can be obtained. The importance of understanding soil stratigraphy and its influence on permeability when designing deep excavations is illustrated by the Underground car park at the House of Commons project (Brown et al., 2023a). In the latter project fine sand and silt deposits were discovered within the London Clay and showed high horizontal permeability, which meant a risk of hydraulic uplift. The risks from this hazard was mitigated by using 30-meter-deep diaphragm walls that extended into the underlying homogeneous clay. Hence, it is crucial to carry out detailed investigations to map the permeability and inhomogeneities of the soil deposit. Both field and laboratory methods should be used to obtain a reliable estimate of soil properties and to identify potential hazards, and plan effective measures.

The first presented ground model of Implenia was produced with the help of the computer program Conrad. This method showed significantly lower amounts of silt in the silt and clay layer than the final profile arrived at in this project. Given the site's geological history with layered deposits of silt and clay and the presence of fine-grained soil with coarse parting as silt, it is crucial to analyze the soil profile with a method that considers the behaviour of silt with a higher accuracy. This was achieved by the evaluation method for CPT proposed by (Schneider et al., 2008), which indeed indicated a silty clay and silt layer. The presence of silt layers within the clay thus became a key factor for the analysis, especially in terms of permeability, which is crucial for understanding how water moves through the soil and how the pressure distribution changes during and after excavation, as explained in the theory by (Brown et al., 2023a).

The developed ground model, highlights a large layer consisting of both silt and clay. In the model however this layer had to be treated as a common layer with

characteristic properties of both materials. The challenge arose when the thickness of the silt layer varied from 0.2 m to several meters, which created problems in the Finite Element analysis performed with Plaxis. The mesh quality created convergence issues precluding an accurate analysis. In addition, it was difficult to obtain reliable model parameters from the Site Investigation carried out in the area. Many of the CRS samples were taken at depths corresponding to the level of the silt layer, but as CRS mainly works for cohesive soils, i.e. clay, these values were considered to represent the clay between the silt layers. As a result, samples for the actual silt properties between the clays were missing except for the evaluation of the CPT data.

In order to capture the characteristic behaviour of the silt, empirical values of the permeability were used. In order to treat the two materials together, the characteristic properties of the soil material were combined in a weighted average based on the percentage of clay and silt. This was done primarily for permeability because an accurate estimate of this parameter is critical as it controls the rate and extent of consolidation, which in turn affects the response in time for the settlements. In the final result of the parametric analysis, the density was also averaged, which is an important factor in obtaining a correct assessment of the settlements.

Another important observation was that the horizontal permeability was found to be significantly higher than the vertical, which affects the groundwater flow and thereby the stability of the soil during excavation. This anisotropy can lead to uneven settlement and potentially damage inducing ground deformations.

Another important aspect investigated was whether the model would depend on OCR or POP. Since the evaluated OCR values decreased with depth, it was decided to use POP in PLAXIS analyses according to Karstunen and Amavasi, 2017. The soil test results showed that a reduction in POP for clay produced a greater settlement and a result that corresponded more closely to the actual settlement. This parameter did not influence the silt, which retained its original POP value, while the clay POP was lowered in the parametric study.

8.2 Unloading effect

Excavating the soil within the excavation reduces the overburden pressure at the excavation bottom and results in heave from unloading in the numerical model (*Figure 6.4* and *Figure 6.5*). The heave is mainly attributed to the phase where the excavation progresses and the following consolidation phase. The excavation phase is modelled with a plastic (undrained) calculation type due to the presumed fast workmanship and excavation. The unloading effect in the phase leads to negative excess pore pressures developing and immediate heaving (*Figure 6.6*). The immediate heave depends mainly on the soil stiffness and is elastic (Gaba et al., 2017). Moreover, the sensitivity analysis revealed that the stiffness parameters $\kappa*$, ν_{ur}, and $\lambda*$ for silt and clay control the numerical output and the final settlement. Higher values (hence lower stiffness) resulted in more heave and subsequent settlements.

Altogether this suggests that the immediate vertical displacement depends on the stiffness. Nevertheless, no soil tests with unloading-reloading loops from which the κ can be evaluated are available. The negative excess pore pressures arising during the unloading indicates that there is a delayed heaving process. Consequently, the model exhibits both short and long-term heaving. The second phase is governed by consolidation (flow of groundwater towards the zone with negative porewater pressures). The contractor excavated long trench sections to increase the efficiency. The numerical model accounts for this construction approach by having a consolidation phase of 14 days when the final excavation level is reached. In the consolidation stage, the negative excess pore pressures dissipate, leading to the generation of heave. The shape of the heave curve coupled with the dissipation of negative excess pore pressure, indicates that mechanical swelling is ongoing.

The immediate and time-dependent unloading responses contribute to a significant heave in the numerical model. The major contribution to the accumulated heave arises from the excavation process. The numerical unloading effect cannot be compared to the project site, as the excavation bottom level was not monitored during excavation works. Given that the numerical output shows significant heave at excavation bottom, the question is if the same behaviour happened at the site. The unloading response is showed to be governed by the soil stiffness.

8.3 Reloading effect

Backfilling of the excavation increases the overburden pressure on the excavation bottom, resulting in significant settlements and positive excess pore pressure development as shown in *Figure 6.4*, *Figure 6.5*, and *Figure 6.6*. This construction sequence in the numerical model involves backfilling, removing the embedded retaining walls and supports, and letting the site consolidate. The global trend of the settlement curve shows an immediate and a consolidation settlement driven by the dissipation of positive excess pore pressures.

The approach of backfilling the numerical model was accompanied by numerical challenges related to the mobilisation of tensile strength in the backfilling material and to the pipe installation procedure (*Figure E.5* in Appendix E). The final solution encompassed accepting small tensions and inserting elevated values of c'_{ref} in the backfilling material. This approach is only meant to prevent the backfilling soil body from collapsing in the numerical calculation. The vertical displacement throughout the excavation is measured in the layers beneath the backfilling material to minimise the influence of the workaround in the overlying layer. Moreover, an excavation bed was placed on top of the excavation bottom in the construction project before laying the pipe. The numerical calculation required lateral soil support on the sides of the pipe and keeping newly activated soil elements dry to converge. This can be the reason for the fluctuations in the excess pore pressure in the model during the backfilling.

The backfilling was performed to restore the overburden pressure at the excavation

bottom and bring the effective stress back to approximately the same level as before the excavation. The backfilling material used in the model is based on an interpretation of the material specified in the construction documents. However, since there are no measurements of the actual backfilling material, the model relies on literature values for similar materials. This introduces uncertainty in comparing the numerical output to the monitored pipe settlements at the site.

The major settlement in the numerical model arise immediately from the increase in overburden pressure and minor additional settlements results from consolidation of the model. The unloading effect has been shown to be stiffness-dependent. Subsequent reloading of the excavation increases the overburden pressure at the excavation bottom. Immediate settlements of the bottom can occur when the overburden pressure is below the pre-consolidation pressure and thus in the overconsolidated regime where strains are generally elastic. When the overburden pressure exceeds the pre-consolidation pressure, the soil enters a normally consolidated state, and plastic deformations typically develop. Backfilling was performed to restore the effective stress state. Hence, the settlements at the excavation bottom (and the pipe settlements) during backfilling are likely due to an elastic rebound effect. Minor contributions to settlements arise from consolidation, which can occur because the reloading rate is faster than the pore water flow rate in the soil.

8.4 Wall removal effects

The removal of the embedded walls creates a cavity. The loss of lateral support for the backfill and the retained ground only results in minimal deviations in the global settlement trendline. Franzén et al. (2000) attributed significant settlements to removing sheet piles in a field test of pipe laying in excavated trenches in soft clay. Longer sheet piles resulted in larger pipe settlements. This behaviour is not evident in the settlement curve in the numerical output. Consequently, the removal effects of the embedded retaining wall is potentially underestimated in the numerical output. The removal effect at construction site for the pipe was probably larger than the numerical model suggests.

8.5 Additional factors contributing to vertical displacements of the excavation bottom

The evolution of the vertical displacement at the excavation bottom after unloading has been assessed, showing dependency on soil stiffness and delayed effects driven by consolidation in the long term. This section will assess additional factors that can influence the overall numerical analysis and contribute to differences between the numerical model and the construction site. The geotechnical hazard of hydraulic uplift due to the permeable stratum underneath the less permeable excavation bottom has been assessed in the model. Given the ground profile developed in this project, the geotechnical structure no longer fulfils *Equation 3.9*. The influence of

the former factor is recognised, and the contribution to the total heave is uncertain. Given that the heave develops immediately in the model and thus long before the excavation reaches a critical level for the hydraulic uplift. This contribution is not considered as major but can influence the result.

The excavation is in clay, which typically exhibits very low permeability. Below the excavation lies layered silty soil with alternating layers of low and high permeability. The excavation extends below the static groundwater level and is kept dry. Embedded retaining walls, penetrating underlying water-bearing strata, can induce water flows at the wall-soil interface and result in vertical displacements of the excavation base (Gaba et al., 2017).

The sheet pile walls were driven and removed by means of vibration. Additionally, a plate compactor was used to compact the excavation bed. Installation and removal of sheet piles walls was recognised as a source for ground movements by Fredriksson et al. (2018). Vibration is a form of dynamic loading and cyclic shearing (Knappett & Craig, 2019). This action can raise excess pore pressures, and at a critical point the effective stress becomes zero, resulting in induced soil liquefaction. Franzén et al. (2000) saw that pipes laid in an excavated trench on a bottom where workers walked more developed larger settlements and attributed it to clay disturbance. All these factors can contribute to soil disturbance and thus differences between the numerical model and the construction site. Their influence is recognised in this project. Nevertheless, the mechanisms are not clear and are too challenging to model accurately in the scope of this project.

Furthermore, the monitored pipe was not in service during the level monitoring. Hence, the pipe can settle more when taken in service. Water flowing through the system increasing the overburden pressure on the soil beneath the excavation, resulting in positive excess pore pressures. Dissipation of the water pressure results in further consolidation settlements.

8.6 Soil test and sensitivity

In order to achieve a correct model linked to the site-specific conditions, it is important to conduct soil tests to compare the calculated values with the measured values from lab tests on samples retrieved from the ground. Soil tests evaluated the stiffness parameters (κ, λ and ν_{ur}) and the strength parameters (ϕ', K_0^{nc}, and K_0) for clay and silt against the given saturated values from the field for triaxial and CRS tests. A good way to compare the evaluated values from the soil test against the measured values from CRS is to plot the oedometer modulus against the vertical effective stress. The measured oedometer modulus from CRS can then be compared against the newly calculated oedometer modulus using the R. Larsson, 2008 relationship for the extracted values from the soil test. The results of the oedometer modulus and the adjustment of the CRS curve are presented in *Appendix C* and *Appendix D* in *Figure C.4* and *Figure D.4* below, where the curve has been primarily adapted to M_L and not M_0. This is because there were difficulties in evaluating the

first part of the CRS curve that is connected to M_0 to only κ^* since this parameter is usually evaluated for unloading and reloading. However, it is possible to connect κ^* to the slope of the first part of the CRS curve.

Another difficulty was that the M_0 value had to be multiplied by 3 to reflect the actual field response, which cannot be done in PLAXIS for soil tests. Hence, the measured oedometer modulus from CRS (without adjustment for real field conditions) and the values from the soil test are significantly lower than the initial values, as only these values have accounted for the real field conditions. *Figure C.4* and *Figure D.4* in *Appendix C* and *Appendix D* indicates that the calculated M_0 value is lower than that in the field condition, suggesting that a lower value for κ^* should better match the higher actual M_0value. Therefore, κ^* was further investigated in a sensitivity analysis and a parametric study, concluding that a higher κ^* should be used to match the real settlement curve. However, literature from (Olsson, 2010) points out that a lower value of κ^* should be chosen to represent a more realistic M_0 value for the SSC model, and that this value should not perfectly match the CRS curve.

Considering this, all other parameters were evaluated in a sensitivity analysis to investigate whether it was possible to adjust the other parameters and still achieve the true settlement curve. The result was that κ^* had to be increased, but as little as possible, to match the true settlement curve. The parameters mainly adjusted to achieve the true settlement curve were the strength parameters (ϕ', K_0^{nc}, and K_0) as well as the input parameters ρ and permeability. A final result for the soil test, incorporating the values from the parametric study, showed that the new values for κ^* differed the most from the actual field value for for M_0 both silt and clay.

The primary adjustment of the CRS curve was instead made to M_L, which is associated with the slope of the last part of the CRS curve and is related to the value of λ^*. This adjustment was made using a higher λ^* and shifting the curve to the right by slightly increasing the initial stress. The reason λ^* is related to $M_L$is that the value of the preconsolidation stress is close to the value of the final vertical effective stress. This confirms the result because the final effective stress is not significantly higher than the preconsolidation stress. A final result for the soil test with the values from the parametric study was produced to compare the result against the correct measured values. The result of the parametric study in *Appendix C* showed that the new value for λ^* for clay deviated from the measured value from CRS for M_L, as shown in *Figure C.3*, and the result for silt in *Appendix D* with the new value of λ^* for silt, the slope of M_L matches the value better according to *Figure D.4*.

The values of λ, κ^* och ϕ' were also crucial for adapting the triaxial tests. The results of the soil test showed significantly more divergent curves for the parametric study for both silt and clay in *Appendix C* and *Appendix D*. The results in *Figure C.2* and *Figure D.2* clearly illustrate how higher values of κ^* resulted in lower stiffness for the material, while higher values of λ and ϕ' resulted in higher stress levels. This outcome clearly indicates how lower stiffness values and higher stress levels

are associated with ground movements and lead to a larger settlement curve. It is important to note, however, that while the values from the parametric study achieve the true settlement curve, they do not exactly match the graphs from the CRS and triaxial tests.

8.7 Economical and environmental impact

When evaluating various construction solutions, it's essential to consider not only the functionality and quality but also the economic and environmental impacts associated with each option. In small shafts, such as those used for pipe laying, four common excavation methods are typically employed: Sheet pile wall, trench box (kojapo), Slope, and Steered JT drilling. While landfill emerges as the optimal solution from both economic and environmental perspectives, slope constructions are heavily constrained by factors such as shaft depth, site conditions, and existing infrastructure. In the Varberg project, for example, the nearby railway posed limitations on the application of slope construction, particularly in deep shafts, as indicated by the contractor. However, for smaller shafts, opting for a sloping solution can offer significant advantages.

The trench box solution emerges as the second-best option from both economic and environmental standpoints. It proves to be significantly more cost-effective than both the Sheet pile wall and Steered JT drilling methods. Additionally, the trench box can be reused to a much greater extent than sheet piles, resulting in a lower environmental impact. From a construction standpoint, both methods require equally large shafts, but the trench box only needs to reach the level of the shaft, whereas the sheet pile requires a depth of 10 meters. This difference may explain settlements observed when piles penetrate the lower aquifer and complex silt layers, leading to ground movement. Unlike the sheet pile method, the trench box solution avoids the need to reach the silt layer, potentially eliminating significant portions of measured settlement. Regarding Steered JT drilling, it presents a compelling environmental advantage as only masses corresponding to the pipe's volume need excavation.

9

Conclusions

This project investigates potential causes of settlements of a newly laid pipeline within an excavated trench supported by sheet pile walls, situated in a clay and a layered silt formation. Numerical modelling was employed to examine the effects of unloading (excavation) and reloading (backfilling). The conclusions of the investigation are as follows:

- The assessment of the ground profile, based on a soil behaviour type (SBT) classification system, indicates that it comprises a layered silt with thin layers of finer and coarser fractions. Given this layered macrostructure and the predominance of clay and silt, the site was best evaluated using the soil behaviour type classification system proposed by Schneider et al. (2008)

- The vertical displacements in the numerical model included both heave and subsequent settlements. Unloading caused immediate heave and mechanical swelling at the excavation bottom, making the time-evolving displacements dependent on both stiffness and permeability. The subsequent settlement during reloading was also shown to be stiffness-dependent and evolving in time. The analysis recognised that the major part of the pipe settlements in the numerical analysis arises from an elastic rebound effect of the excavation bottom. The minor contribution comes from subsequent consolidation settlements. The study also found that the excavation base, given the ground profile, is unstable against hydraulic uplift at a critical excavation depth. This effect can contribute to the unloading and reloading effects. Additional unloading and reloading effects can arise from wall penetration into water-bearing soil layers in the layered silt, as well as from soil disturbance, including wall driving/removal, cavity creation in the soil after wall removal, and working on the excavation bottom.

- In engineering practice of unloading/reloading problems, modelling and the prediction of vertical displacements at the excavation bottom can be improved by conducting triaxial and oedometer tests with unloading/reloading loops. This approach leads to more reliable stiffness parameters. The numerical analysis also shows that understanding the immediate unloading effect can help in predicting the subsequent excavation bottom settlements. Faster excava-

tion, pipe laying, and backfilling minimise the influence of mechanical swelling, thereby facilitating more predictable settlements during backfilling.

- An alternative approach for laying pipes in excavated trenches, instead of using braced excavations, is employing trench boxes. This method has the potential to reduce soil disturbance caused by wall installation and removal effects. The shorter embedded walls minimise the cavity loss from wall removal and, thus, minimise settlements. The risk of having vertical displacements from water due to penetration of permeable water-bearing layers beneath the excavation level can also be mitigated. The trench box system was also proven superior to sheet piling in terms of economic and environmental aspects.

9.1 Recommendations for further studies

Further studies are proposed in investigating the behaviour of silt and layered silt. Furthermore, ground movements in excavations arise from a complex interaction of multiple factors. The influence of soil disturbance from construction machinery during installing embedded retaining structures and compaction can be be investigated. Once the key mechanisms are recognised, further studies are proposed in numerical modelling of these behaviours. An enhanced understanding of the soil disturbance associated with sheet piling can result in a more accurate comparison to a trench box approach and resulting settlements.

Bibliography

Amundsen, H. A., Emdal, A., Sandven, R., & Thakur, V. (2015). *On engineering characterisation of a low plastic sensitive soft clay* (tech. rep.). Norwegian University of Science and Technology.

Andresen, A., & Kolstad, P. (1979). The NGI 54-mm samplers for undisturbed sampling of clays and representative sampling of coarser materials, state of the art on current practice of soil sampling.

Azizi, F. (1999). *Applied Analyses in Geotechnics, First edition*. CRC Press.

Bjerrum, L., & Aitchison, G. D. (1973). Problems of soil mechanics and construction on soft clays and structurally unstable soils (collapsible, expansive and others). *8th International Conference on Soil Mechanics and Foundation Engineering*.

Brown, M., Burland, J., Chapman, T., Higgins, K., Skinner, H., & Toll, D. (2023a). *ICE Manual of Geotechnical Engineering, Second edition, Volume I*. Emerald Publishing Limited. https://doi.org/10.1680/icemge.66816

Brown, M., Burland, J., Chapman, T., Higgins, K., Skinner, H., & Toll, D. (2023b). *ICE Manual of Geotechnical Engineering, Second edition, Volume II*. Emerald Publishing Limited. https://doi.org/10.1680/icemge.66830

Christensen, S. (1995). *Long-term processes in geomaterials : creep parameters from oedometer tests on illitic clays*. SINTEF Geotechnical Engineering.

Franzén, G., Spetz, T., & Sällfors, G. (2000). Settlement of sewer pipes in soft clay installed in a trench. *International Society for Soil Mechanics and Geotechnical Engineering*.

Franzén, G., & Spetz, T. (1998). *Spontens inverkan vid ledningsläggning i lös lera* (tech. rep.). Chalmers University of Technology.

Fredriksson, A., Kullingsjö, A., Ryner, A., & Stille, H. (2018). *Sponthandboken*. Pålkommissionen (Commission on Pile Research).

Gaba, A., Hardy, S., Doughty, L., Powrie, W., & Selemetas, D. (2017). *Guidance on Embedded Retaining Wall Design (C760D)*. CIRIA (Construction Industry Research and Information Association).

Geological Survey of Sweden. (2023). Kartvisaren Jordarter 1:25 000-1:100 000. https://apps.sgu.se/kartvisare/kartvisare-jordarter-25-100.html

Golder Associates AB. (2020). *Ledningsomläggningar östra sidan E2113* (tech. rep.).

Implenia AG. (n.d.). Varberg Tunneln FAS 2. https://implenia.com/en/references/detail/ref/varberg-tunneln-fas-2-1/

Karlsrud, K., & Hernandez-Martinez, F. G. (2013). Strength and deformation properties of Norwegian clays from laboratory tests on high-quality block samples. *Canadian Geotechnical Journal*, *50*(12). https://doi.org/10.1139/cgj-2013-0298

Karstunen, M., & Amavasi, A. (2017). *BEST SOIL: Soft soil modelling and parameter determination* (tech. rep.). Chalmers University of Technology.

Knappett, J., & Craig, R. F. (2019). *Craig's Soil Mechanics* (9th ed.). CRC Press. https://doi.org/10.1201/9781351052740

Larsson, P.-E., Bengtsson, R., & Eriksson, L. (1997). *Prediction of settlements of embankments on soft, fine-grained soils. Calculation of settlements and their course with time* (tech. rep.). Swedish Geotechnical Institute.

Larsson, R. (1986). *Consolidation of soft soils* (tech. rep.). Swedish Geotechnical Institute.

Larsson, R. (1995). *Jordmaterialet silt - geotekniska egenskaper och deras bestämning* (tech. rep.). Swedish Geotechnical Institute.

Larsson, R. (2008). *Jords egenskaper* (tech. rep.). Swedish Geotechnical Institute.

Larsson, R., Sällfors, G., Bengtsson, P.-E., Alén, C., Bergdahl, U., & Eriksson, L. (2007). *Skjuvhållfasthet - utvärdering i kohesionsjord* (tech. rep.). Swedish Geotechnical Institute.

Löfroth, H., Fritzson, H., Holmén, M., Lundström, K., Rudebeck, D., Abed, A., Karstunen, M., Jia, Q., & Laue, J. (2024). *Långsamma skred i skiktad siltig jord : Förstudie – BIG A2022-01* (tech. rep.). Swedish Geotechnical Institute (SGI).

Lunne, T. A., Berre, T., & Strandvik, S. O. (1997). Sample Disturbance Effects in Soft Low Plastic Norwegian Clay.

Magnusson, O. (1975). Deformationer i en schaktbotten av lera. *Statens råd för byggnadsforskning*, *Rapport R21:1975*.

McRostie, G. C., Morissette, L., & St-Louis, M. W. (1996). Bottom-heave control of a deep sensitive clay excavation in Ottawa, Canada. *Canadian Geotechnical Journal*, *33*(6). https://doi.org/10.1139/t96-122

Mesri, G., & Castro, A. (1987). Cα/Cc Concept and K0 During Secondary Compression. *Journal of Geotechnical Engineering*, *113*(3). https://doi.org/10.1061/(ASCE)0733-9410(1987)113:3(230)

Olsson, M. (2010). *Calculating long-term settlement in soft clays - with special focus on the Gothenburg region* [Licentiate thesis]. Chalmers University of Technology.

Parry, R. H. G., & Wroth, C. P. (1981). Shear Stress-Strain Properties of Soft Clay. https://doi.org/10.1016/B978-0-444-41784-8.50007-1

Påsse, T. (1990). *Beskrivning till jordartskartan Varberg NO*. Geological Survey of Sweden (SGU).

Persson, J. (2004). *The Unloading Modulus of Soft Clay: A Field and Laboratory Study* [Licentiate thesis]. Chalmers University of Technology.

Persson, J. (2007). *Hydrogeological Methods in Geotechnical Engineering: Applied to settlements caused by underground constructions* [Doctoral dissertation]. Chalmers University of Technology.

Robertson, P. K. (1990). Soil classification using the cone penetration test. *Canadian Geotechnical Journal*, *27*(1). https://doi.org/10.1139/t90-014

Robertson, P. K. (2009). Interpretation of cone penetration tests — a unified approach. *Canadian Geotechnical Journal*, *46*(11). https://doi.org/10.1139/T09-065

Robertson, P. (2016). Cone penetration test (CPT)-based soil behaviour type (SBT) classification system — an update. *Canadian Geotechnical Journal*, *53*(12). https://doi.org/10.1139/cgj-2016-0044

Sällfors, G. (1975). *Preconsolidation pressure of soft, high-plastic clays* [Doctoral dissertation]. Chalmers University of Technology.

Schneider, J. A., Randolph, M. F., Mayne, P. W., & Ramsey, N. R. (2008). Analysis of Factors Influencing Soil Classification Using Normalized Piezocone Tip Resistance and Pore Pressure Parameters. *Journal of Geotechnical and Geoenvironmental Engineering*, *134*(11). https://doi.org/10.1061/(ASCE)1090-0241(2008)134:11(1569)

Svenskt Vatten AB. (2023). Investeringsbehov och framtida kostnader för kommunalt vatten och avlopp - en analys av investeringsbehov 2022–2040. (Rapport: R2023-02).

Swedish Institute for Standards. (1991a). *Geotekniska provningsmetoder - Kompressionsegenskaper - Ödometerförsök, CRS-försök - Kohesionsjord*. (SS 27126).

Swedish Institute for Standards. (1991b). *Geotekniska provningsmetoder - Skjuvhållfasthet - Direkta skjuvförsök, CU- och CD-försök - Kohesionsjord*. (SS 27127).

Swedish Institute for Standards. (2007). *Eurocode 7: Geotechnical design - Part 2: Ground investigation and testing*. (SS-EN 1997-2:2007).

Swedish Institute for Standards. (2011). *Sustainability of construction works - Assessment of environmental performance of buildings - Calculation method*. (SS-EN 15978:2011).

Swedish Institute for Standards. (2023). *Geoteknisk undersökning och provning - Fältprovning - Del 1: Spetstrycksondering med elektrisk spets, CPT och CPTU (ISO 22476-1:2022)*. (SS-EN ISO 22476-1:2023).

Swedish Transport Administration. (2022). Varbergstunneln, Västkustbanan, Varberg–Hamra. https://www.trafikverket.se/vara-projekt/projekt-i-hallands-lan/varbergstunneln/#om_projektet

Terzaghi, K., Peck, R., & Mesri, G. (1996). *Soil Mechanics in Engineering Practice* (3rd ed.). John Wiley & Sons.

Varberg Kommun. (2021). Varbergs järnväg. https://varberg.se/varbergvaxer/varbergstunneln/ny-station-i-centrum/jarnvagens-historia

Ward, W. H. (1957). The Use of Simple Relief Wells in Reducing Water Pressure Beneath a Trench Excavation. *Géotechnique*, *7*(3). https://doi.org/10.1680/geot.1957.7.3.134

Wood, D. M. (1991). *Soil Behaviour and Critical State Soil Mechanics*. Cambridge University Press. https://doi.org/10.1017/CBO9781139878272

A

Borehole

Table A.1: Compilation of selected boreholes and analysed tests.

Name	CPTu	Piston	FC	FVT	DSS	CRS	CAUC
U01G36	X	X	X	X	X	X	
U01G40	X	X	X	X	X	X	X
U05G02	X						
U05G04	X						
U05G06	X						
U05G07	X	X	X	X	X	X	
U05G08	X						
U05G09	X						
U05G11	X						
U05G12	X	X	X	X	X	X	
U05G13	X	X	X	X	X	X	X
U05G14	X						
U05G15	X						
U05G16	X	X	X	X	X	X	
U05G17	X	X	X	X	X	X	X
U05G18	X	X	X	X	X	X	
U05G20	X	X	X	X	X	X	
U05G22	X						
U05G24	X						
U05G25	X						
U05G54	X	X	X	X	X	X	X
U17G04	X	X	X	X			
U17G05	X	X	X	X	X	X	
U17G06	X	X	X	X			
U17G25	X	X	X	X			
U17G27	X	X	X	X			
U34G02	X						
U34G03	X						
U34G04	X						
U34G06	X	X	X				
14T2037	X						
N122-07	X						

B

Soil properties

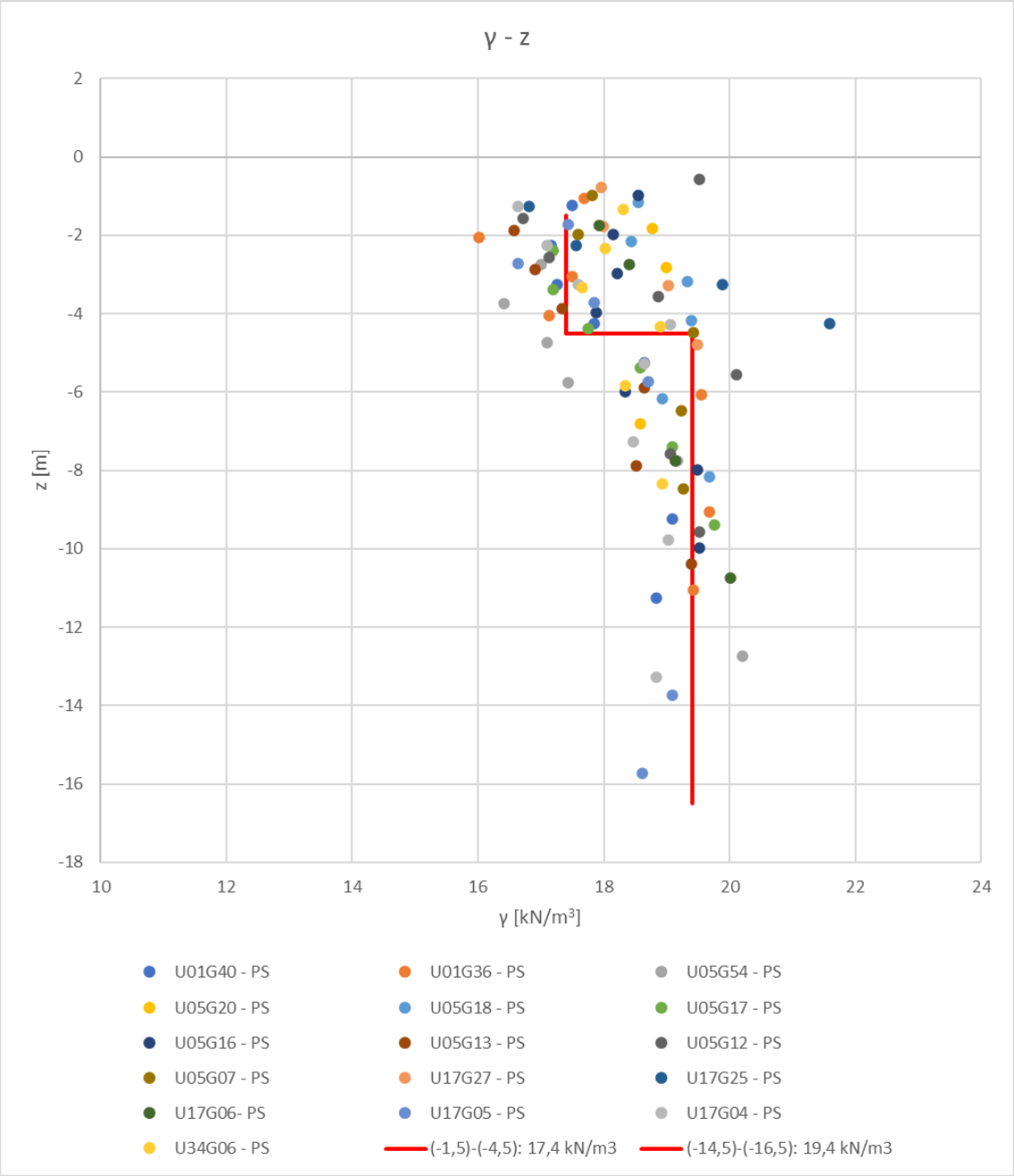

Figure B.1: Soil unit weight plotted against level.

Figure B.2: Undrained shear strength plotted against level.

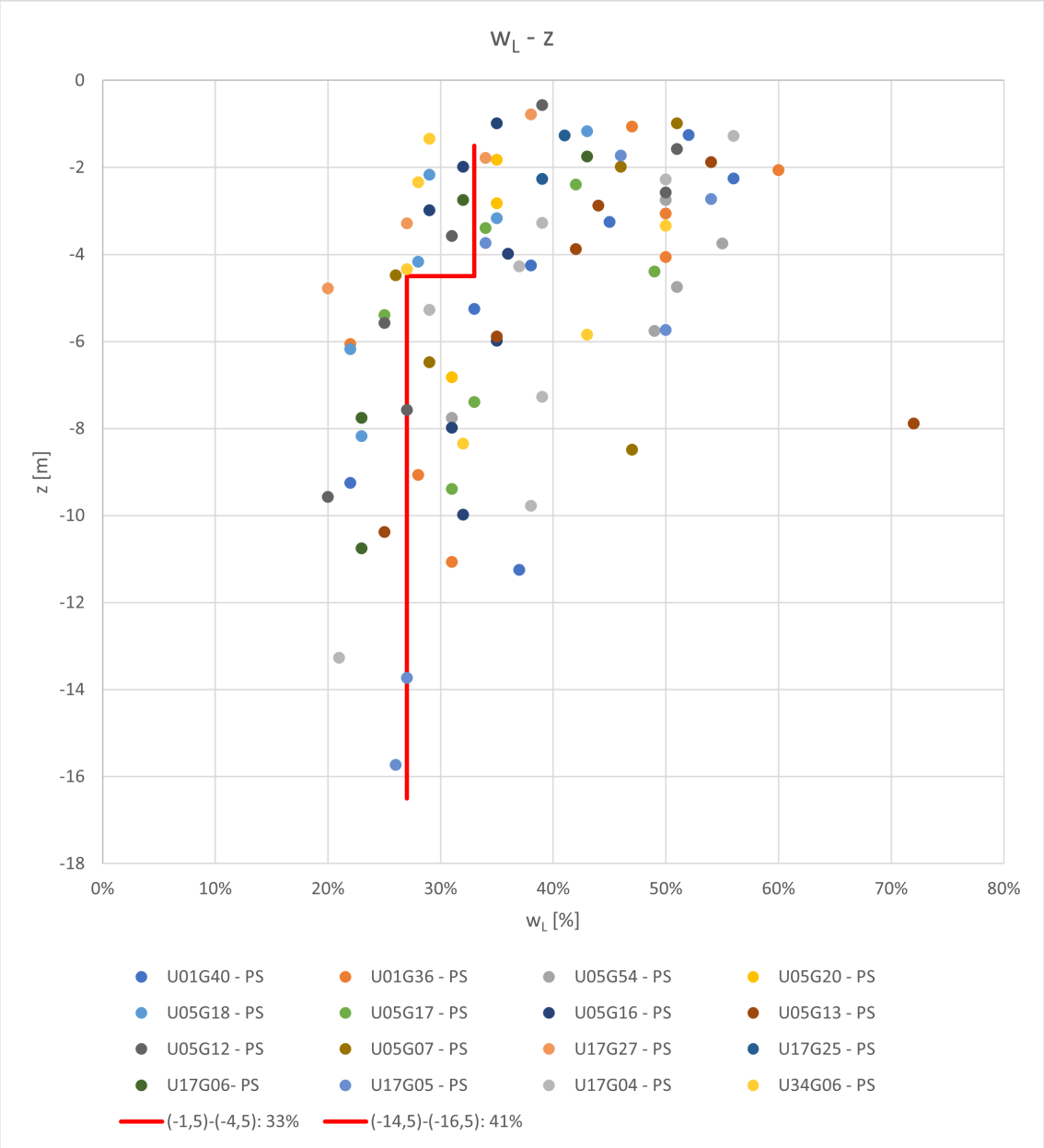

Figure B.3: Liquid limit plotted against level.

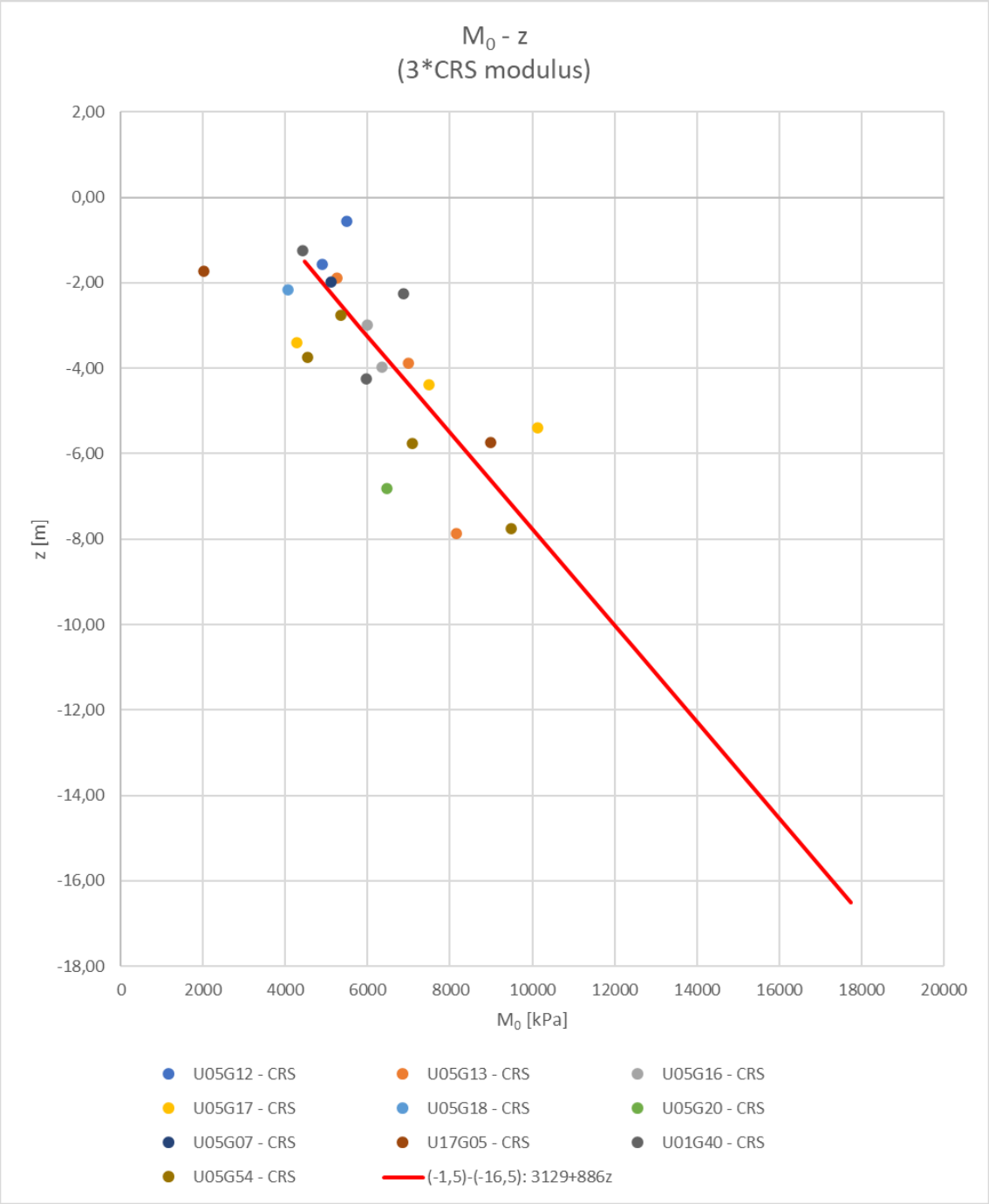

Figure B.4: Oedometer modulus (M_0) plotted against level. The red line represents the selected values for the initial analysis in PLAXIS before the soil test. Due to the limited number of measurement points in the silt layer, the same slope of the trend line for the clay was also applied to the silt and then verified through the soil test.

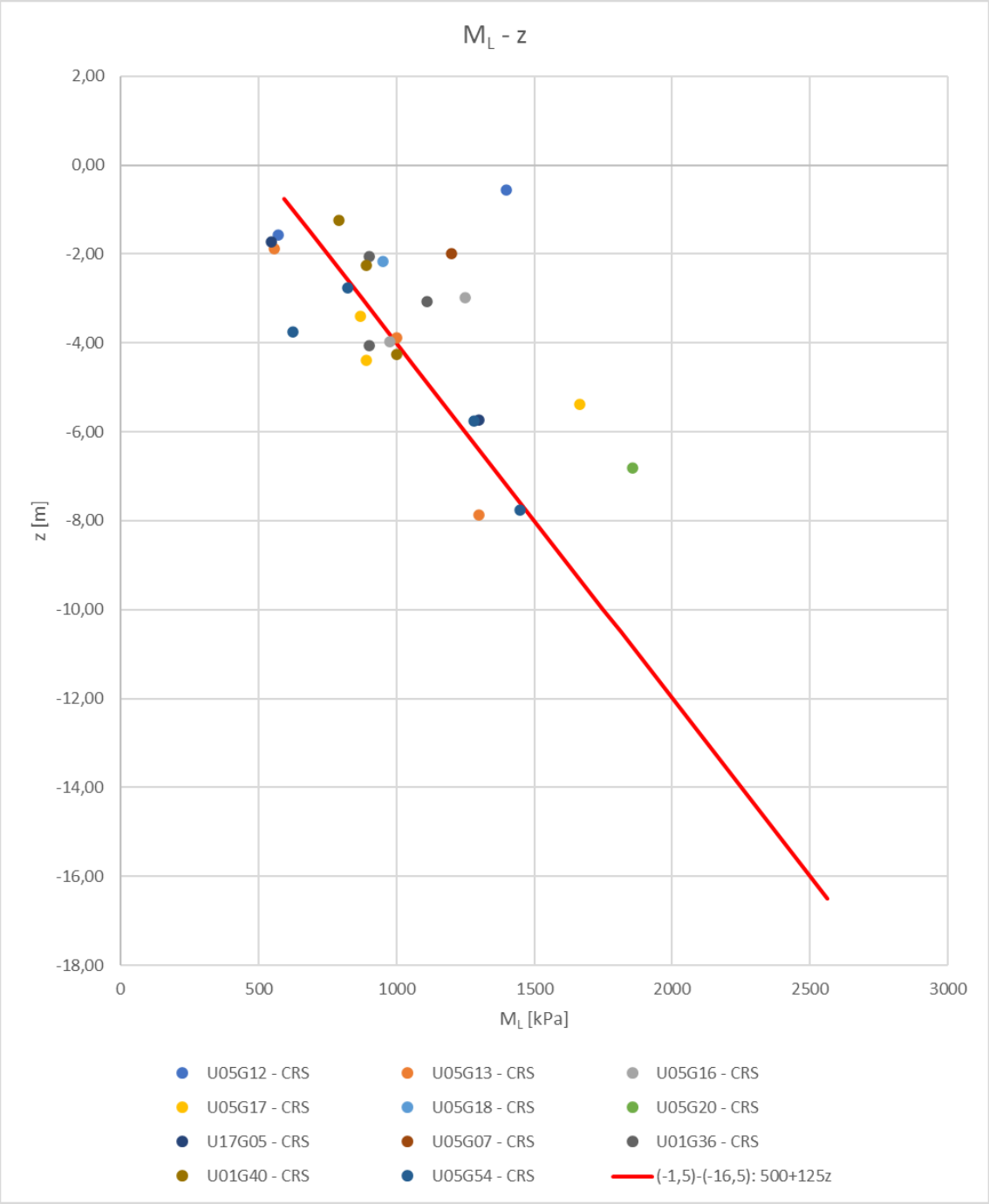

Figure B.5: Oedometer modulus (M_L) against level. The red line represents the selected values for the initial analysis in PLAXIS before the soil test. Due to the limited number of measurement points in the silt layer, the same slope of the trend line for the clay was also applied to the silt and then verified through the soil test.

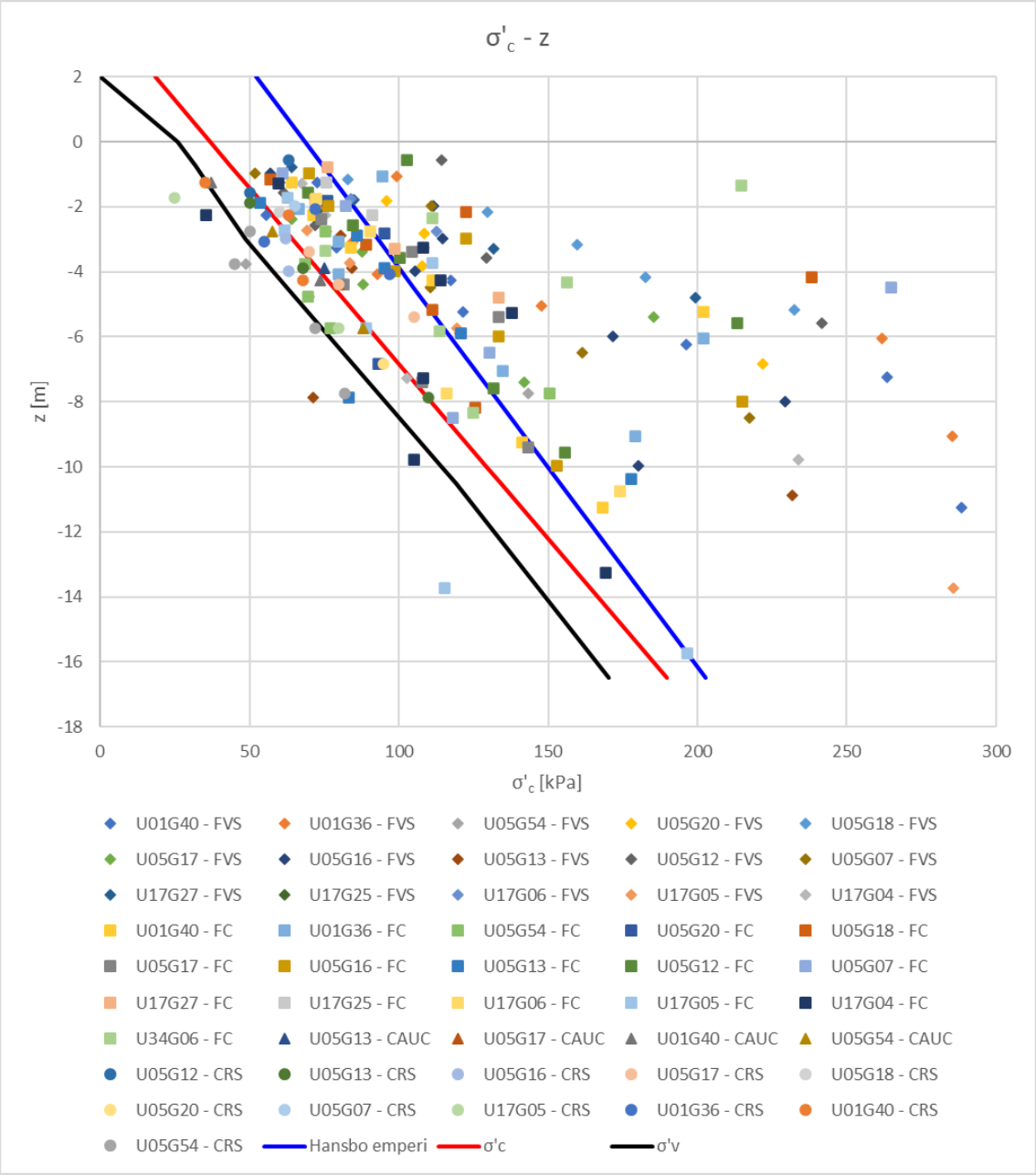

Figure B.6: Preconsolidation pressure against level.

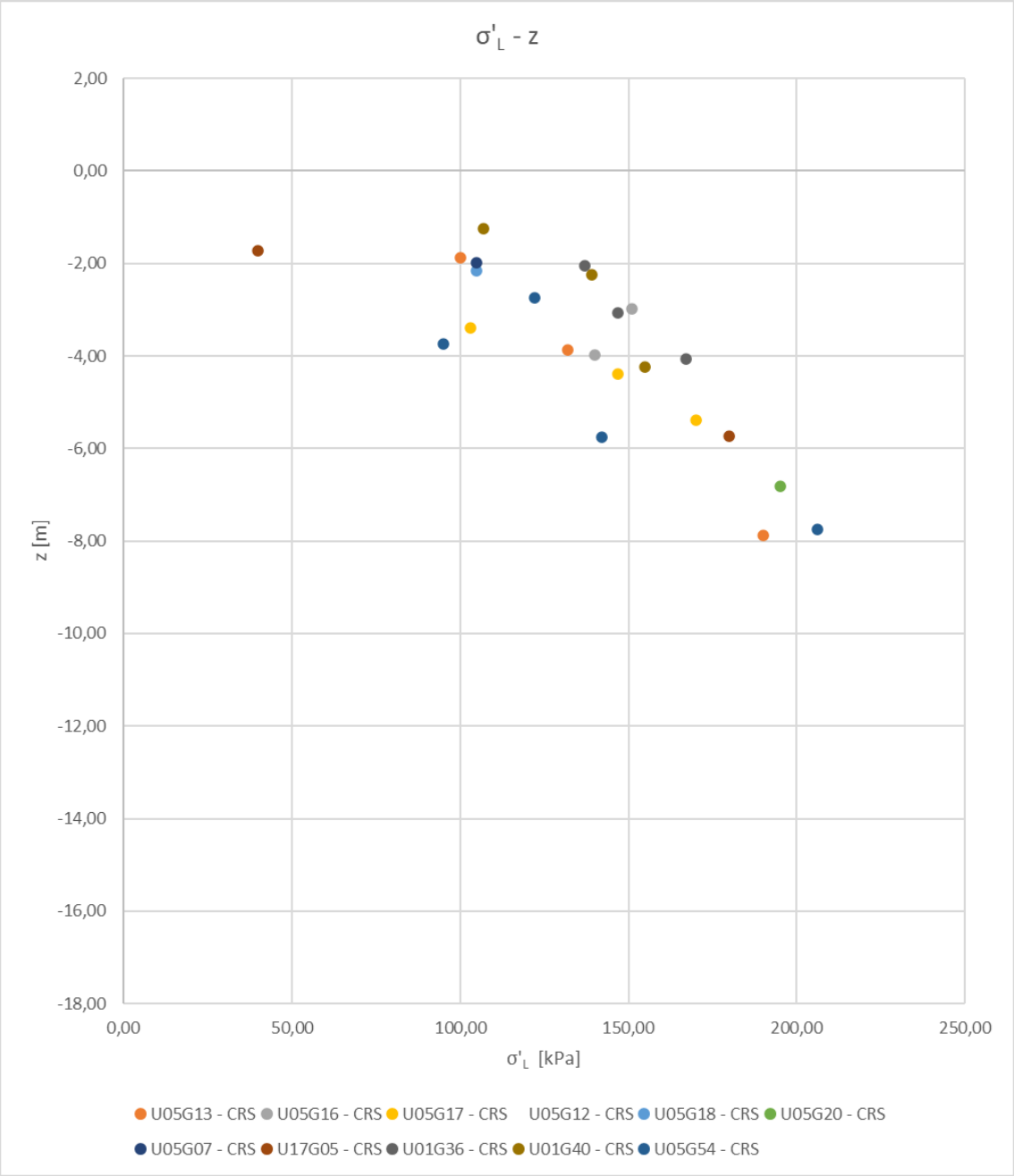

Figure B.7: Limit pressure plotted against level.

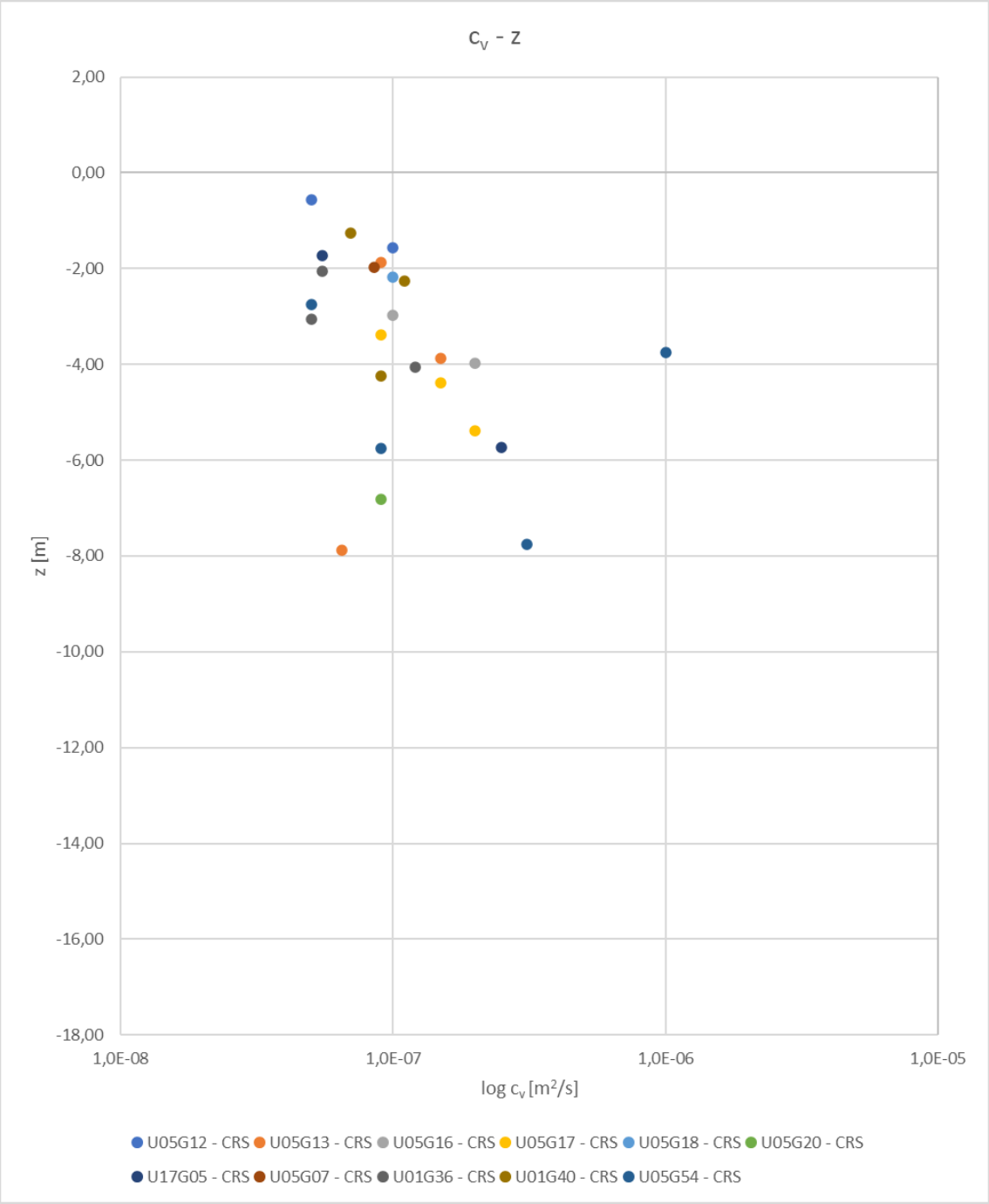

Figure B.8: Consolidation coefficient plotted against level.

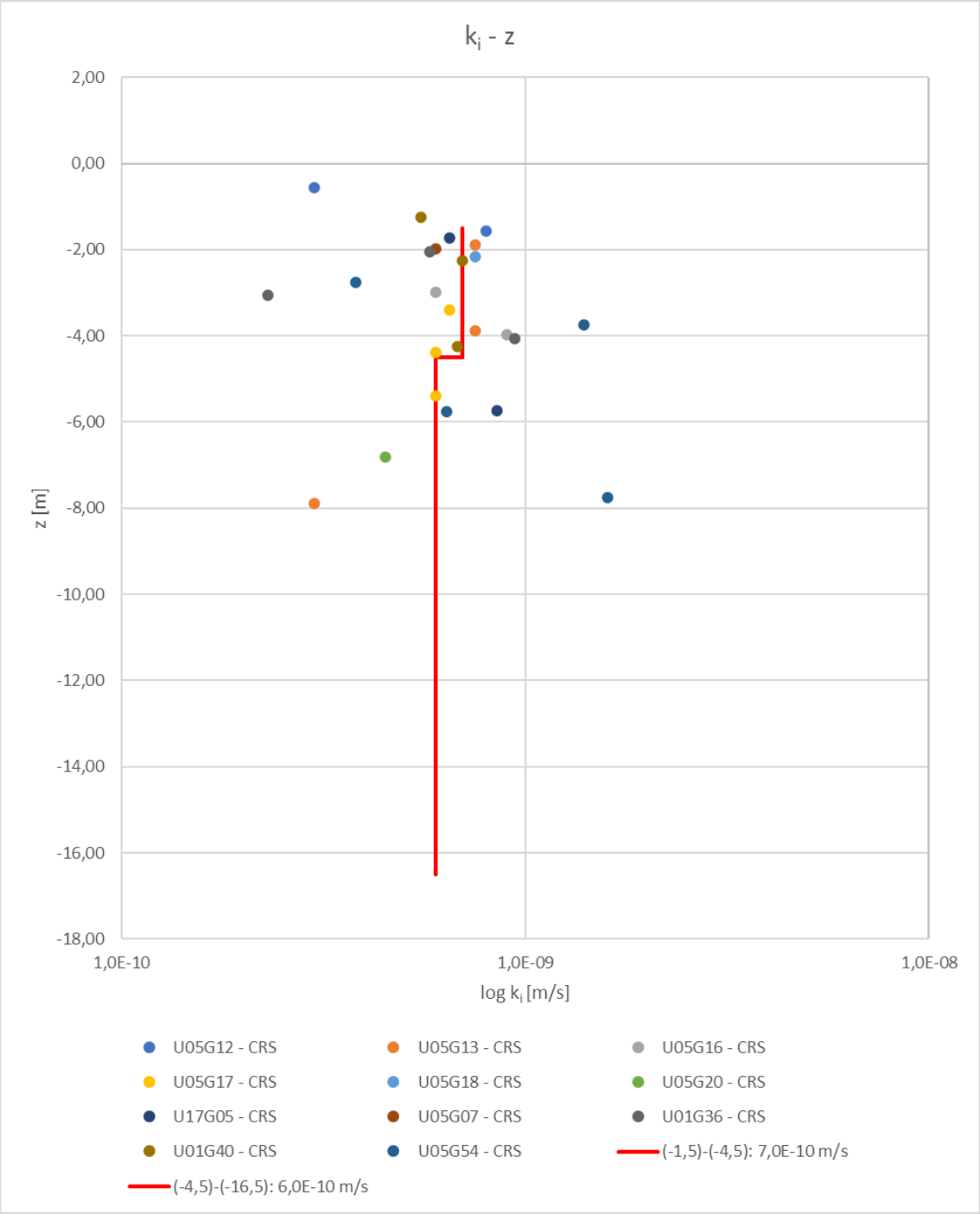

Figure B.9: Permeability plotted against level. The red line shows the selected values for the initial analysis in PLAXIS before the soil test. Due to the limited number of measurement points in the silt layer, the slope for the trend line was determined by averaging the lowest values and applied to the entire silt layer, and then verified through the soil test.

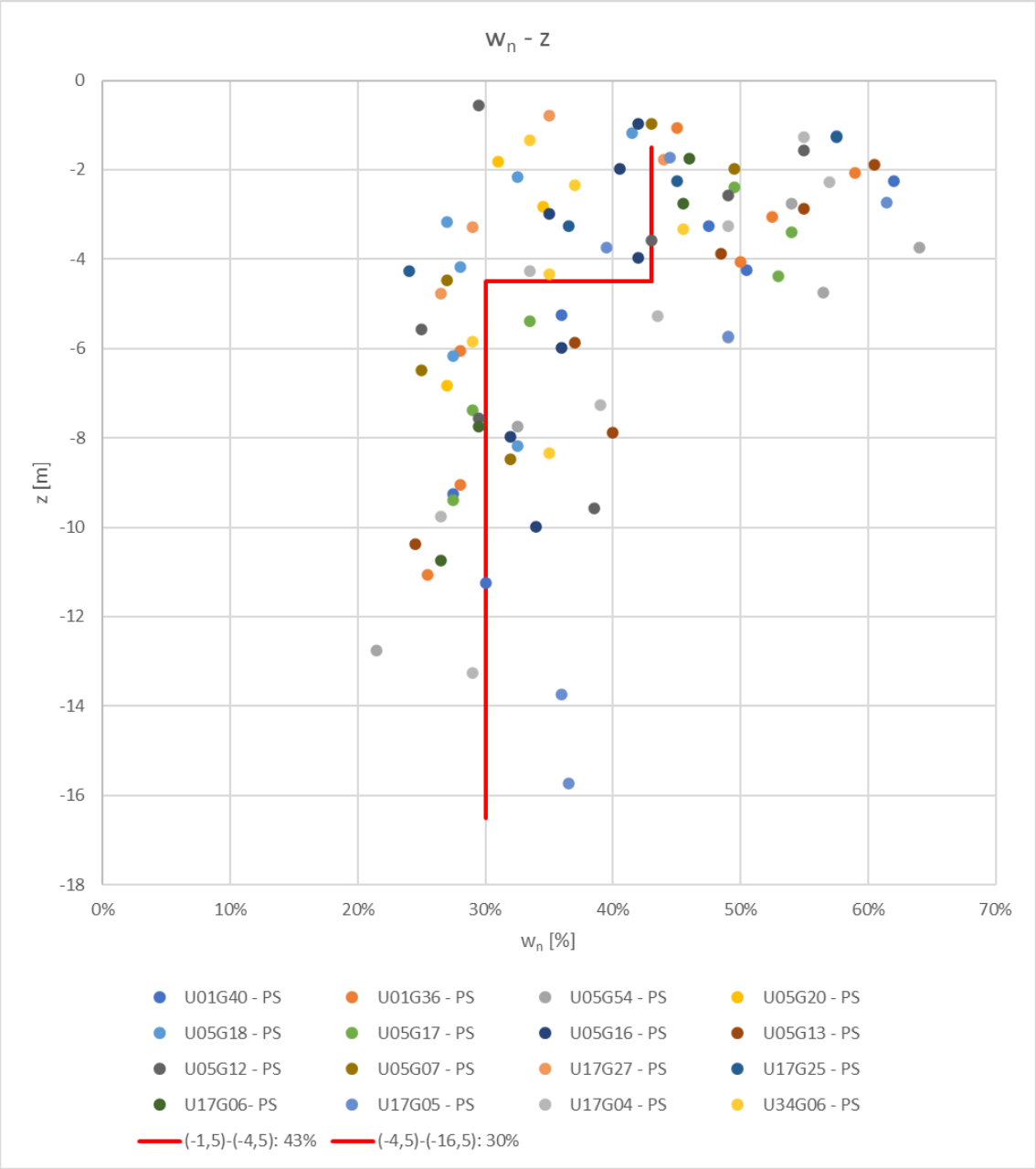

Figure B.10: Water ratio plotted against level.

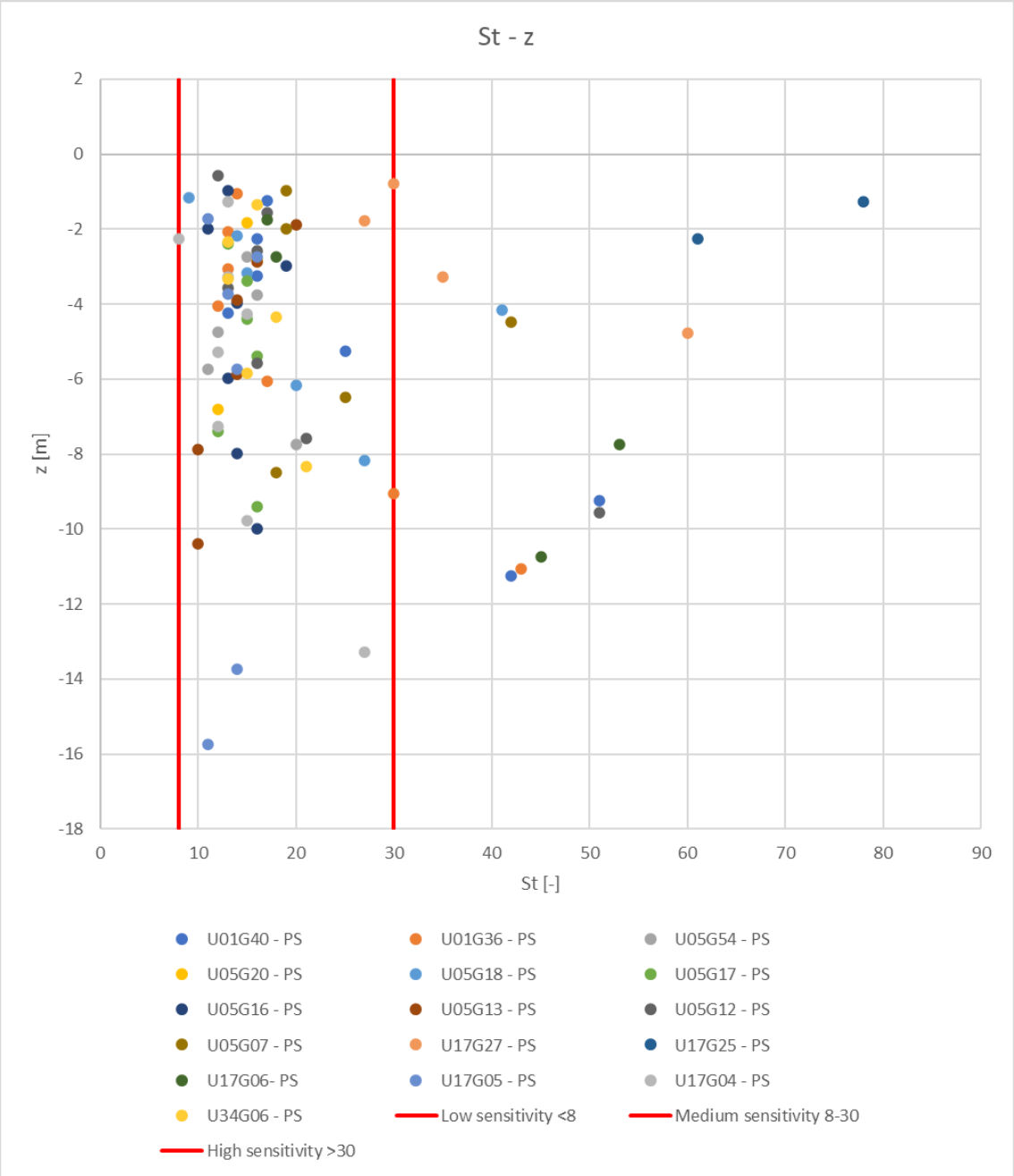

Figure B.11: Sensitivity plotted against level.

C

Soil test Clay

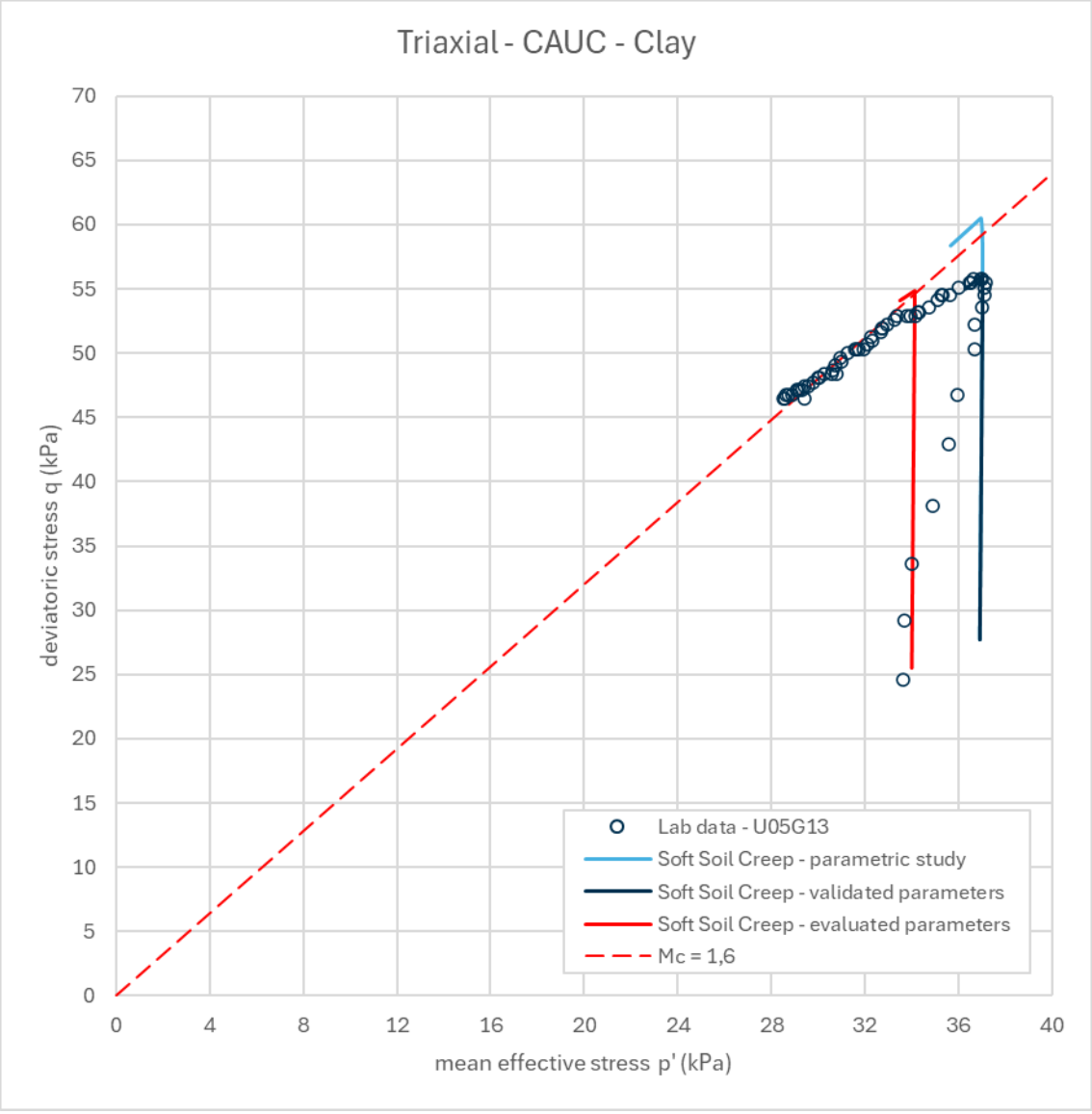

Figure C.1: $p' - q$ plot showing triaxial (CAUC) test stress paths for clay.

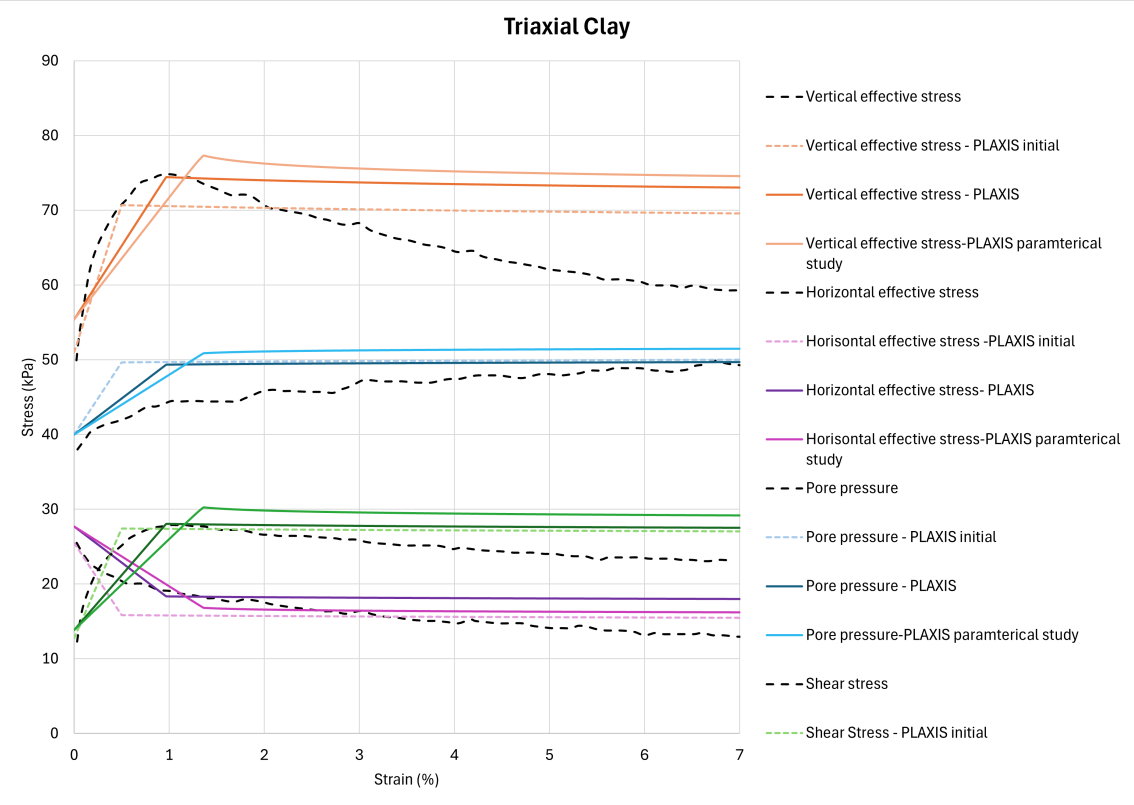

Figure C.2: Stress paths for clay for the triaxial test, the original values in PLAXIS soft soil model, the values from the soil test in PLAXIS soft soil model, and the values from the PLAXIS parametric study for soft soil model for vertical effective stress, horizontal effective stress, shear stress, and pore pressure.

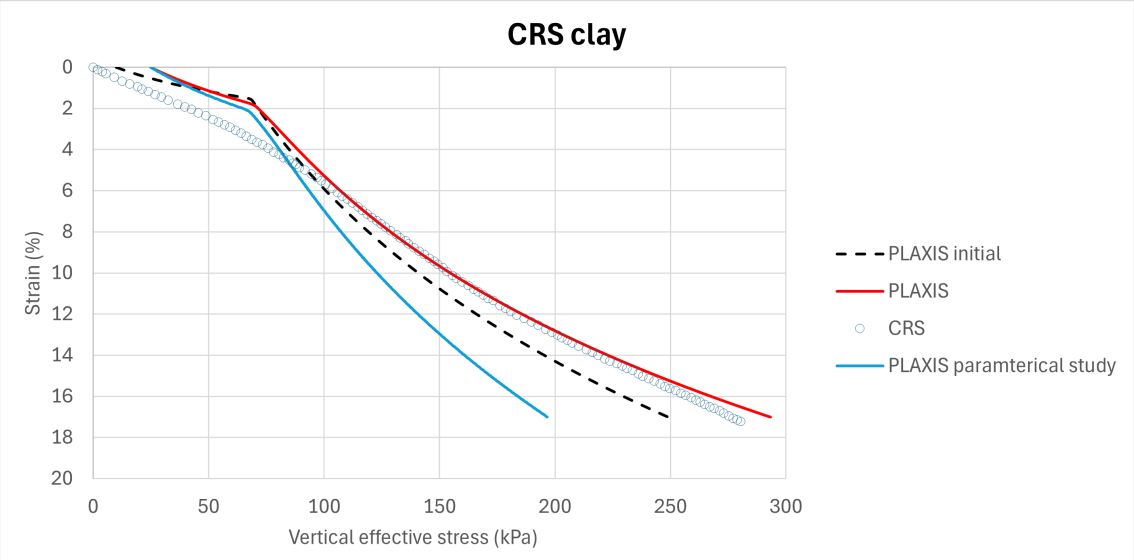

Figure C.3: The plot shows the results for clay for the CRS test, the original values in PLAXIS soft soil model, the values from the soil test in PLAXIS soft soil model, and the values from the PLAXIS parametric study for soft soil model for the plot of vertical effective stress against strain.

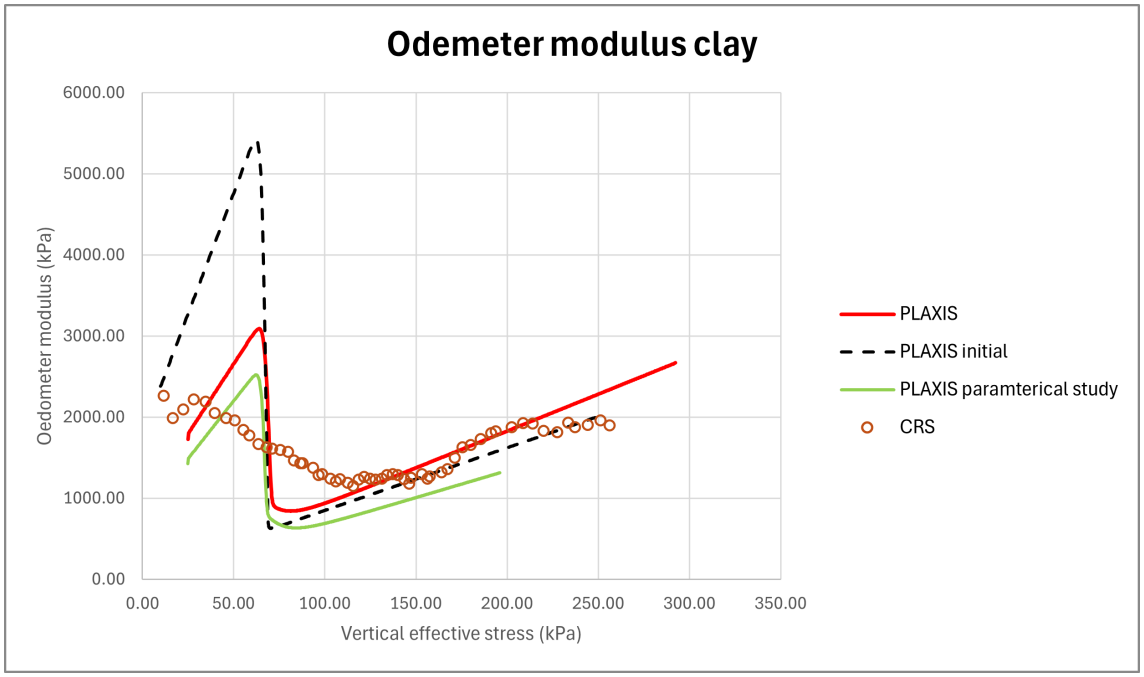

Figure C.4: The results of the oedometer modulus for clay are shown for the CRS test, the original values in PLAXIS soft soil model, the values from the soil test in PLAXIS soft soil model, and the values from the PLAXIS parametric study for soft soil model.

D

Soil test Silt

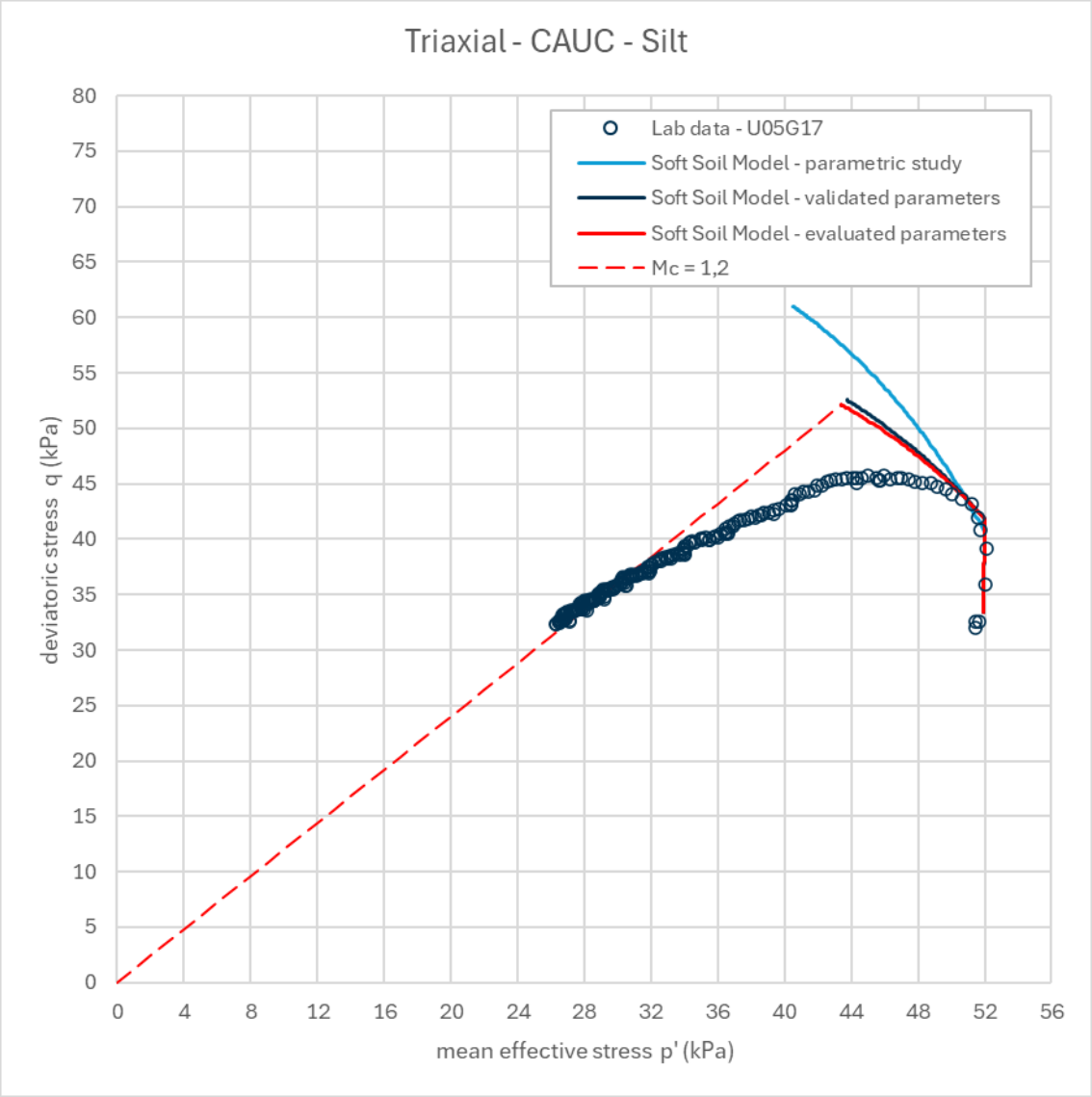

Figure D.1: $p' - q$ plot showing triaxial (CAUC) test stress paths for silt.

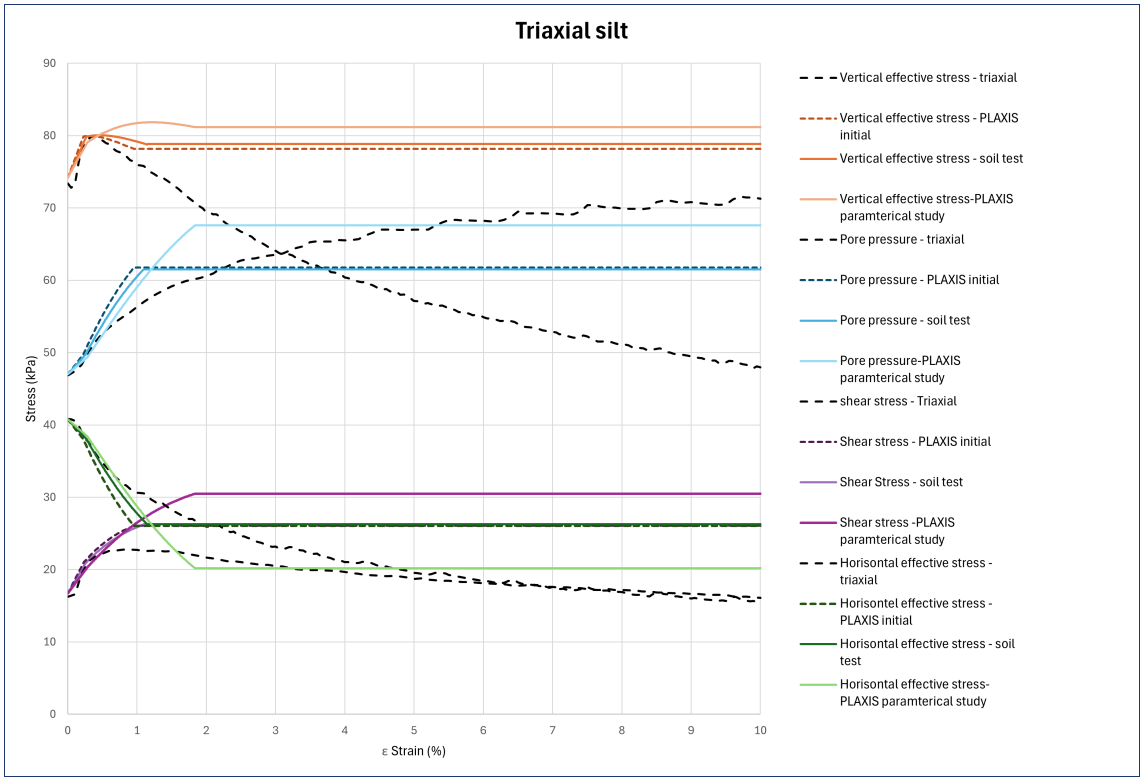

Figure D.2: The plot shows the results for silt for the triaxial test, the original values in PLAXIS soft soil model, the values from the soil test in PLAXIS soft soil model, and the values from the PLAXIS parametric study for soft soil model for vertical effective stress, horizontal effective stress, shear stress, and pore pressure.

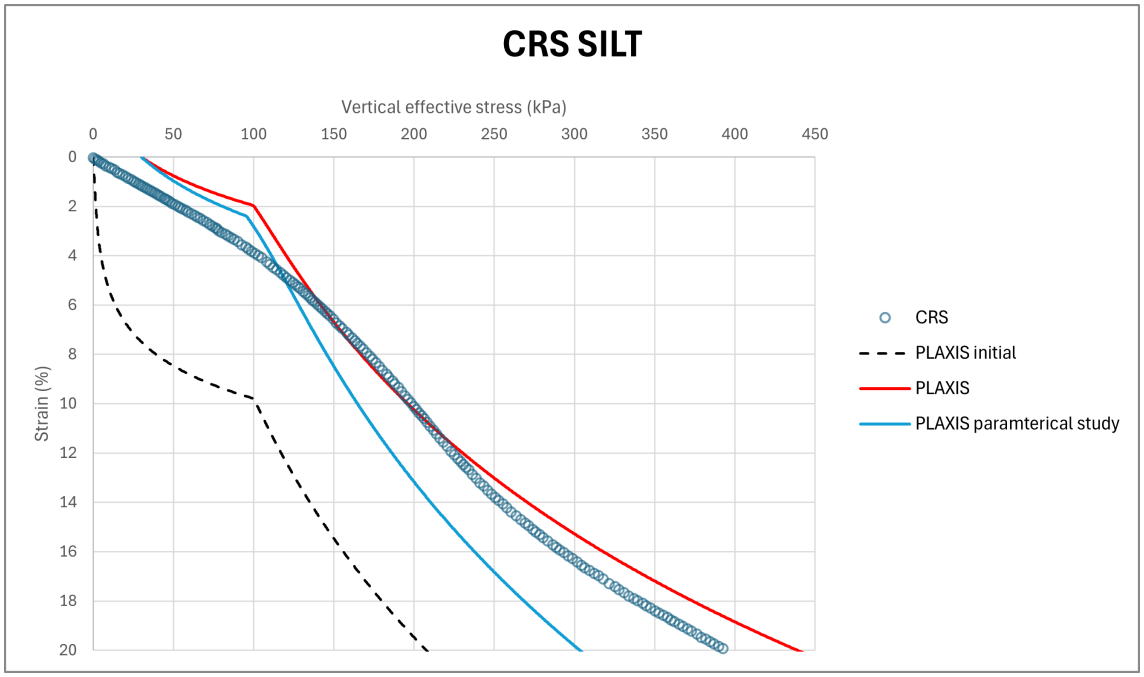

Figure D.3: The results for silt are shown for the CRS test, the original values in PLAXIS soft soil model, the values from the soil test in PLAXIS soft soil model, and the values from the PLAXIS parametric study for soft soil model for the plot of vertical effective stress against strain.

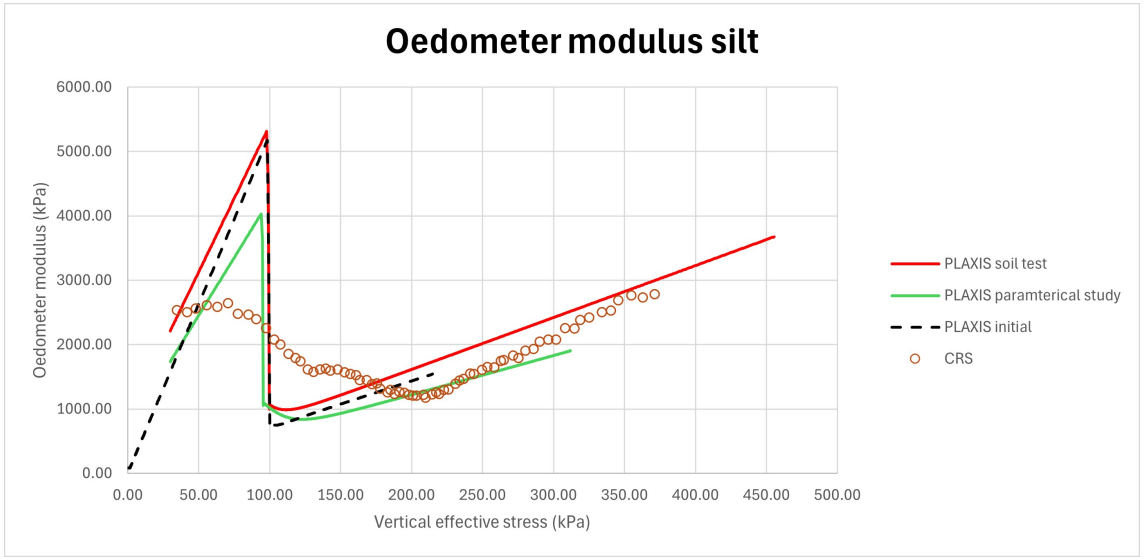

Figure D.4: The results of the oedometer modulus for silt for the CRS test, the original values in PLAXIS soft soil model, the values from the soil test in PLAXIS soft soil model, and the values from the PLAXIS parametric study for soft soil model.

E

Numerical Results

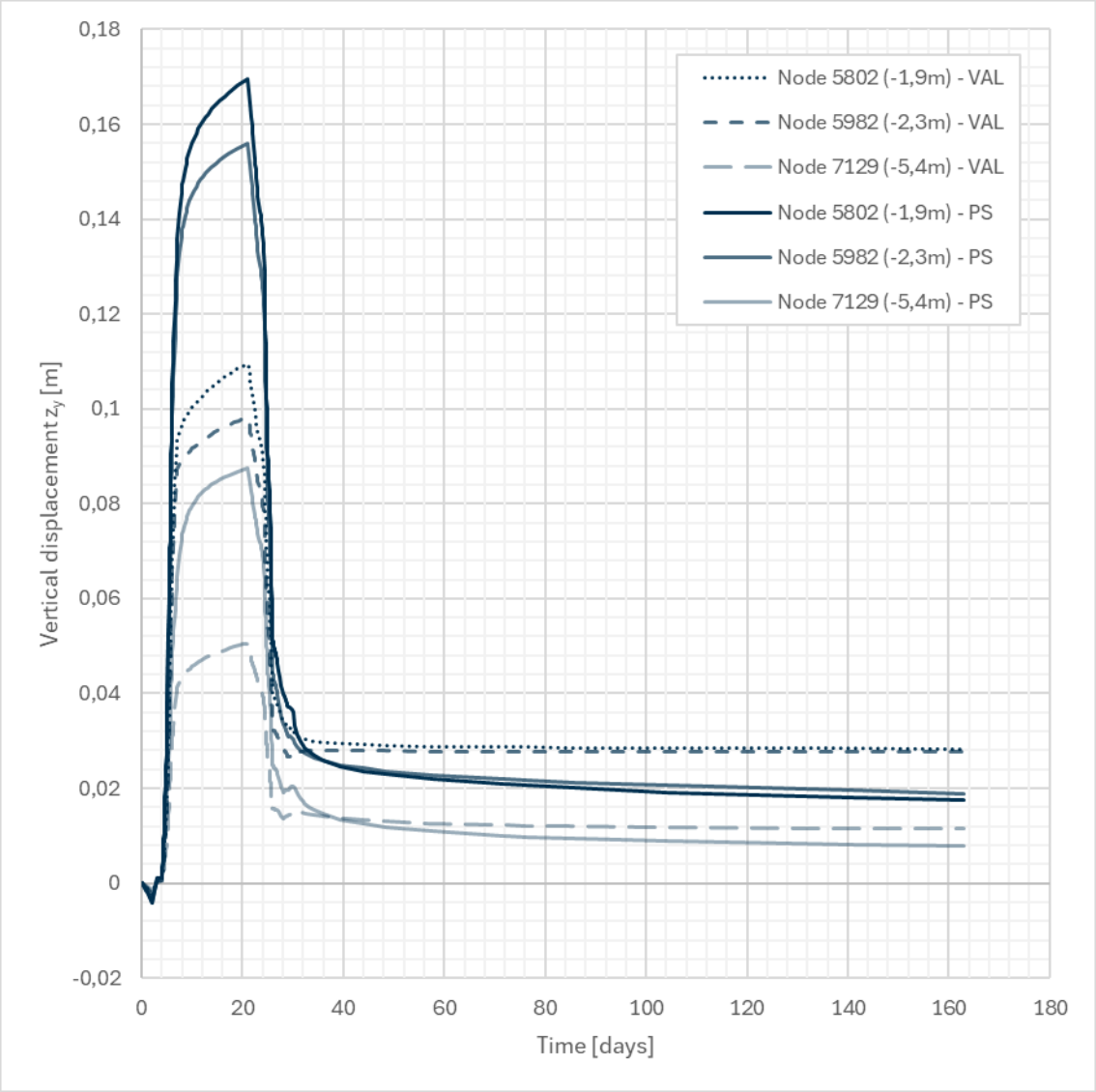

Figure E.1: The vertical displacement of the excavation bottom is shown at various depths (nodes) plotted against the total calculation time.

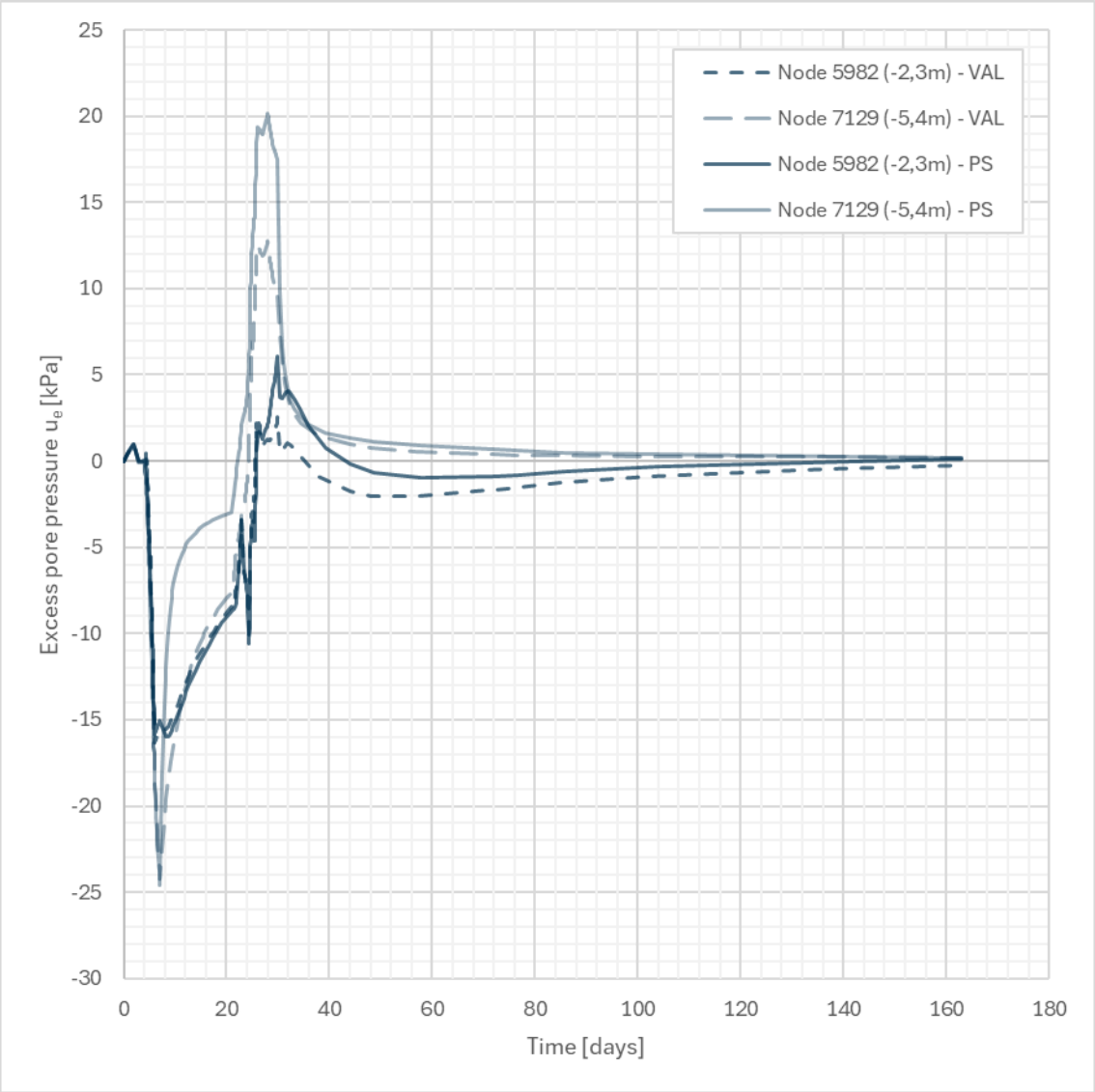

Figure E.2: The evolution of excess pore pressure plotted against the total calculation time.

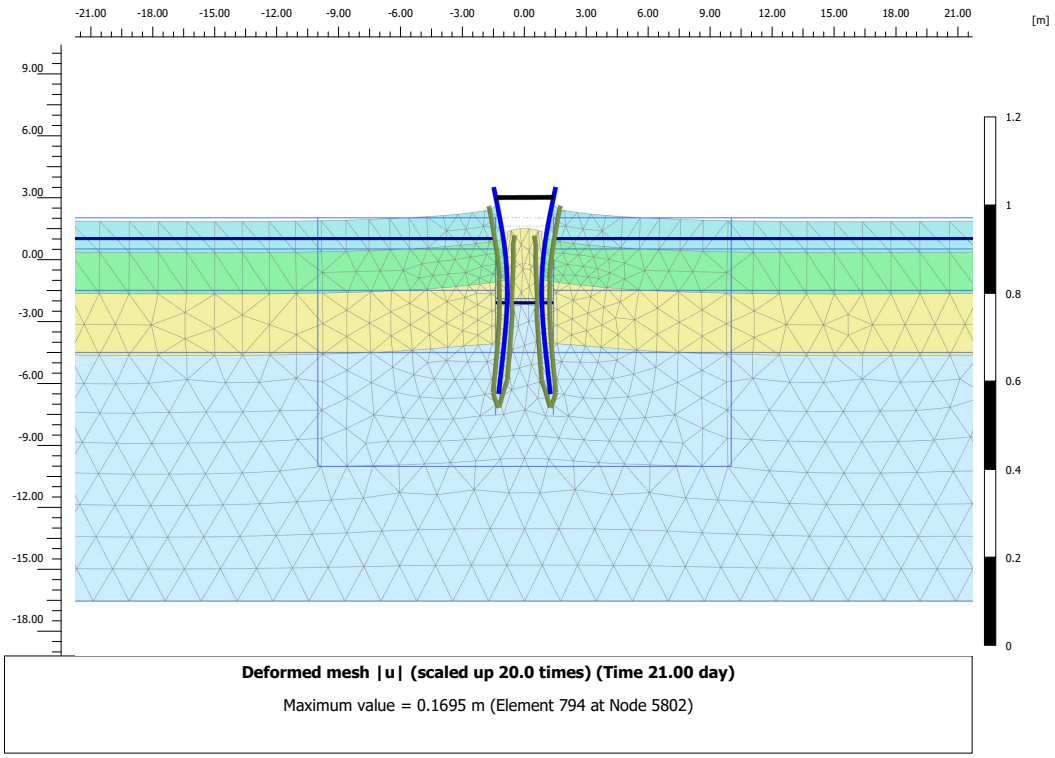

Figure E.3: Illustration of the deformed mesh after unloading of the excavation.

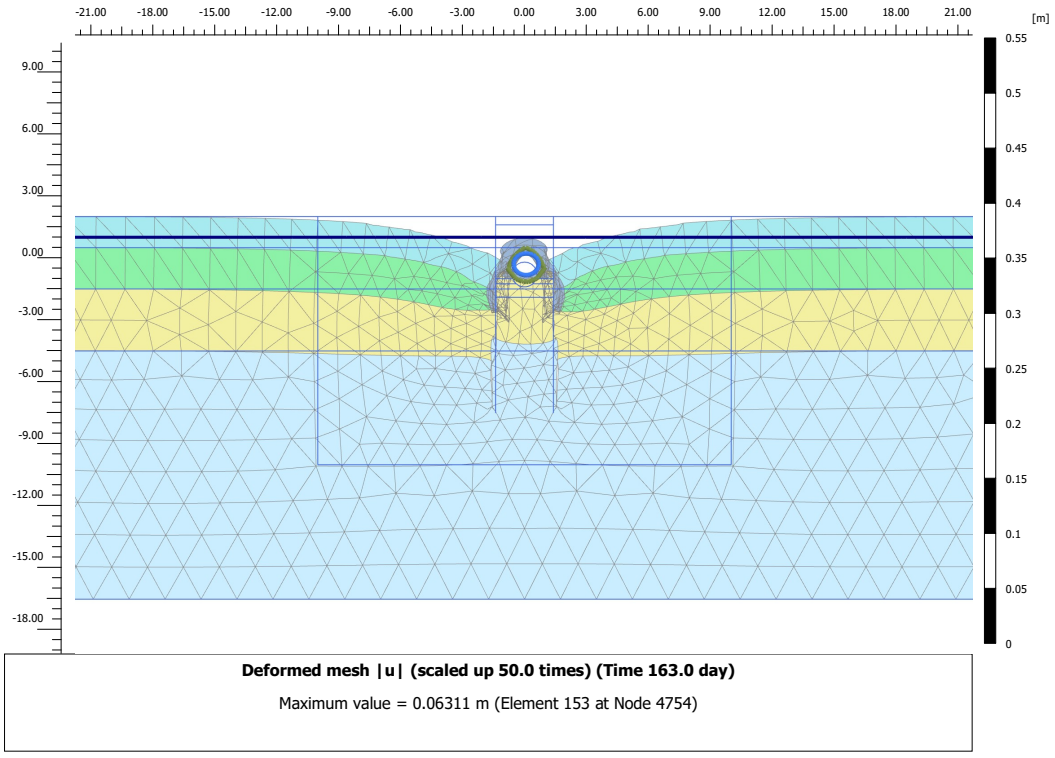

Figure E.4: Illustration of the deformed mesh after the final consolidation step.

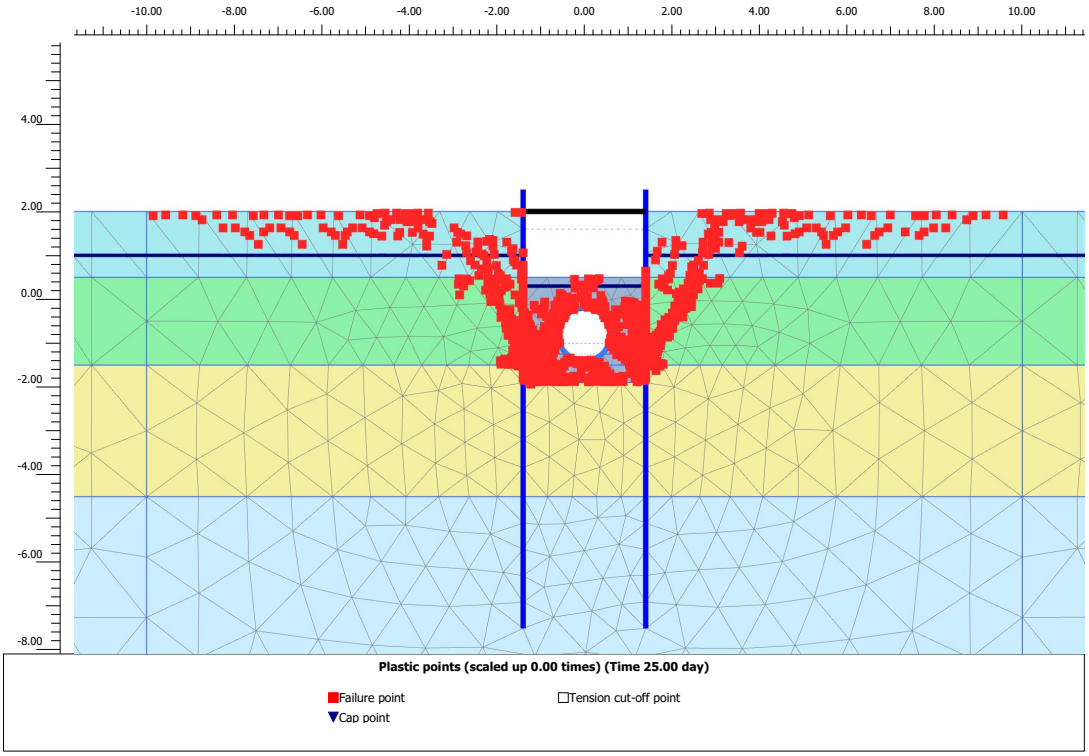

Figure E.5: Illustration of plastic points in the numerical model during reloading (backfilling).

DEPARTMENT OF ARCHITECTURE AND CIVIL ENGINEERING
CHALMERS UNIVERSITY OF TECHNOLOGY
Gothenburg, Sweden
www.chalmers.se

CHALMERS
UNIVERSITY OF TECHNOLOGY